Three-phase ac-dc power supply design and experiments using a sic based power module

By

Chintan A. Raval

B.E., Gujarat Technological University, 2014

A THESIS

Submitted in partial fulfillment of the requirements for the degree

MASTER OF SCIENCE

Department of Electrical and Computer Engineering
College of Engineering

KANSAS STATE UNIVERSITY
Manhattan, Kansas

2017

Approved by:

Major Professor
Dr. Behrooz Mirafzal

Copyright

Abstract

The rise of Wide Band Gap (WBG) devices has brought excitement in the field of Power converters. The WBG based converter can operate at the very high frequency and temperature making them ideal to use in harsh environments. The commercialization of WBG devices such as SiC and GaN MOSFETs has made it interesting for power engineering professionals all over the world. The use of WBG devices capable of operating at high switching frequencies reduces the overall system size dramatically with added benefit of improved power quality at high temperature. The main goal of this thesis is to design and test an AC-DC converter based on a SiC power module. The designed rectifier can be considered an active rectifier equipped with a controller to constantly provide feedback for modification of switching signals to get the desired output voltage. The designed active rectifier converts the varying frequency input power supply into rectified DC voltage while keeping the power factor of the system to unity. This thesis covers elementary information on power supply design, switching schemes and design of the controller. System arrangement will provide more light on the use of Six Channel MOSFET Gate Driver from CREE with the overall experimental setup. The experimental analysis will summarize the behavior of the system where information on achieved rectification, effect on the line currents at the generator and concluding power factor representation is described.

Table of Contents

List of Figures

List of Tables

List of Abbreviations

AC	Alternate Current
DC	Direct Current
PWM	Pulse Width Modulation
WBG	Wide Band Gap
UPF	Unity Power Factor
RMS	Root-Mean-Square
FF	Form Factor
TUF	Transformer Utilization Factor
CT	Center Tapped
P	Primary Windings of transformer
S	Secondary Windings of transformer
PFC	Power Factor Correction
THD	Total Harmonic Distortion
CCM	Continuous Conduction Mode
DCM	Discontinues Conduction Mode

Acknowledgements

I am grateful for the support of Dr. Behrooz Mirafzal who is just not my major advisor but also a mentor. I would like to express my gratitude to my lab-mates for their support, wisdom and for a very healthy lab environment. Thank you, K-State for having me first as an International Exchange Student and after that a full time graduate student. My sincere appreciation for the Department of Electrical & Computer Engineering for giving me opportunity to work as a Teaching Assistant with talented professors and the hardworking undergraduate students. I would like to extend my sincere gratitude to my committee members Dr. Anil Pahwa and Dr. Shelli Starrett for being part of my advisory committee.

Dedication

I dedicate this work to my beloved belated parents *Arun* and *Indira*, my entire family and my friends. I would not have come this far away without your love and support!

Chapter 1 - Introduction

1.1 Motivation

AC-DC converters or rectifiers find application in day-to-day life as a front end to DC-AC converters and DC-DC converters with buck, boost or buck boost capabilities. Most low power applications use diode bridge rectifiers. Bridge rectifiers naturally have effect on AC mains so in high power applications it becomes very important to design systems, which can have control on these sinusoidal currents. In on the move systems, it is important to have smaller system size. Many investigations have been reported in the literature to reduce the size and weight of their proposed systems with the use of wide band gap devices [1]-[5]. The research on Si devices is in such a state where limitations of physical properties of material are being encountered. Conventional power devices have limitations such as switching speed of the devices, efficiency etc. Therefore, the overall system is huge in size and weight. The recent advancement and commercialization in the field of wide band gap (WBG) power devices has allowed researchers to go on higher switching frequencies and harsher environment for the switching devices. Higher switching frequency has significant impact on reducing the size of the magnetic components, which are essential for power applications [1]. The reverse blocking capability of this material is remarkable that leads to the possibility of using very high DC bus voltage. Due to physical properties of wide band gap devices, it is possible to go on higher frequencies.

A novel AC/DC converter or rectifier, which is essentially an active rectifier, is proposed in this thesis, focusing on operating at Unity Power Factor (UPF) and reduced the overall system size.

1.2 Problem Statement

The objective of this thesis is to design and test an active rectifier. The active rectifier, which is required to ensure a UPF operation with the use of smaller size of magnetic components required for the rectifier. A three –phase AC generator operating at different speeds provides the AC supply voltage, which is varying in frequency and magnitude. The operation of UPF implies that the input currents are sinusoidal and in phase with the input voltages assuming the input voltages are sinusoidal.

1.3 State of Art

Wide Band Gap devices

Wide Band Gap (WBD) semiconductors are semiconductors made up of material, which has wider band gap – energy gap between valence band and conduction band. The wider band gap implies that it will take more energy for electrons to move from valence band to conduction band. Wider band gap represents the strength of crystal bonds in material. Fig. 1.1 shows the difference of energy gap between different material classes.

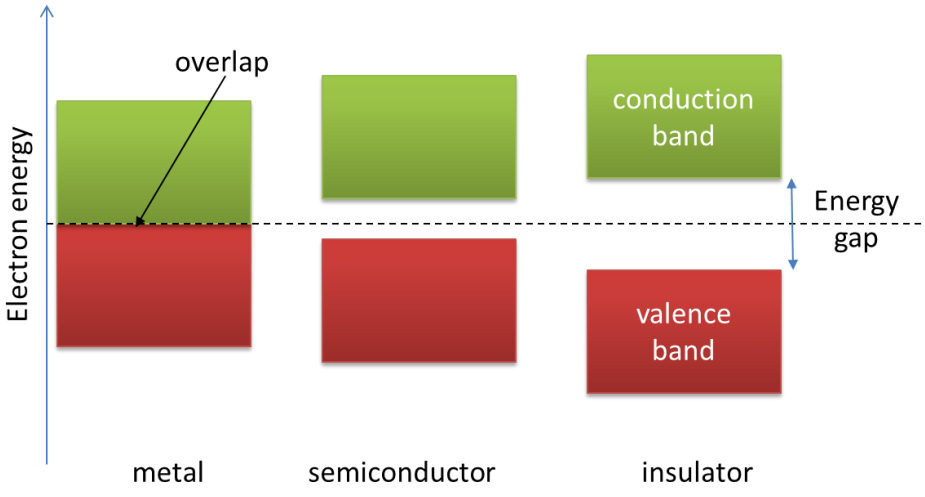

Fig. 1.1: Energy bandgap in materials

The term wide band gap semiconductors cover entire family of materials consisting of SiC (Silicon Carbide), GaN (Gallium nitride), Aluminum Nitride (AIN) and semiconductor diamond (C) etc. Fig. 1.2 shows comparison of band-gap of different semiconductors materials. This property has numerous advantages. To name a few, WBD has low carrier concentration n_i and the energy required to cross the band gaps is high so that the concentration of electrons that cross the band gap is smaller than that of typical Si devices.

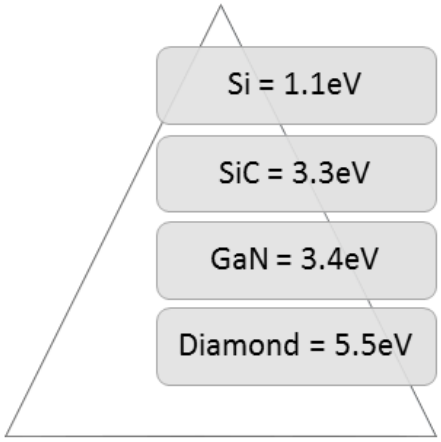

Fig. 1.2: Band gap of semiconductors materials

The leakage currents are proportional to n_i or ${n_i}^2$ so the devices can operate at much higher temperatures [1]. The dielectric breakdown field-strength of WBD is approximately 10 times that of Si devices. SiC devices can be made to have a thinner drift layer or in other words high doping concentration, so they have very high breakdown voltage and small resistance compared to Si devices [1]. Furthermore, WBD have reduced energy losses, higher-voltage operations, higher operating frequency, and improved power quality when compared to typical Si material semiconductors [3]. Table 1.1 extracted from [3] summarizes the key properties of different semiconductor materials.

Table 1-1: Key properties for semiconductor materials [3]

Parameter	Si	4H-SiC	GaN	Diamond
Energy bandgap E_g (eV)	1.1	3.3	3.4	5.5
Critical electric field E_c (MV/cm)	0.25	2.2	3	10
Electron drift velocity V_{sat} (cm/s)	1×10^7	2×10^7	2.2×10^7	2.7×10^7
Thermal conductivity λ (W/cm-K)	1.5	4.9	1.3	22

Apart from the advantages of WBG semiconductors, there are several challenges associated with these semiconductors such as increased EMI, high di/dt and dv/dt and increased system cost [5]. In this thesis, the experimental results highlights the advantages explored from the SiC MOSFETs with reduced system size.

1.4 Contribution

The key contribution of this research is the development of an active UPF rectifier based on SiC MOSFET gate driver module operable at high switching frequencies [> 50 kHz], receiving the supply voltage from variable speed three-phase generator and using smaller size of magnetic components as filter. This thesis also summarizes basic power supply design, popular switching schemes and elementary information on design of the controllers. The experimental analysis will highlight the behavior of the system at certain power rating while keeping the power factor of the system near unity as the AC supply voltage varies in both frequency and magnitude. Furthermore, the research performed for this thesis assists the design of an active rectifier with inputs and outputs to the system given.

1.5 Outline of Thesis

This thesis is comprised of six chapters. Apart from this introductory chapter where overview is present, Chapter 2 will provide comprehensive summary on different rectifier topologies, power factor corrector rectifiers, brief information on importance of power factor correction and harmonic mitigation.

Chapter 3 addresses sine pulse width modulation switching technique (SPWM) and third harmonic injection in spwm (THIPWM), basic discussion on controller design for the system to achieve Unity Power Factor and generation of precharge pulses for the system.

Chapter 4 will shed light on the proposed experimental setup, simulation of system and details on the setup including SiC gate driver, use of dSpace and FPGA.

Chapter 5 will highlight the result and analysis from the setup. Finally, conclusion and future use of the system is discussed in final chapter.

Chapter 2 - Literature Study

Rectifiers are the devices used to convert AC voltages into DC. These converted voltages are then applied to different types of loads. Some of these loads require high voltage, some require high current and some require both. This rectification is in most cases unidirectional. An ideal rectifier is the one that produces a minimum ripple in DC voltage. Most rectifiers are supplied from a line transformer at the utility side; it is vital to minimize the use of these bulky transformers in modern power electronics. This chapter briefly provides discussion on the classification of rectifiers, their advantages, and limitations. Towards the end of the chapter, there is a brief discussion on prominent power factor corrector three-phase rectifier: Vienna rectifier. To explain the classification some of the rectifier parameters are necessary to address.

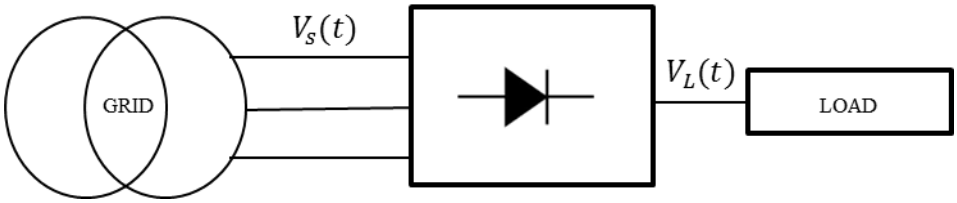

Fig. 2.1: Basic rectifier circuitry

Fig. 2.1 shows a basic rectifier circuitry. Where, $V_S(t)$ is the instantaneous input voltage and $V_L(t)$ is the instantaneous rectified load voltage. For the ease of discussion in this chapter, the diodes and thyristors are considered as ideal i.e. there is no forward voltage drop, no reverse recovery time and they do not have turn on – off delays. In addition, the load is purely resistive so voltage and load current have similar waveforms.

The average DC voltage on load can be written as:

$$V_{DC} = \frac{1}{T}\int_0^T V_L(t)dt \qquad (2\text{-}1)\ [6]$$

Where V_{DC} is the average DC voltage.

The root-mean-square (rms) value of the load voltage can be expressed as:

$$V_L = \sqrt{\frac{1}{T}\int_0^T {V_L}^2(t)dt} \tag{2-2}$$

Where V_L is the load voltage.

The currents can be written as,

$$i_L(t) = \frac{V_L(t)}{R_L} \tag{2-3}$$

$$I_{DC} = \frac{V_{DC}}{R_L} \tag{2-4}$$

$$I_L = \frac{V_L}{R_L} \tag{2-5}$$

Where I_{DC} is average value of load current and I_L is the rms value of load current.

2.1 Basic Rectifier parameters

Rectifier parameters are useful in comparing the performance of different rectifier structures. Although there are many parameters, the parameters discussed in this section are mostly elementary.

2.1.1 Form Factor (FF):

Form Factor (FF) of a rectifier is the ratio of the root-mean-square value to the mean value of voltages.

$$\text{FF} = \frac{V_L}{V_{DC}} \tag{2-6}$$

2.1.2 Rectification Ratio (RR):

Rectification ratio (Rectification efficiency) can be expressed as the ratio as,

$$\eta = \frac{P_{DC}}{P_L + P_D} = \left(\frac{1}{FF}\right)^2 \tag{2-7}$$

Where

$$P_{DC} = V_{DC} \cdot I_{DC} \quad (2\text{-}8)$$

$$P_L = V_L \cdot I_L \quad (2\text{-}9)$$

$$P_D = R_D \cdot {I_L}^2 \quad (2\text{-}10)$$

Here, P_D is the power losses in the rectifier. R_D is the equivalent resistance of rectifier. In case of ideal switches $R_D = 0$.

2.1.3 Ripple Factor (RF):

Ripple Factor is a measure of the ripple content. It denotes smoothness of voltage waveform in the output of the rectifier or the quality of rectification.

$$RF = \frac{V_{AC}}{V_{DC}} = \frac{\sqrt{{V_L}^2 - {V_{DC}}^2}}{V_{DC}} \quad (2\text{-}11)$$

Where $V_{AC} = \sqrt{{V_L}^2 - {V_{DC}}^2}$ is the rms value of the ac component of the load voltage V_L.

2.1.4 Transformer Utilization Factor (TUF):

Transformers provide isolation between the input of the rectifier and grid. TUF is the ratio of the DC output power to the transformer volt-ampere (VA) rating required by the secondary winding [6].

$$TUF = \frac{P_{DC}}{V_s I_s} = \frac{P_{DC}}{\frac{VA_p + VA_s}{2}} \quad (2\text{-}12)$$

Where, VA_p and VA_s are power ratings at primary and secondary of the transformer.

2.2 Classification of Rectifiers

Rectifiers have evolved to a mature state. There have been many rectifier topologies since the evolution of diodes and thyristors. Uncontrolled or line-commutated rectifiers usually consist of diodes. Most diode rectifiers have fixed frequency input AC voltages, fixed DC output voltage. Controlled rectifiers or Phase-control rectifiers have control on switching devices and usually

consist of thyristors where the thyristors act as a switch and have two states: ON state and OFF state (i.e. achieved by providing suitable gate trigger pulse). In the case of diode rectifiers, load current flows when diodes conduct and in the case of phase rectifiers, the load current flows when the thyristors conduct. Fig. 2.2 shows an attempt to classify the rectifiers based on their operational control **[6].**

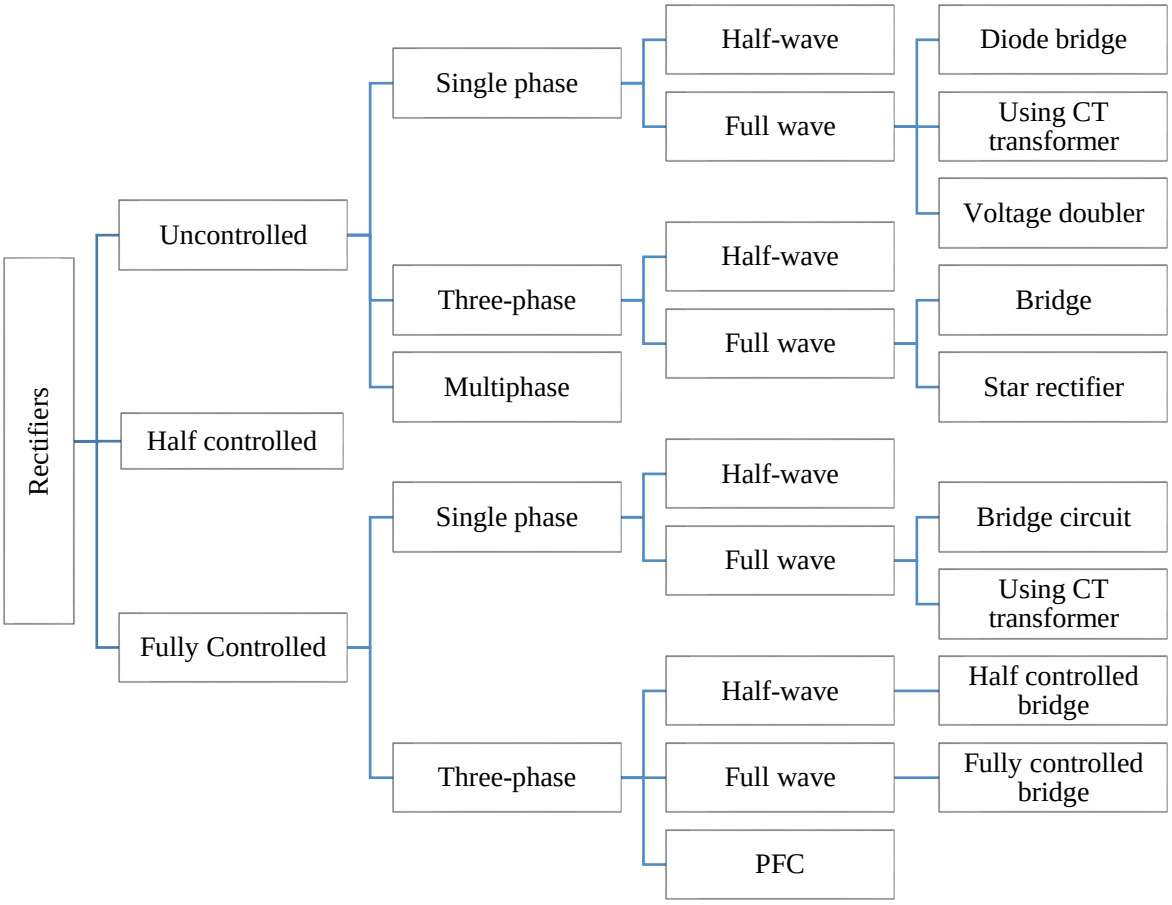

Fig. 2.2: Rectifier Classification [6]

Apart from these two categories shown Fig. 2.2, there are many hybrid rectifier constructions proposed by researchers, which are popular in the industry. Traditional rectifiers are usually constructed using diodes. These diode rectifiers are also vital in the home and in industrial equipment to feed in-between DC link to electronic circuitry. To include all the constructions and the state of the art of these

constructions can be very prolonged. Another rectifier classification, based on the direction of power flow, regenerative rectifiers can be found in the literature [10] [11]. In the following sections, few of the most common rectifier constructions are discussed.

2.2.1 Uncontrolled Rectifiers:

2.2.1.1 Single-phase Half-wave Diode Rectifier:

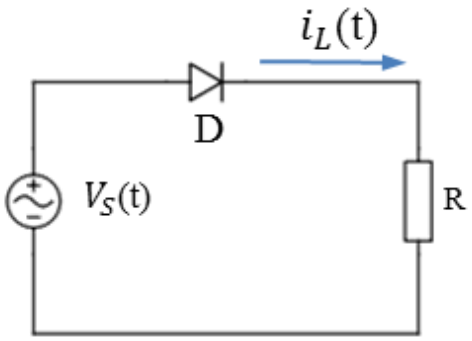

Fig. 2.3: 1 - ϕ unidirectional half-wave rectifier

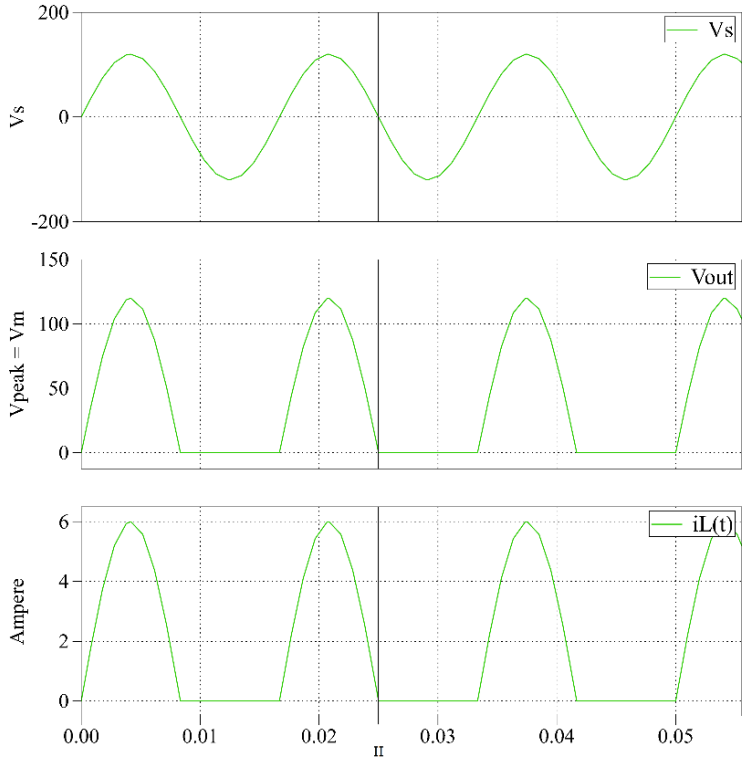

Fig. 2.4: Voltage and current waveform of 1 - ϕ half-wave rectifier

As shown in the Fig. 2.3, the 1 - ϕ half-wave diode rectifier with resistive load gives the fixed average output voltage. The diode conducts during the positive half of cycle (i.e. T/2). During the negative half cycle, the diode is reverse biased and acts as an open circuit. From observation of the voltage and current relationship of this circuitry, peak voltage $V_{peak} = V_m$. The inverse voltage seen by the diode in its blocking state is the negative half cycle of the AC voltage $V_s(t)$.

Using the equation 2-1,

$$V_{DC} = \frac{1}{T}\int_0^T V_L(t)dt$$

$$= \frac{1}{2\pi}\int_0^{\pi} V_s \sin(\omega t)dt = \frac{V_s}{\pi} \quad (2\text{-}13)$$

Similarly,

$$V_L = \sqrt{\frac{1}{T}\int_0^T {V_L}^2(t)dt}$$

$$= \sqrt{\frac{1}{2\pi}\int_0^{T} {V_s}^2 \ \sin^2(\omega t)\ dt} = \frac{V_s}{2} \quad (2\text{-}14)$$

$$I_{DC} = \frac{V_{DC}}{R_L} = \frac{V_s}{\pi \cdot R_L} \quad (2\text{-}15)$$

$$I_L = \frac{V_L}{R_L} = \frac{V_L}{2*R_L} \quad (2\text{-}16)$$

$$FF = \frac{V_L}{V_{DC}} = \frac{\pi}{2} \quad (2\text{-}17)$$

$$RR = (\frac{1}{FF})^2 = 0.405 \quad (2\text{-}18)$$

$$RF = \frac{V_{ac}}{V_{DC}} = \frac{\sqrt{{V_L}^2 - {V_{DC}}^2}}{V_{DC}} = 1.21 \quad (2\text{-}19)$$

2.2.1.2 Single-phase full-wave diode rectifier:

Full-wave rectifier using CT(Center Tapped) transformer uses both halves of secondary AC. Diode D1 conducts during the first half cycle and Diode D2 conducts during the other half

cycle. The center tap provides the return path for current to flow. The load current I_L flows through the common point of the diodes through the resistor. Combining the output of two of these half-wave rectifiers, 1- ϕ full-wave rectification in load achieved. The full-wave diode rectifier using center-tapped transformer is showing Fig. 2.5.

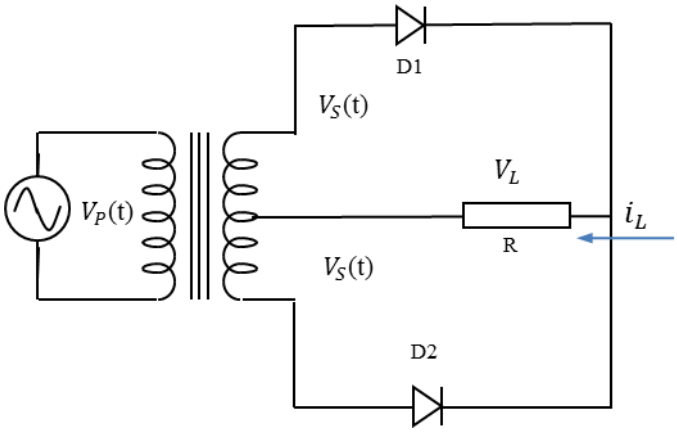

Fig. 2.5: 1 - ϕ Full-wave rectifier using CT transformer [8]

Using the equation 2-1,

$$V_{DC} = \frac{1}{T}\int_0^T V_L(t)dt$$

$$= \frac{2}{2\pi}\int_0^{\pi} V_s \sin(\omega t)dt = 2\frac{V_s}{\pi} \quad (2\text{-}20)$$

$$V_L = \sqrt{\frac{1}{T}\int_0^T {V_L}^2(t)dt}$$

$$= \sqrt{\frac{1}{\pi}\int_0^T {V_s}^2 \ sin^2(\omega t)\ dt} = \frac{V_s}{\sqrt{2}} \quad (2\text{-}21)$$

$$I_{DC} = \frac{V_{DC}}{R_L} = 2\frac{V_S}{\pi * R_L} \quad (2\text{-}22)$$

$$I_L = \frac{V_L}{R_L} = \frac{V_L}{\sqrt{2} * R_L} \quad (2\text{-}23)$$

$$FF = \frac{V_L}{V_{DC}} = \frac{\pi}{2\sqrt{2}} = 1.11 \quad (2\text{-}24)$$

$$RR = \left(\frac{1}{FF}\right)^2 = 0.81 \quad (2\text{-}25)$$

$$RF = \frac{V_{ac}}{V_{DC}} = \frac{\sqrt{V_L{}^2 - V_{DC}{}^2)}}{V_{DC}} = 0.483 \quad (2\text{-}26)$$

Although this rectifier performs better than the half-wave, there are some drawbacks. When D1 conducts, D2 see the inverse voltage of both the secondary in the blocking state. Fig. 2.6 shows the most commonly used bridge rectifier.

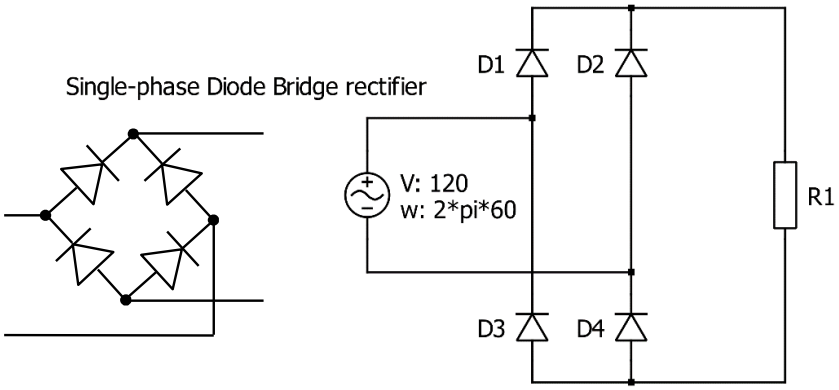

Fig. 2.6: 1 - ϕ full-wave diode-bridge and diode-bridge rectifier

The bridge rectifier has the similar waveform that of CT rectifier but the construction of this rectifier is simple. Output waveform shown in the Fig. 2.7 displays the voltage and current relationship of the 1- ϕ full-wave diode rectifier using center-tapped transformer and the diode bridge. During the positive half cycle, diodes D1 and D4 conduct, providing V_{out}. During the negative half cycle, diodes D2 and D3 conduct, providing V_{out}. In each cycle, all the diodes conduct for the same amount of time.

The following table adapted from [6] summarizes the rectifier parameters for single-phase rectifiers as discussed in the prior section.

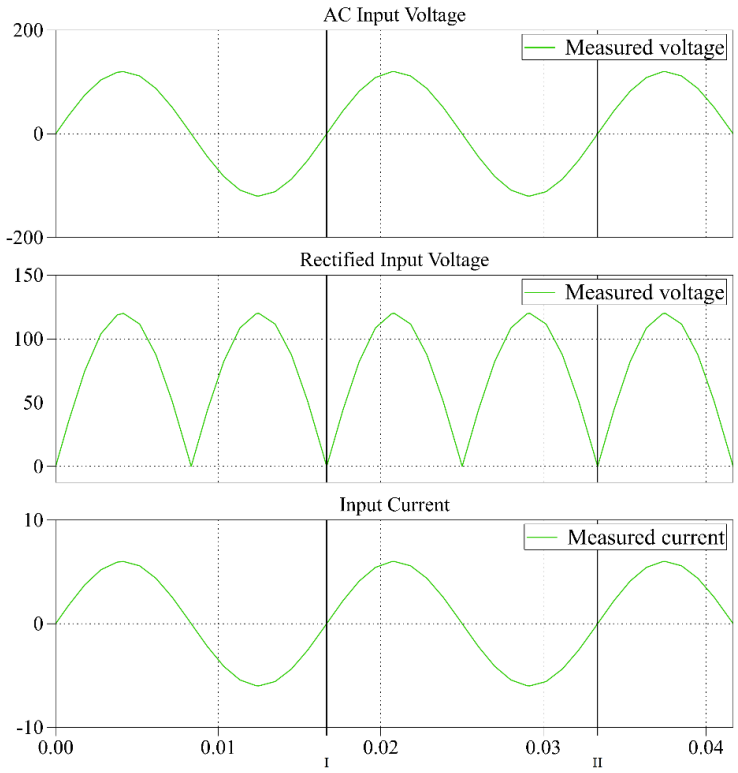

Fig. 2.7: Voltage and current waveform of 1 - ϕ full-wave rectifier

Table 2-1: Parameters for single-phase diode rectifiers

	Half-wave Rectifier	CT Rectifier	Diode Bridge
Form Factor	1.57	1.11	1.11
Rectification Ratio	0.405	0.81	0.81
Ripple Factor	1.21	0.482	0.482
Peak Repetitive reverse voltage (V_{RRM})	3.14 V_{DC}	3.14 V_{DC}	1.57 V_{DC}
rms Input voltage per transformer leg V_s	2.22 V_{DC}	1.11 V_{DC}	1.11 V_{DC}
Output ripple frequency f_r	6 f_i	12 f_i	12 f_i
Diode Average Current	1.00 I_{DC}	0.50 I_{DC}	0.50 I_{DC}
Transformer rating primary VA	2.69 P_{DC}	1.23 P_{DC}	1.23 P_{DC}
Transformer rating secondary VA	3.49 P_{DC}	1.75 P_{DC}	1.23 P_{DC}

The values in the table are in terms of V_{DC}.

2.2.1.3 Variations in single-phase rectifier circuitry:

Voltage multiplier:

Voltage multipliers are specified rectifier circuitry, which theoretically produces a voltage which is an integer multiple of the AC peak value. Voltage multipliers are usually employed when very high-voltage sources are required, the current demand is small and regulation is not important in the rectifier system [9]. The voltage doubler circuit converts the peak of AC input voltage V_m to direct voltage output $2 \cdot V_m$ by transferring charge from one capacitor to another during the positive half cycle and recharging the first capacitor without discharging the other capacitor in the negative half cycle [9].

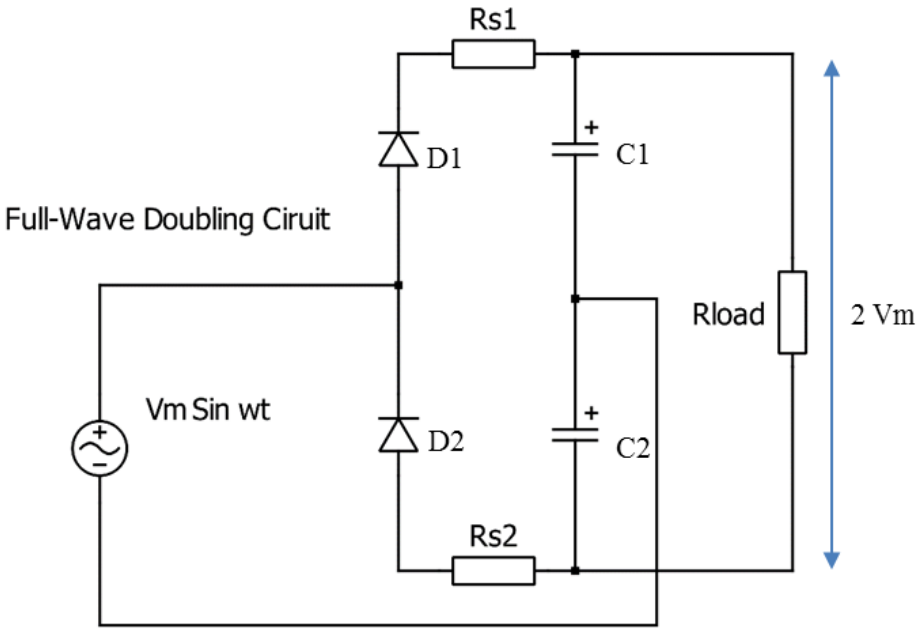

Fig. 2.8: 1 - ϕ Full-wave Doubling circuit

The operation of this circuit is as follows: Diode D1 operates in the positive half cycle and charges the capacitor C1, Diode D2 operates and charges C2 during the negative half cycle. Voltage Doubler circuit exhibits very high inrush currents with input capacitors. Resistors Rs1

and Rs2 restrict these inrush currents. Here, $C1 = C2$ and $R_{S1} = R_{S2}$.

2.2.1.4 Poly-phase rectifier systems:

In the single–way structures i.e. one diode per phase, each diode conducts while, the other diodes are in a blocking state. The operation of these structures becomes more suitable as the number of phases increases. Fig. 2.9 shows the representation of a single-way rectifier with m phases. Each phase has same voltage amplitude and same frequency.

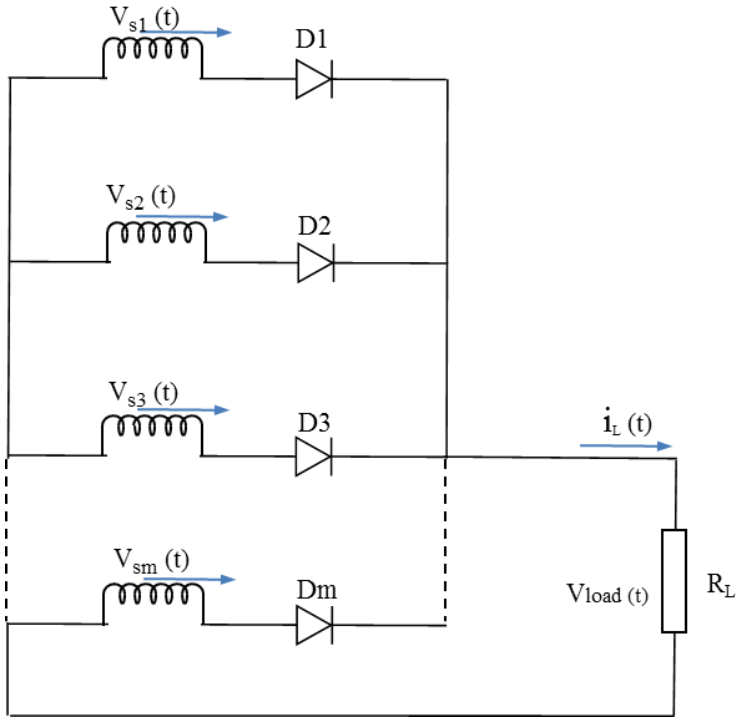

Fig. 2.9: m-phase single way rectifier

Fig. 2.10 shows the waveform of the voltages (here m = 3) and of the current in the load. There is a phase shift of 2π/m rad between the voltages. Each diode conducts for 2π/m rad. It can be seen that in one period there are a specific number of peaks (pulses), depending upon the number of phases and rectifier structure. In single-way structures, the number of pules (p) equals to number of phases (m), i.e. m = p.

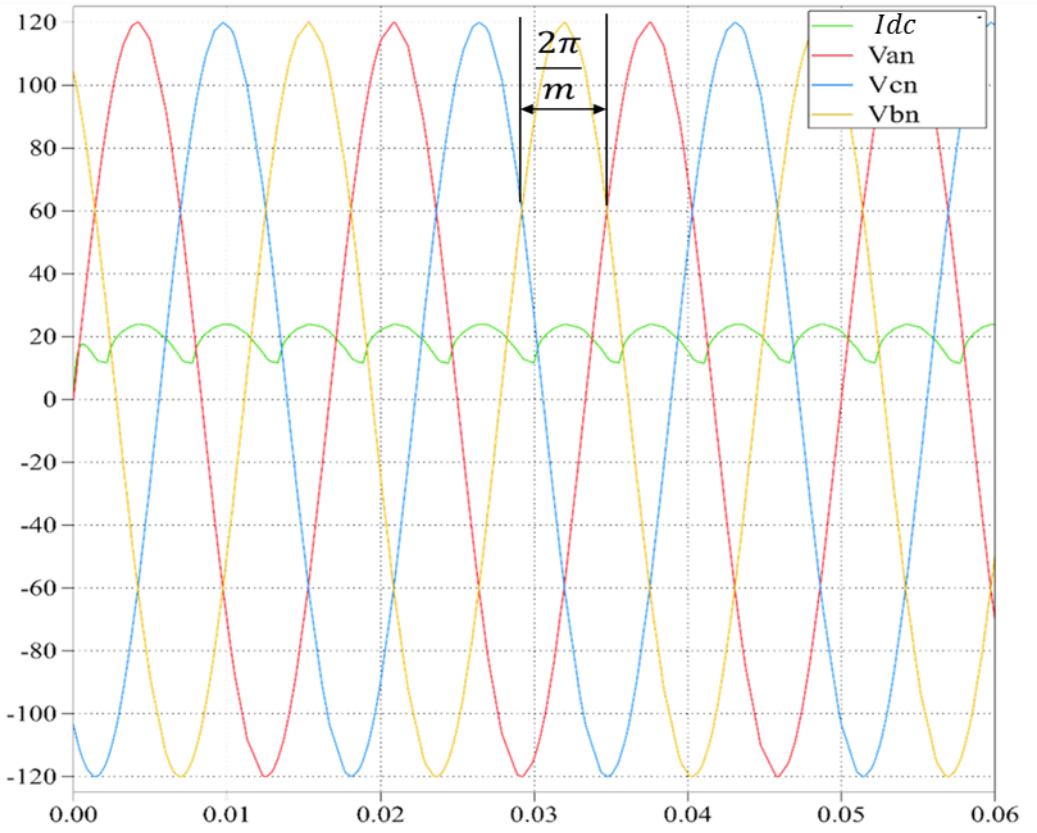

Fig. 2.10: single way rectifier waveform (m = 3)

The rectified voltage V_{DC} can be written by,

$$V_{DC} = \frac{V_S}{2\pi/\mathrm{m}} \int_{-\frac{\pi}{m}}^{\frac{\pi}{m}} cos(\omega t)dt$$

$$= V_S \cdot [\frac{sin(\frac{\pi}{m})}{\frac{\pi}{m}}] \quad (2\text{-}27)[13]$$

$$V_L = \sqrt{\frac{{V_S}^2}{2\pi/m} \int_{-\frac{\pi}{m}}^{\frac{\pi}{m}} cos^2(\omega t)dt}$$

$$= V_S \cdot \sqrt{\frac{1}{2}[1 + \frac{sin(\frac{2\pi}{m})}{\frac{2\pi}{m}}]} \quad (2\text{-}28)$$

From the definition of Form Factor (FF),

$$FF = \frac{V_L}{V_{DC}} = \frac{\sqrt{\frac{1}{2}[1+\frac{\sin(\frac{2\pi}{m})}{\frac{2\pi}{m}}]}}{[\frac{\sin(\frac{\pi}{m})}{\frac{\pi}{m}}]} \quad (2\text{-}29)$$

It is seen from eq. 2-29 that $m \rightarrow \infty \Rightarrow FF = \frac{V_L}{V_{DC}} \rightarrow 1 \Rightarrow RF \rightarrow 0$ (2-30)

It means that by increasing the number of phases in a poly-phase single-way rectifier structures, the rectification can be improved i.e. smoother output voltage. It is possible to increase the number of pulses using a higher number of secondary coils in the secondary transformers.

There is a significant amount of details and variations of these transformers and their interconnections found in the literature. (For more examples, see [[6] [13]) Few basic topologies shown below and are from [6].

A basic 3-ϕ star-rectifier circuit is shown in Fig. 2.11. It is three single-phase half-wave rectifiers combined. The diode in each phase conducts during the period when the voltage on that phase is higher than that of the other two phases.

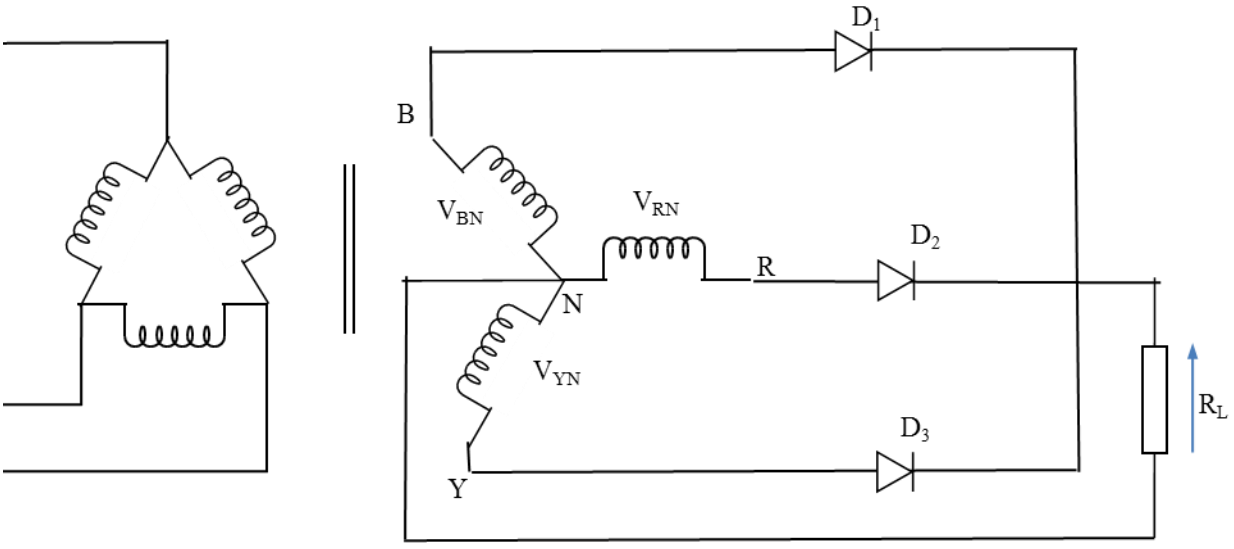

Fig. 2.11: Three-phase star rectifier

The single-phase half-wave rectifier and the three-phase star rectifier shown in Fig. 2.11 have direct currents in the secondary windings which cause transformer core saturation issues [6]. This core saturation can be avoided by having the zig-zag arrangement in secondary windings. The modified circuit is shown in Fig. 2.12. In a three-phase inter-star rectifier each secondary phase voltage is obtained from two equal-voltage secondary windings connected in series. The currents in the primary of the transformer do not sum to zero so it's not preferable to have star-connected primary windings [6].

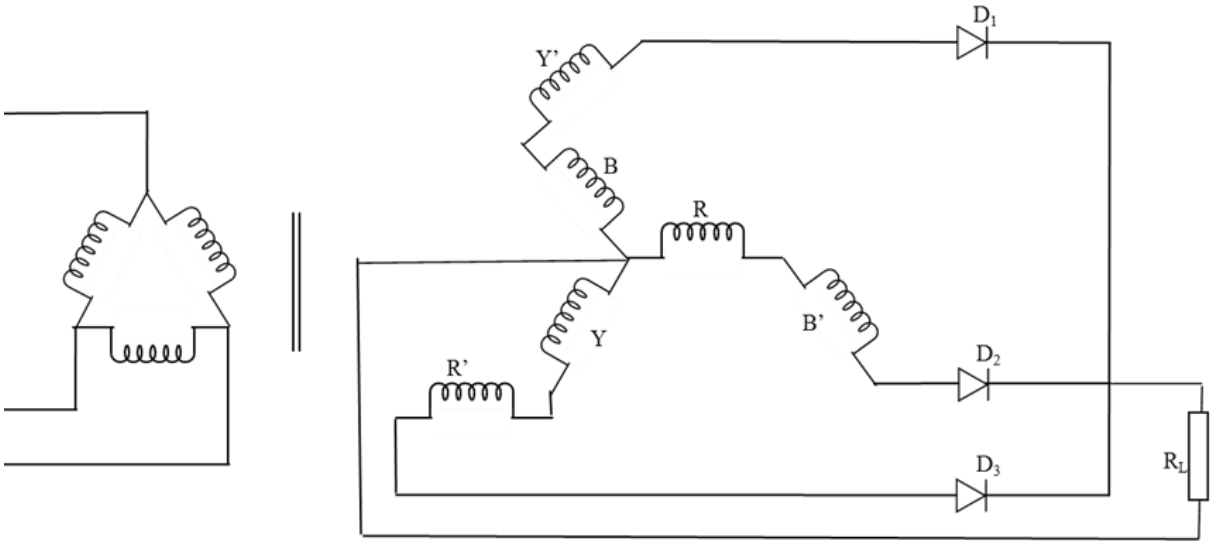

Fig. 2.12 : Three-phase inter-star or zig - zag rectifier

Connection with conventional three-phase mains and using m = 6 six-phase star rectifier can be represented as shown in Fig. 2.14. The diode in each phase conducts when the voltage in that phase is higher than other phases. The diode conducts for $\pi/3$ conduction angle. The disadvantage of this rectifier is that only one rectifying element conducts at a time poorly utilizing secondary of the transformer.

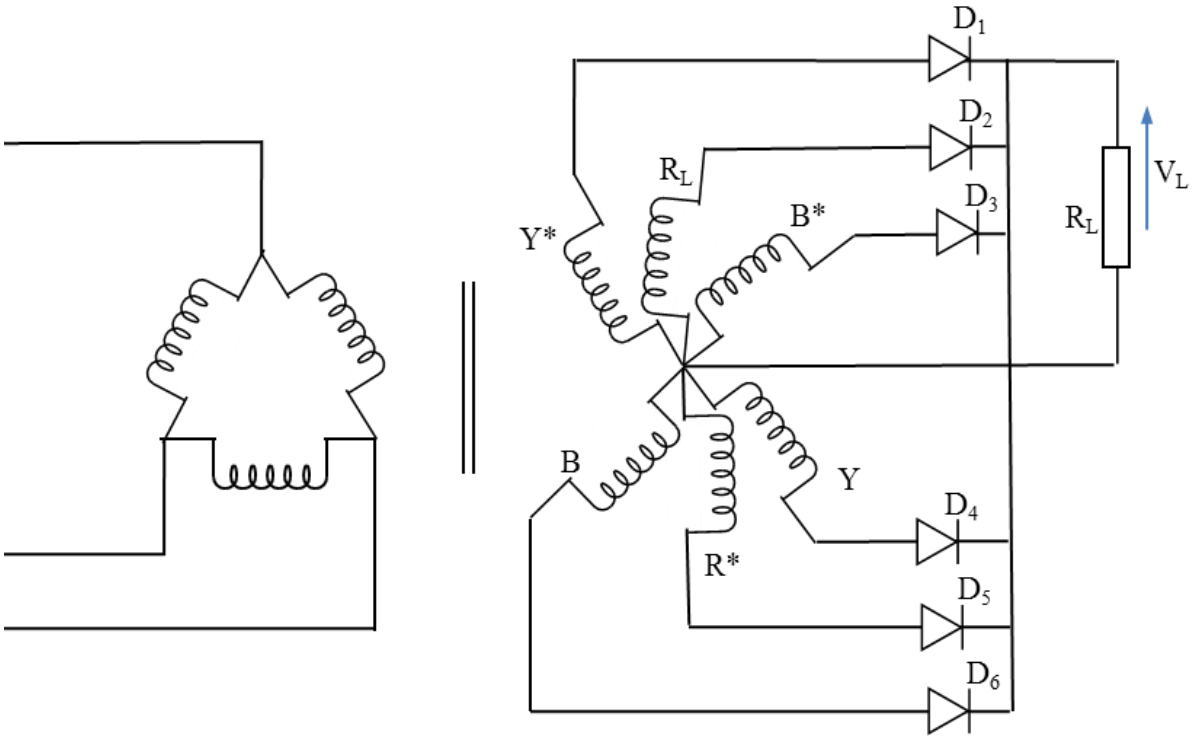

Fig. 2.13 : Six-phase star-connected rectifier recreated from [6]

2.2.1.5 Three - phase diode bridge rectifier

Instead of having a separate winding for a single pulse for each phase, it is possible to reduce the number of windings by having twice number of pulses than phases, i.e. $p = 2m$. Three-phase diode bridge rectifier shown in Fig. 2.15 is most commonly used three-phase diode rectifier circuit for low power applications. The conduction angle of each diode is $2\pi/3$. Each diode conducts in a sequence. The conduction sequence for diodes is 12, 23, 34, 45, 56 and 61. The voltage and current waveforms of the three-phase diode bridge rectifier are shown in Fig. 2.16.

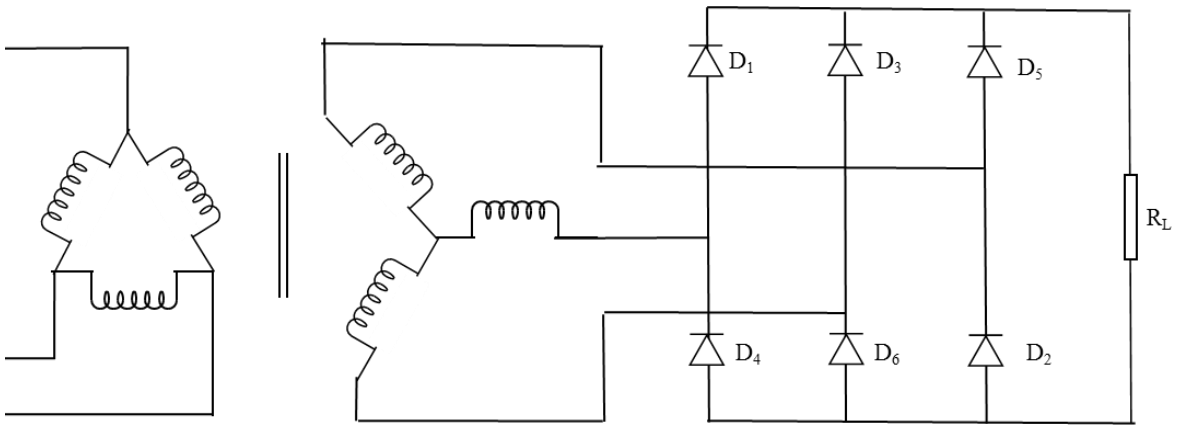

Fig. 2.14: Three-phase diode Bridge rectifier

Using the equation 2-1,

$$V_{dc} = \frac{1}{T}\int_0^T V_L(t)dt = \frac{6}{2\pi}\int_{\frac{\pi}{3}}^{2\frac{\pi}{3}} \sqrt{3}V_m \sin(\omega t)dt$$

$$= \frac{3\sqrt{3}V_m}{\pi} = 1.654 \cdot V_m \quad (2\text{-}27)$$

$$V_L = \sqrt{\frac{1}{T}\int_0^T {V_L}^2(t)dt}$$

$$= \sqrt{\frac{9}{\pi}\int_{\frac{\pi}{3}}^{2\frac{\pi}{3}} {V_m}^2 \sin^2(\omega t)\, dt} = 1.655 \cdot V_S \quad (2\text{-}28)$$

The rms current from each winding can be given by,

$$I_{dc} = \frac{\sqrt{3}\, v_s}{R_L}\sqrt{\frac{2}{\pi}\left(\frac{\pi}{6} + \frac{\sqrt{3}}{4}\right)} \quad (2\text{-}29)$$

$$I_s = \frac{\sqrt{3}\, v_s}{R_L}\sqrt{\frac{1}{\pi}\left(\frac{\pi}{6} + \frac{\sqrt{3}}{4}\right)} \quad (2\text{-}30)$$

$$FF = \frac{V_L}{V_{DC}} = 1.009 \quad (2\text{-}31)$$

$$RF = \frac{V_{ac}}{V_{DC}} = \frac{\sqrt{{V_L}^2 - {V_{DC}}^2)}}{V_{DC}} = 0.042 \quad (2\text{-}32)$$

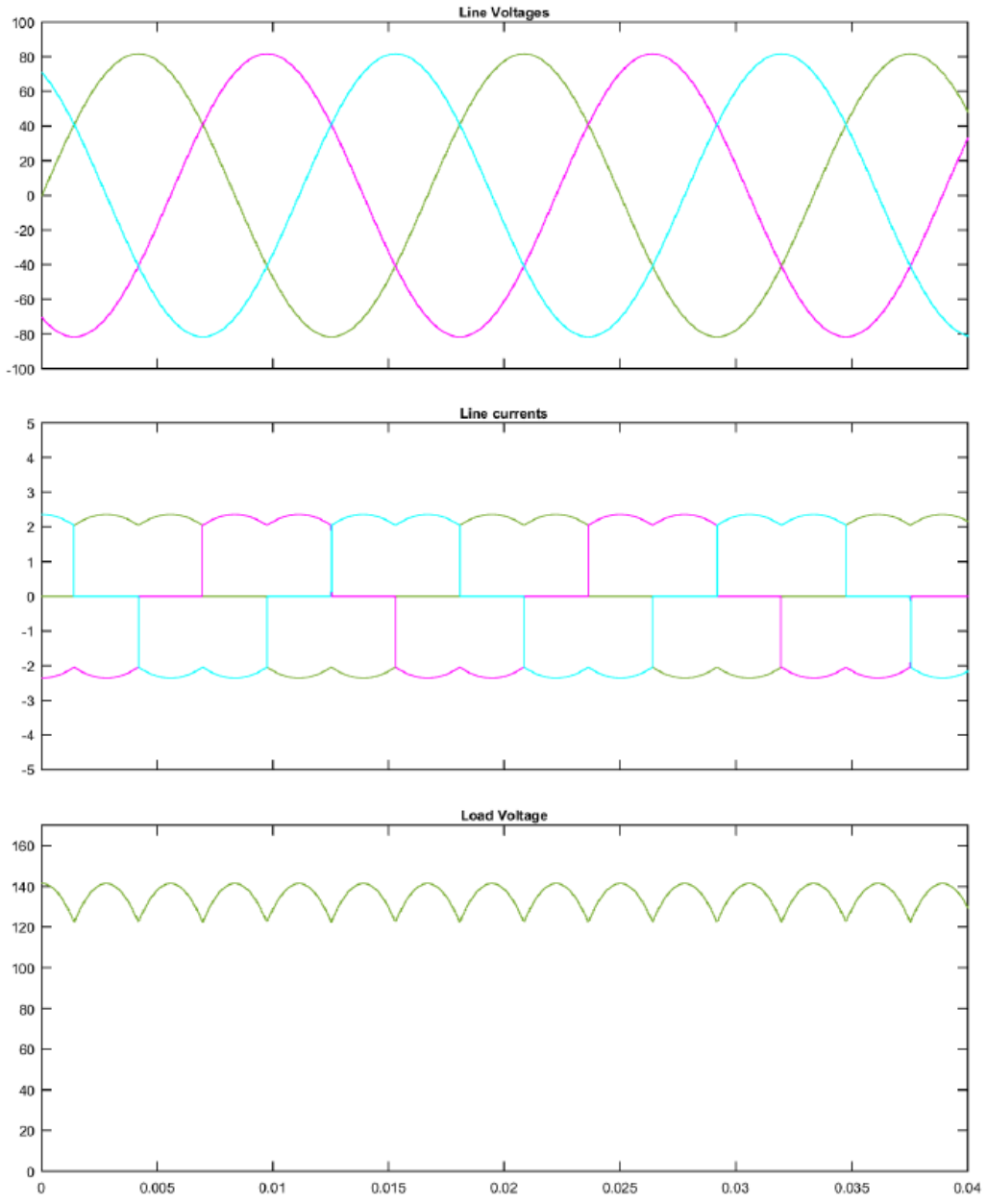

Fig. 2.15: Voltage and current waveform of the three-phase bridge rectifier

In Fig. 2.15, the secondary of the transformer is in Y configuration. It is possible to increase the number of pulses of a diode rectifier without having one phase per conducting element or even in the case of bridge connection. From the three-phase mains distribution, four combinations for the connections at primary and secondary are possible for a distribution transformer: $delta -$

$delta, delta - Y$, $Y - delta$ and $Y - Y$ as shown in Fig. 2.17. Star and delta connected secondary have natural phase shift of $\pi/6$ in output voltage. By connecting star connected and delta connected bridge rectifier together, it is possible to achieve rectification as if it is 12-pulse rectifier.

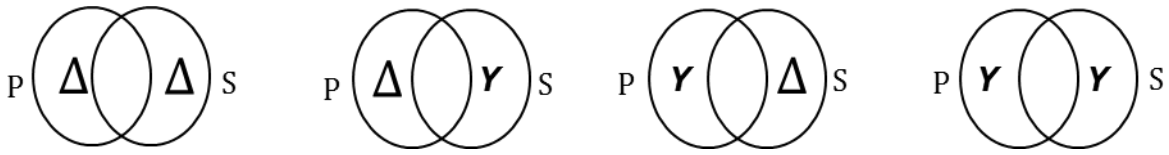

Fig. 2.16: Three-phase transformer connections

A delta primary has three main lines without neutral and avoids excitation unbalance. Each winding is tied to two lines. The delta primary avoids excitation unbalance as the non-sinusoidal exciting currents taken from the supply creates complete ampere-turn balance. As compared to delta secondary with the same turn ratio between primary and secondary, Y secondary has some advantages. Mainly the rectified voltage is $\sqrt{3}$ times higher; the current in the windings is same as in the load and it has an easily accessible common zero-point [13]. In the case of three-phase diode bridge rectifier, any combination of star or delta connected primary and secondary are feasible as the currents in the secondary are symmetrical [6].

2.2.1.6 Six - phase diode series bridge rectifier

Three-phase star connected and delta-connected rectifiers connected in series make the series bridge connection of these multi-pulse rectifiers. The combined output will have double ripple frequency on dc (in this case 12 times the input frequency). Fig. 2.17 shows six-phase series bridge rectifier. Other parameters of this series bridge rectifier are described in Table 2.2[6].

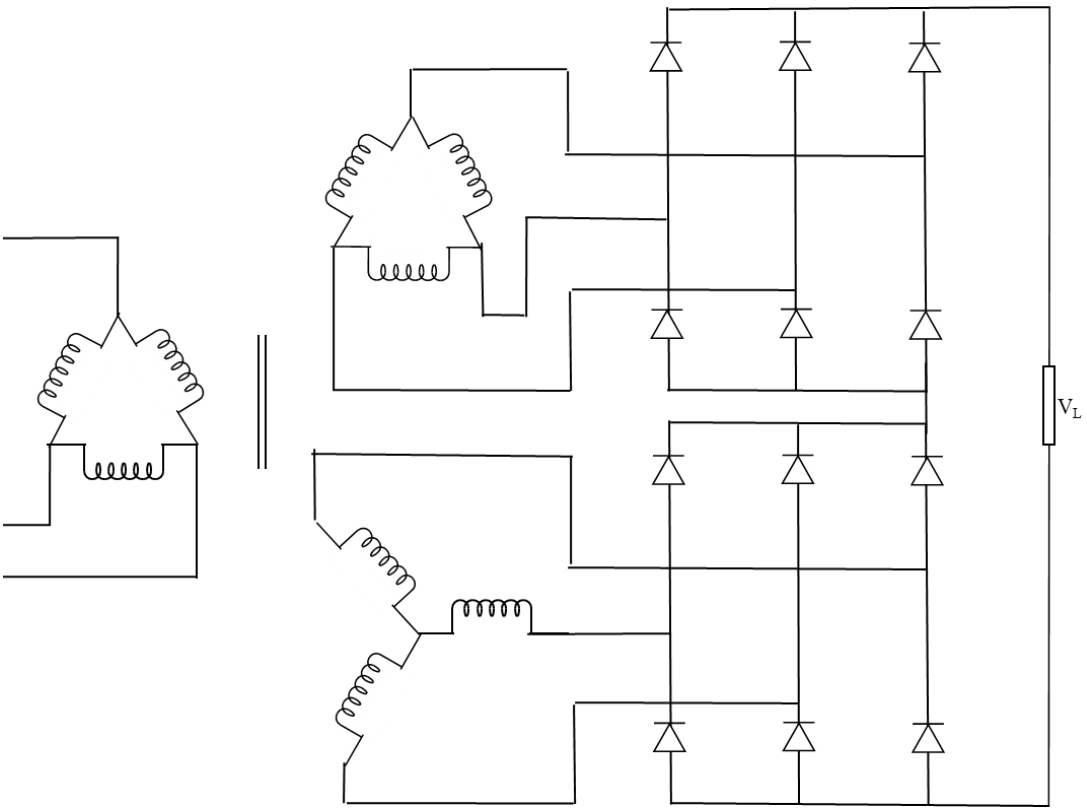

Fig. 2.17: Six-phase series bridge connection [6]

2.2.1.7 Six - phase diode parallel bridge rectifier

Another application by connecting these star and delta connected bridge rectifier is six phase parallel bridge. Fig. 2.18 shows a six-phase parallel bridge rectifier. Six-phase Series Bridge provides a higher voltage at the output; however, to have higher current output, the parallel bridge can be used. Similar to the six-phase series bridge, six-phase parallel bridge has higher ripple frequency (12 times the input frequency)

The table 2.2 from [6] summarizes some important rectifier performance parameters for six-phase rectifiers.

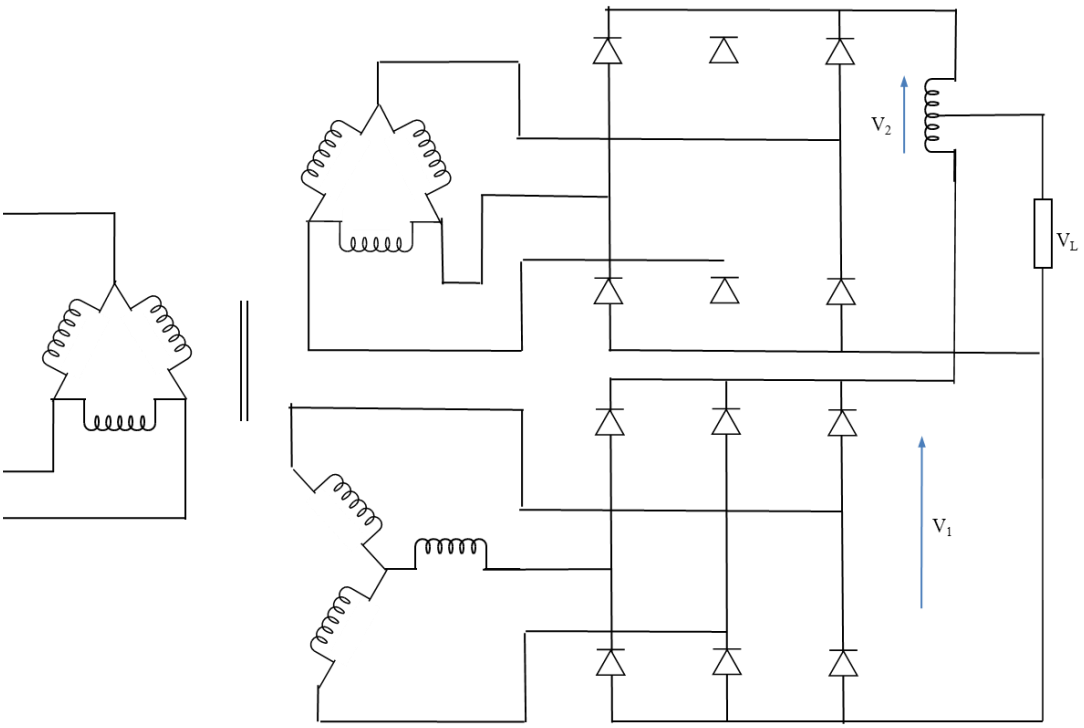

Fig. 2.18: Six-phase parallel bridge connection [6]

Table 2-2: Parameters for six-phase diode rectifiers

Parameter	Six-phase star rectifier	Six-phase series bridge rectifier	Six-phase parallel controlled bridge rectifier (inter-phase transformer)
Form Factor	1.0009	1.00005	1.00005
Rectification Ratio	0.998	1	1
Ripple Factor	0.042	0.01	0.01
Peak Repetitive reverse voltage (V_{RRM})	2.09 V_{dc}	0.524 V_{dc}	1.05 V_{dc}
rms Input voltage per transformer leg V_S	0.74 V_{dc}	0.37 V_{dc}	0.715 V_{dc}
Diode Average Current	0.167 I_{dc}	0.333 I_{dc}	0.167 I_{dc}
Output ripple frequency f_r	6 f_i	12 f_i	12 f_i
Transformer rating primary VA	1.28 P_{dc}	1.01 P_{dc}	1.01 P_{dc}
Transformer rating secondary VA	1.81 P_{dc}	1.05 P_{dc}	1.05 P_{dc}

With more pulses, rectifiers will have better utilization, less ripple, and higher ripple frequency. These high ripple frequency ripples are relatively easier to filter. The advantages of systems with the number of pulses higher than 12 has limitation of increased complexity of the rectifier system [11].

It is important to vary the output of the rectifier to fit the demands. Diode rectifiers provide the output voltage with fixed ratio of input AC voltages. To match the demands, the diodes in the diode rectifiers are substituted with all or some thyristors. The following sections will provide more information on such topologies.

2.2.2 Fully Controlled Rectifiers

Uncontrolled rectifiers do not have control on the voltage converted from AC to DC. This control on converted power is achieved with the use of devices like thyristors, transistors etc. Fully controlled rectifiers can be classified broadly, in terms of their control, as line commutated (thyristor rectifiers) and force commutated rectifiers (PWM rectifiers). This section will provide information on the common commutated rectifier.

2.2.2.1 Single-phase Half-wave Rectifier:

Single-phase half-wave thyristor rectifiers can be constructed as shown in Fig. 2.19. A single thyristor controls the load voltage. The only thyristor in the circuit conducts, when the voltage across thyristor V_T is $+ve$ and a trigger pulse or gate pulse i_G is applied to the gate terminal.

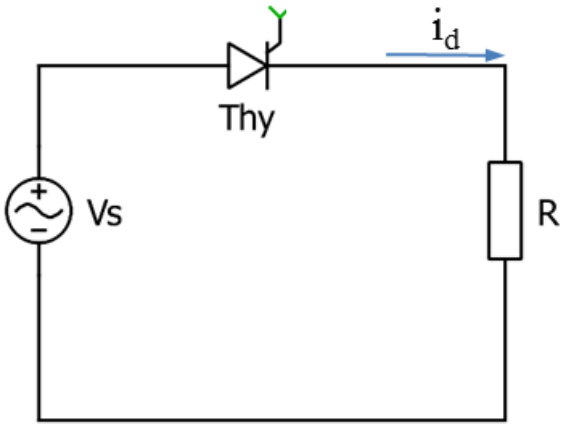

Fig. 2.19: Single-phase thyristor rectifier with resistive load

The control of the load voltage is done by delaying the firing angle α. The *Firing angle* α is measured from the position when a diode naturally conducts. More information on firing angle or delay is in later sections. For the rectifier shown in Fig. 2.19, α is measured from a zero crossing of the supply voltage V_S. For a purely resistive load, Fig. 2.20 shows the voltage and current relationship.

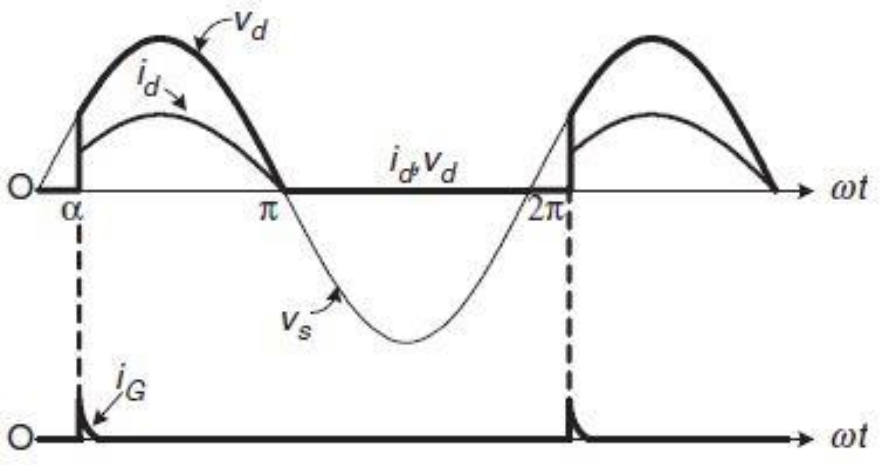

Fig. 2.20: Single-phase thyristor rectifier with resistive load [6]

The thyristor is in non-conducting condition when the voltage across load reaches negative value. Fig. 2.20 shows that the amount of power transferred depends on firing angle α. The average load voltage is given by,

$$V_{dc}(\alpha) = \frac{1}{2\pi}\int_{\alpha}^{\pi} V_{max}\ sin(\omega t)\, d(\omega t)$$

$$= \frac{Vmax}{2\pi}\,(1 + cos\ \alpha) \qquad (2\text{-}33)\ [6]$$

Where V_{max} is peak supply voltage, α is firing angle or delay angle.

2.2.2.2 Single-phase Thyristor Bridge Rectifier:

A single-phase thyristor bridge rectifier with restive load using four thyristors to control load voltage is in Fig. 2.21. Thyristors T1 & T2 receive gate pulses simultaneously making the load voltage during the positive half cycle of source voltage. Thyristors T3 & T4 receive gate pulses simultaneously making load voltage during negative half cycle. Single-phase thyristor bridge rectifiers are line commutated as two gate pulses are applied simultaneously keeping the other two thyristors in OFF state.

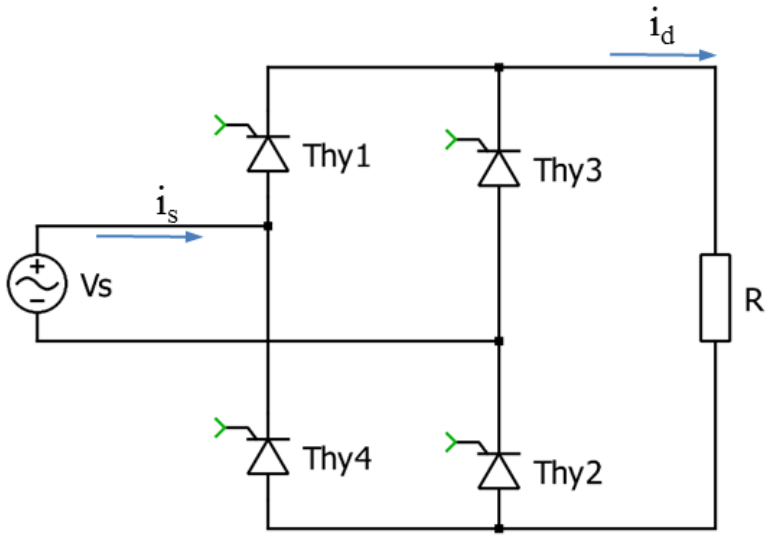

Fig. 2.21: single-phase thyristor bridge with resistive load

The mean value of load voltage with resistive load is determined by,

$$V_{dc}\,(\alpha) = \frac{1}{\pi}\int_{\alpha}^{\pi} V_{max}\ sin(\omega t)\, d(\omega t)$$

$$= \frac{Vmax}{\pi}\,(1 + cos\,\alpha) \qquad (2\text{-}34)$$

Fig. 2.22 shows voltage and current relationship for single-phase thyristor bridge. The currents i_{g1} , i_{g2} , i_{g3} and i_{g4} are gate pulse currents.

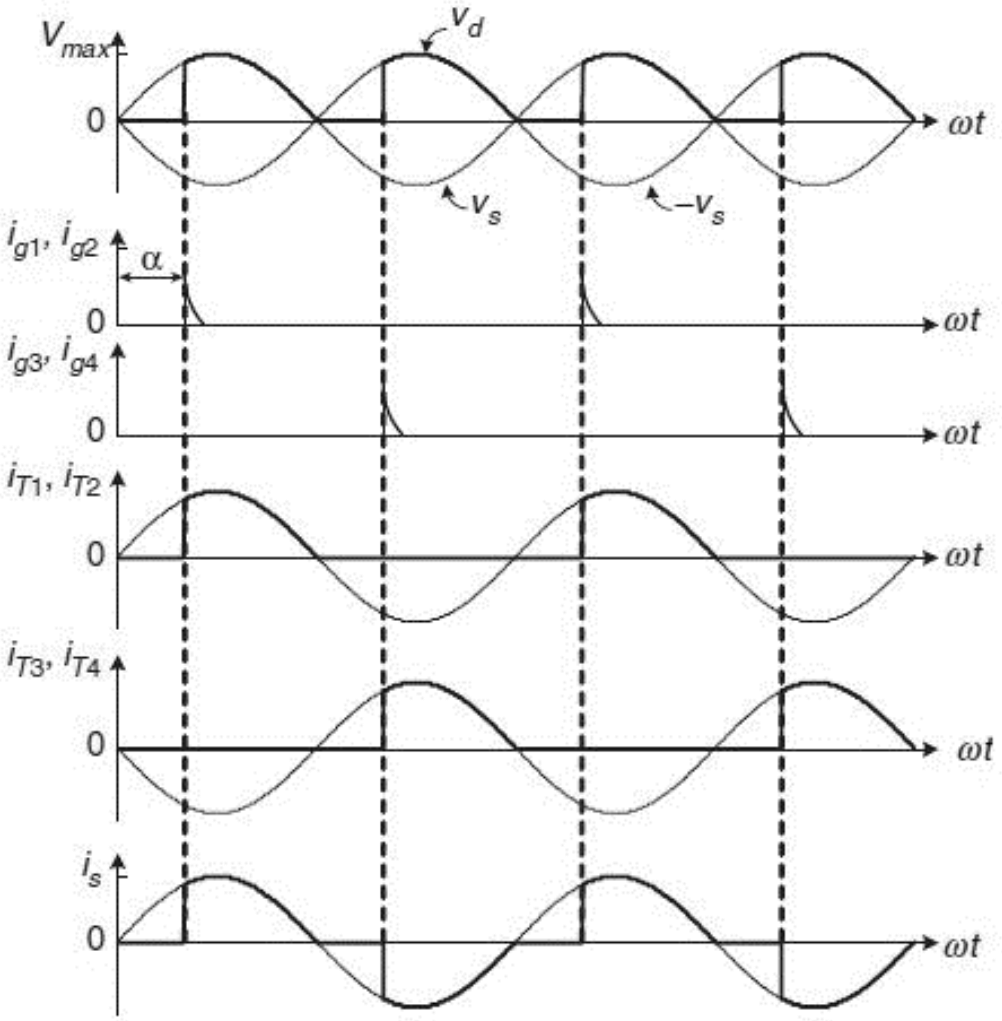

Fig. 2.22: Waveform of single-phase thyristor bridge with resistive load [6]

2.2.2.3 Three-phase controlled rectifier:

Three-phase controlled rectifiers can be half-wave or full-wave (bridge or six pulse) rectifiers. The construction of these rectifiers is similar to that of diode rectifiers discussed in previous chapters. This section will provide information on three-phase fully controlled rectifiers. A fully controlled thyristor rectifier, replacing diodes with thyristors, is in Fig. 2.24.

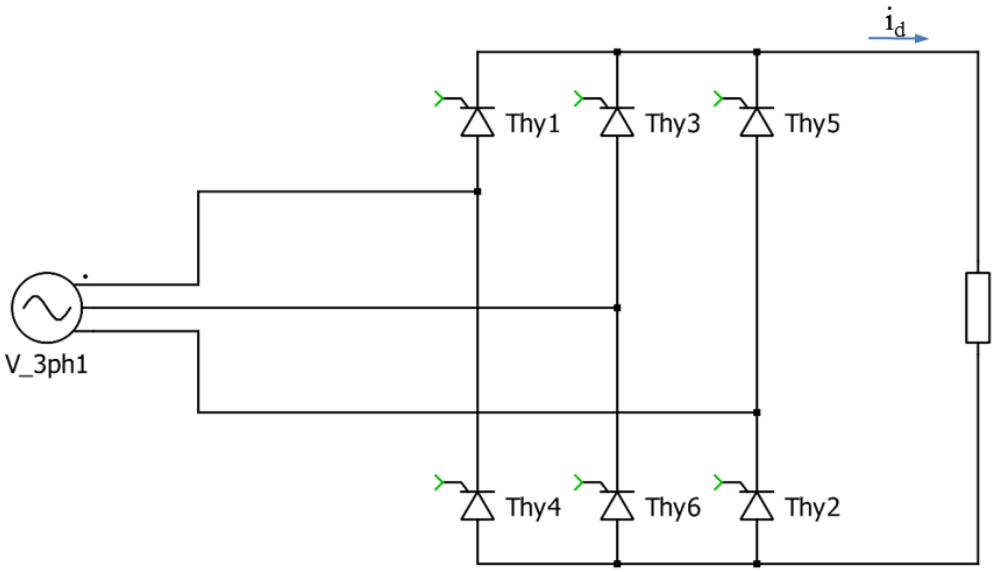

Fig. 2.23: Three-phase thyristor rectifier with resistive load

Like the single-phase full-wave thyristor rectifiers, two sets of thyristors receive gate pulses at the same time making a path for current to flow through load and go back to source. It is important to provide gate pulses with appropriate delay. This delay is essentially the firing angle in degrees or radians. The *firing angle* α as shown in the waveform of the three-phase controlled rectifier Fig. 2.25, is comprised between the time instant when the thyristor will naturally conduct as of diode and the time instant when the gate pulse is applied. Load voltage is represented as function of the firing angle by,

$$V_{dc}\,(\alpha) = \frac{6}{2\pi}\int_{\alpha}^{\frac{\pi}{3}+\alpha} \sqrt{3}Vs\ sin\left(\omega t + \frac{\pi}{3}\right) d(\omega t)$$

For $0 \leq \alpha \leq \frac{\pi}{3}$ (2-35)

$$V_{dc}(\alpha) = \frac{3}{\pi}\sqrt{3}Vs\ cos(\alpha)$$

$$= 1.65\, V_s\, cos(\alpha) \quad 2\text{-}36)$$

$$V_{dc}(\alpha) = \frac{6}{2\pi}\int_{\alpha}^{\frac{2\pi}{3}} \sqrt{3}Vs\ sin\left(\omega t + \frac{\pi}{3}\right) d(\omega t)$$

For $\frac{\pi}{3} \leq \alpha \leq \frac{2\pi}{3}$ (2-37)

$$V_{dc}(\alpha) = \frac{3}{\pi}\sqrt{3}Vs\,[1 + cos\left(\alpha + \frac{\pi}{3}\right)] \quad (2\text{-}38)$$

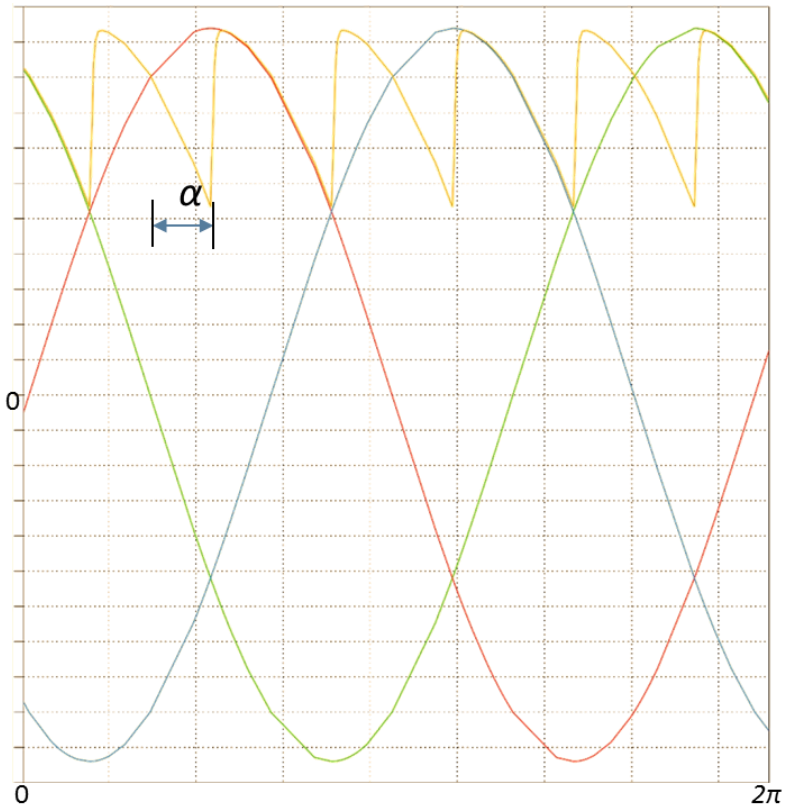

Fig. 2.24: Waveform for *3-ϕ* thyristor rectifier resistive load (simulated at $\alpha = 60°$)

More results of the different simulated waveforms with different firing angles are in Fig. 2.26. Equations of V_{dc} are valid only when the thyristors are operating in continuous condition mode. A *continuous conduction mode* of thyristor rectifier is the duration when DC voltage at the

load is always positive. This is correct in case of the resistive loads. However, in practical situations, the load is not always purely resistive. A dis*continuous conduction mode* of thyristor rectifier is the duration of time when the DC voltage attains negative value due to the inductive load. Mathematical analysis of both the operations is in Appendix A.

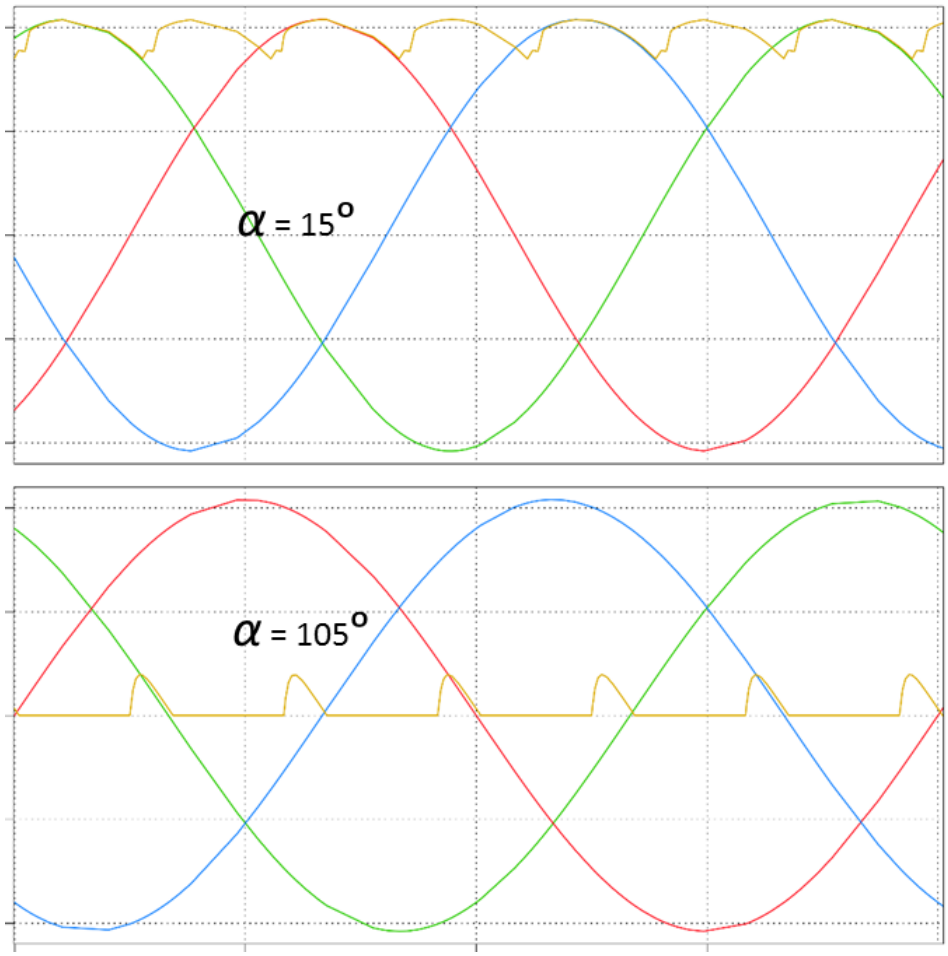

Fig. 2.25: Waveform for three-phase thyristor rectifier for different firing angles

Until now, the assumption is that the commutation of these thyristors in the circuit is instant. However, the thyristors are not ideal in practical applications. More information on the commutation is presented in later parts of this chapter.

2.2.3 Half- Controlled Rectifiers

Half-controlled or semi-controlled rectifier topologies, as the name suggests have limited control on the output voltage. All or only some diodes are replaced with thyristors depending upon applications.

2.2.2.1 Single-phase half-controlled rectifier systems

A semi-controlled full-wave bridge rectifier can be configured in multiple ways as shown in Fig. 2.27 to Fig. 2.30. Operation of these topologies are simple. During positive half cycle, i.e. positive V_s , Thyristor 1 receives trigger pulse and the current flows through load and returns via diode D3. During negative half cycle, $Thy\ 2$ receives trigger-pulse and the current flows through load and returns via diode D4. Thyristor $Thy\ 1$ and D3 conducts during $\alpha < \omega t < \pi$. Thyristor $Thy\ 2$ and D4 conducts during $\pi < \omega t < 2\pi$.

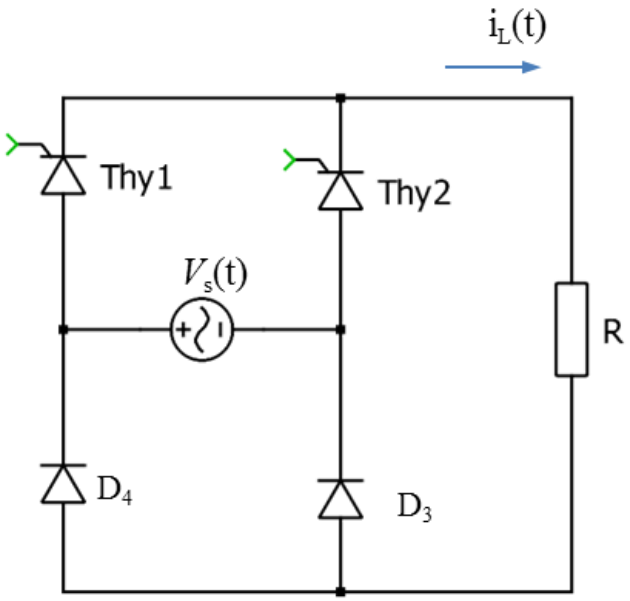

Fig. 2.26: Single-phase half-controlled rectifier Configuration 1

Operation of other configurations shown in Fig. 2.28 is like the one in shown Fig. 2.27.

The average voltage can be given by,

$$Vdc\ (\alpha)\ = \frac{1}{\pi}\int_{\alpha}^{\pi+\alpha} V_{max}\ sin(\omega t\ )\, d(\omega t)$$

$$= \frac{2\,V_{max}}{\pi}\cos\alpha \qquad (2\text{-}39)$$

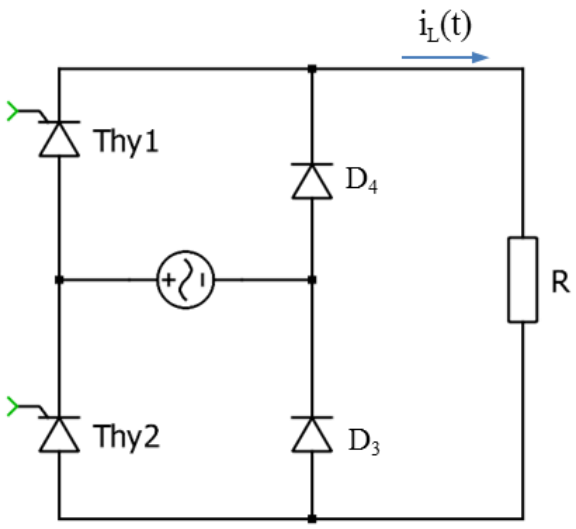

Fig. 2.27: Single-phase half-controlled rectifier Configuration 2

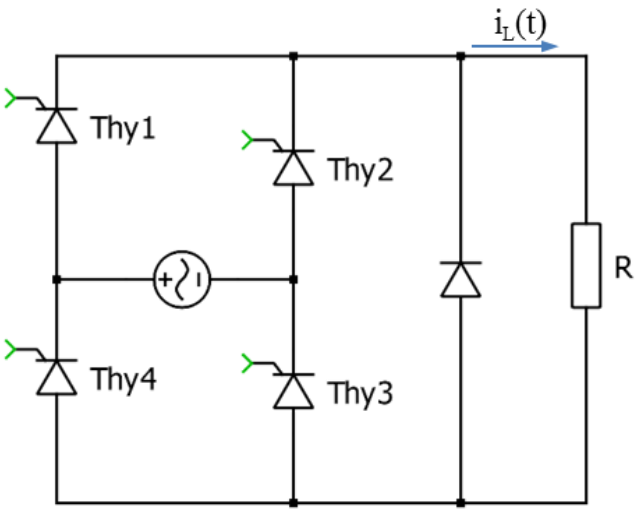

Fig. 2.28: Single-phase half-controlled rectifier

In configuration 3, thyristors Thy1 and Thy3 receive gate pulses when $\alpha < \omega t < \pi$. During $\alpha < \omega t < (\pi + \alpha)$, the diode conducts and output of the bridge circuit is clamped to zero. During $(\pi + \alpha) < \omega t < 2\,\pi$, Thy2 and Thy4 conducts.

2.2.2.2 Three-phase half-controlled rectifier systems

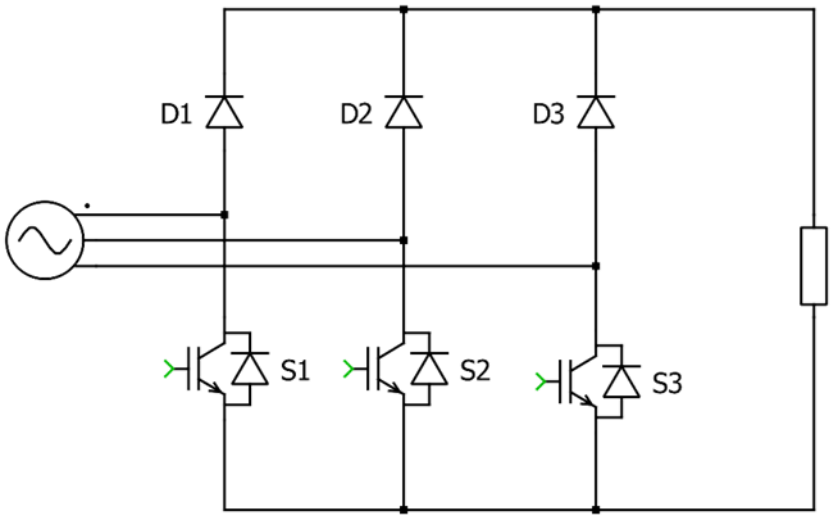

Fig. 2.29: Three-phase half-controlled rectifier

The three-phase half-controlled rectifier is combination of diode-bridge and three-phase thyristor bridge. Three-phase fully controlled converter can work as both rectifier and inverter depending upon the firing angle α. When $\alpha < 90°$ the operation is considered as rectifying and when $\alpha > 90°$ the operation is inverting or the inverter mode operation. If the application is just for rectifying operation than upper or lower switches can be replaced with the diode.

Replacing the switches with diode make the rectifier to operate only in continuous conduction mode i.e. voltage will be positive at all the times. The advantage of half-controlled rectifier is that diode are used instead of all thyristors making the cost lower as in general switching devices are more expensive than the diodes.

The average dc voltage can be given as,

$$V_{dc}(\alpha) = \frac{3\sqrt{2}\,V_{max}}{2\,\pi}(1 + \cos\alpha) \qquad \text{(2-40) [6]}$$

This half-controlled bridge is mostly used to make rectified dc to feed another VSI in series. One such application of this circuit is shown in Fig. 2.30.

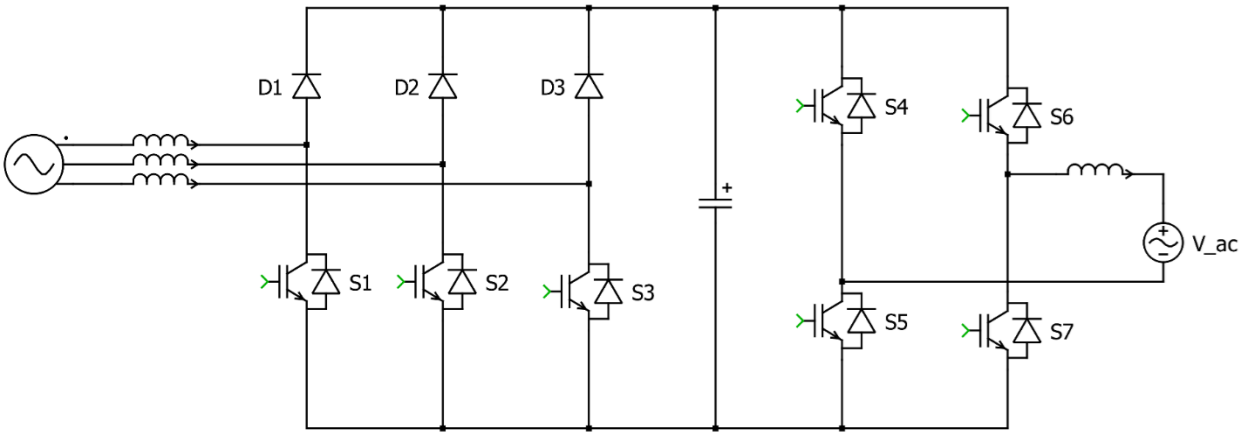

Fig. 2.30: *3-ϕ* half-controlled rectifier for wind turbine system recreated from [12]

2.2.4 Popular rectifier topologies for PFC: Vienna Rectifier

Thyristor rectifiers are line commutated as previously stated, other transistor devices such as IGBTs, MOSFETs and GTOs are commonly used with power factor corrector rectifiers. This section will provide some information on one popular rectifier topology of Power Factor Correctors (PFC) rectifiers: The Vienna rectifier.

As shown in Fig. 2.31 a Vienna rectifier uses unidirectional switches, which consist of multiple diodes surrounding the switch. A six-switch active PWM rectifier and Vienna rectifier have similar advantages in power factor correction. Both have sinusoidal input currents and controlled dc voltage. However, the AC-DC controlled rectifiers shown in the previous section are two level and six switches whereas the Vienna rectifier is a three level and three switch. The disadvantages of Vienna type rectifiers are that they are unidirectional due to inherent nature of the circuit; it takes four diodes to realize a bi-directional switch for each leg.

This rectifier is one type of three-switch boost converter making it vulnerable to inrush currents. Input stage creates a DC voltage across two switches connected to voltage source responsible for load voltage. Four diodes around the switches allow bidirectional current flow so

the rectifier can be operated in similar fashion to the three-phase bridge but with the single switch in each leg. Construction of this type of rectifier is complex and requires specific type of current control techniques. The advantage of Vienna rectifier is that it is made using only three power switches making it less expensive compared to conventional controlled rectifiers.

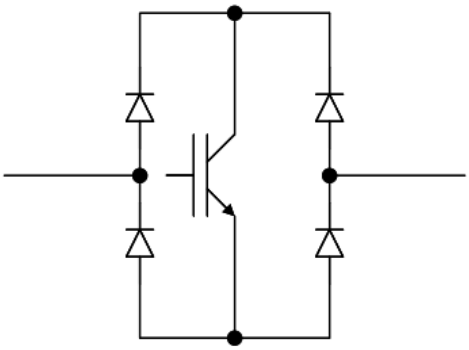

Fig. 2.31: Unidirectional switch representation

As shown in Fig. 2.32, Vienna rectifier features a split DC-rail. As previously mentioned, these are three switch rectifiers and the control is only required for three switches. This rectifier essentially works as a two-switch boost rectifier with one of the switches switched at the line frequency and the other two switches switched at very high frequency [16].

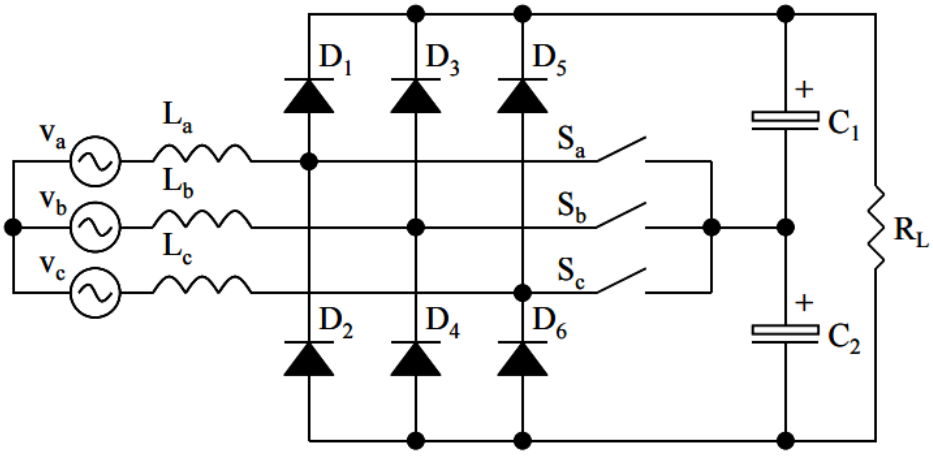

Fig. 2.32: Three-phase three level Vienna Rectifier [16]

Having one switch always at input frequency, the Vienna rectifier is seen as two separate boost rectifiers each for boosting C1 and C2 respectively. This makes another disadvantage of this type of rectifier, as they require higher output voltage for higher boost ratio. Fig. 2.33 shows simulated Vienna rectifier circuit and Fig. 2.34 shows the output waveform from the simulated circuit.

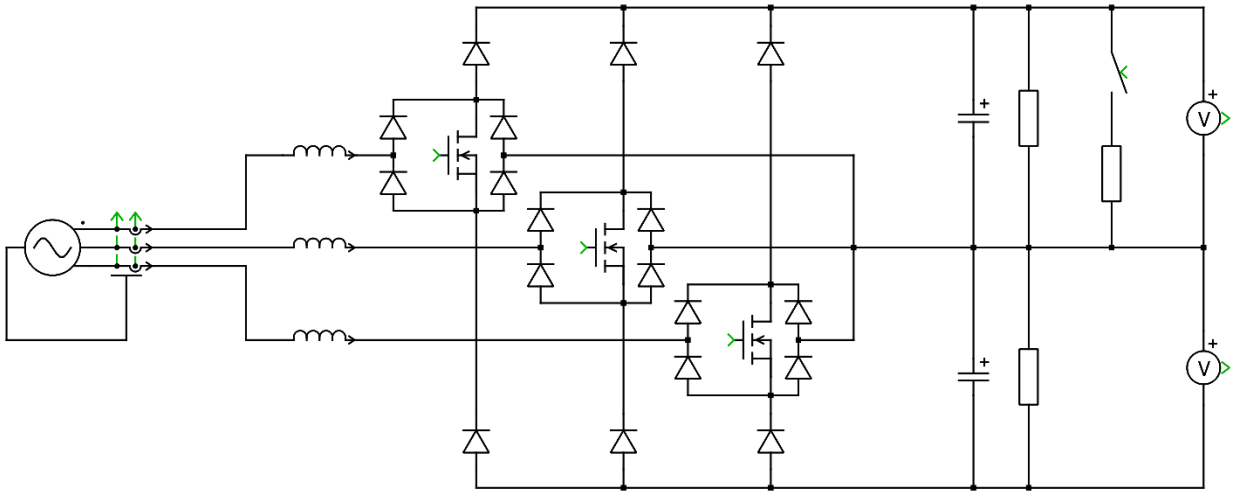

Fig. 2.33: Recreated Vienna rectifier PLECS model [21]

Vienna rectifier operates on hysteresis control technique. However, the generation of switching schemes can be SPWM or any other. Fig. 2.35 shows a basic concept of hysteresis control. The controller fixes the two current bands. The switching of the switches is within the boundaries set up by these bands. Switching frequency is controlled by the current control bands. It requires second control loop to balance the output of the two capacitors. One major advantage of this control technique is that harmonics are distributed over a wide range of frequencies [16]. Another control scheme is fixed frequency control where frequency remains constant only the pulse width is varied. Discussion on fixed frequency type control will be discussed in Chapter 3.

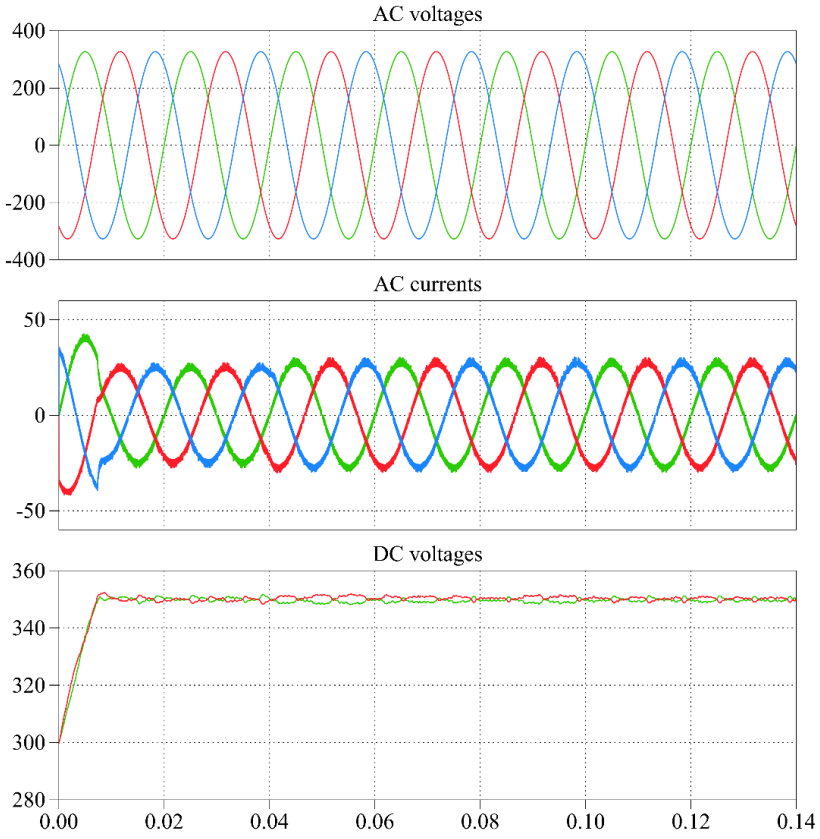

Fig. 2.34: Waveform of Vienna rectifier PLECS model

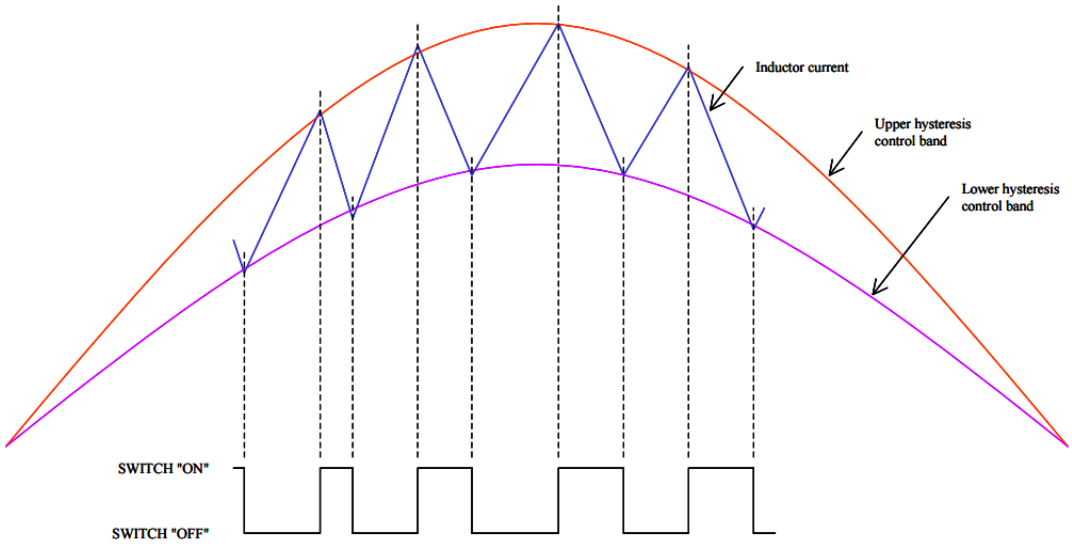

Fig. 2.35: Basis Hysteresis control for three-phase active rectifier [21]

2.3 Commutation and Harmonics Distortion

As previously stated the commutation of the thyristor is not instant. In practical application, it is not possible, as current transfer between two phases will take some finite amount of time. It is sometimes referred as overlap time depending upon the phase-to-phase voltage between the acting thyristors and line inductance [6]. During this overlap time, the phase-to-phase voltage drops on the inductors L_S. It should be noted that during commutation time two switches are in short circuit condition for a small amount of time reducing the output DC voltage and average voltage.

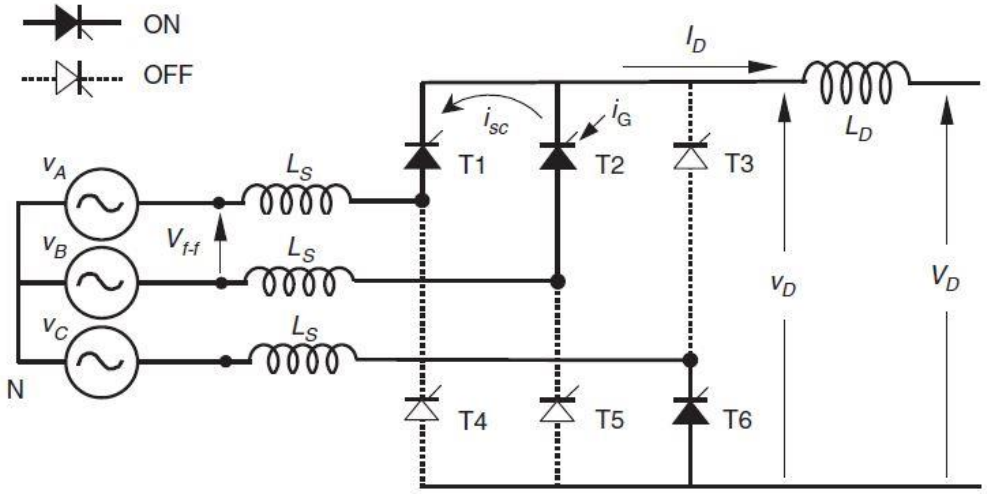

Fig. 2.36: Commutation representation

From the Fig.2.38 before commutation, the current I_D was passing through *thy* T1. During the commutation period, current I_D remains constant, short circuit current i_{sc} returns to mains through *thy* T1. *Thy* T1 is OFF when $I_D = i_{sc}$. Similarly, current I_D passes through *thy* T2. This ultimately affects the output DC voltage as the phase with bigger instantaneous voltage value suffers a voltage drop and low instantaneous phase suffers sudden surge in voltage.

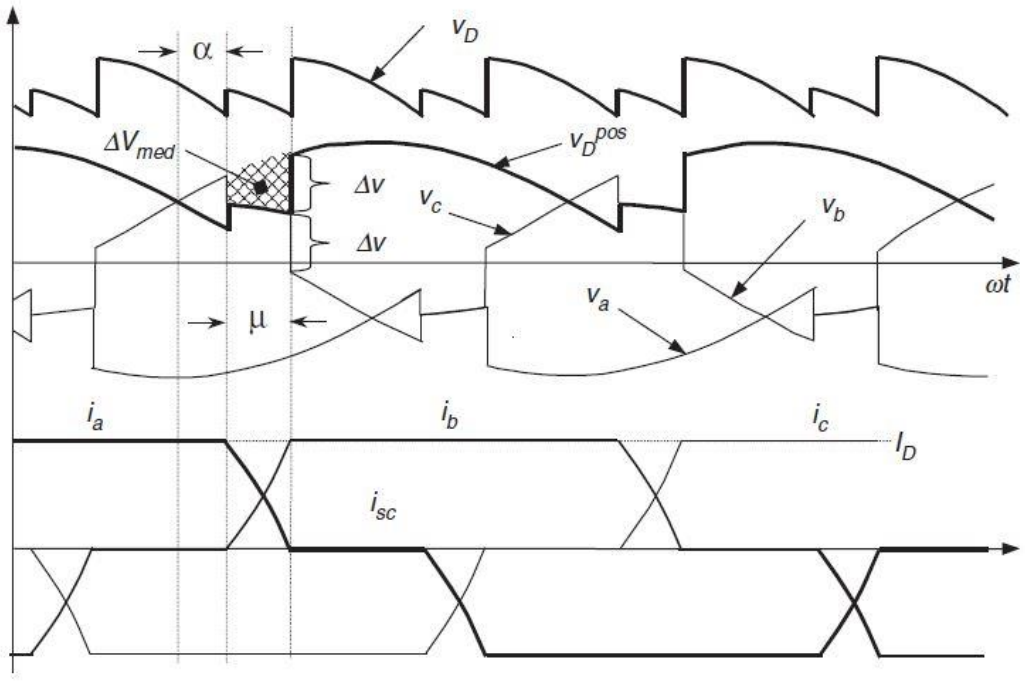

Fig. 2.37: Effect of overlap angle μ on voltages and currents [14]

2.3.1 Harmonics and PF:

When a sinusoidal voltage is applied to certain type of load, the current drawn by the load is proportional to the voltage applied and impedance. This current follows the voltage waveform. The loads are called linear loads if the voltage and current follow one and another without any distortion in their sinusoidal waveform shape. Some linear loads are resistive heaters, synchronous motors, constant speed induction motors etc. The loads are called nonlinear loads if the loads cause the current to vary disproportionally with respect to voltage. Some examples of nonlinear loads are variable frequency drives, typical diode bridge rectifier, switch mode power supply etc. Non-linear loads produce a significant number of harmonics in the system. Harmonics produced by linear loads are smaller than non-linear loads. Major sources of harmonics are thyristors or switching devices, rotating machines, and transformers.

The harmonics in line currents do not deliver real power in load making a drop-in power factor and ultimately dropping the efficiency of the system. High peak harmonics can trigger circuit breakers in the system for protection. Each component in the power system exhibits the effects of harmonics in one way or another and is subject to the damage and inefficient performance.

Power factor gives an estimate of how effectively the real power is utilized in the system. The Total Harmonic Distortion (THD) shows the degree of distortion in line voltages and line currents Fig. 2.38 shows typical poor power factor voltage and current waveform representation in the presence of harmonics. Where, $V_l(t)$ is line voltage, $i_l(t)$ is line current and $V_c(t)$ is the rectified DC voltage for a rectifier system.

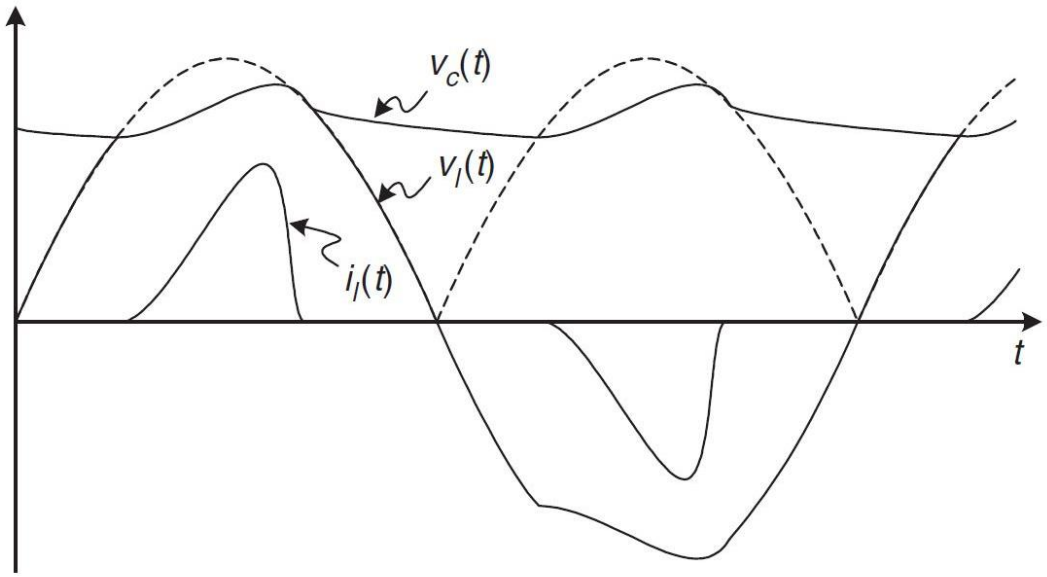

Fig. 2.38: Typical poor power factor voltage and current waveform [7]

Calculation of power factor is the resultant relationship between active, reactive, and apparent power. Power Factor Correction (PFC) concept reduces the reactive component Q, apparently reducing apparent power. The basic way of correcting PF is to add a capacitor in parallel

with the load, which provides reactive for the system instead of supply. This section will provide basic information on power factor and THD mitigation.

2.3.2 Power factor and displacement power factor

When the loads are non linear or the system is non linear, the power factor should not be calculated using traditional method.

$$cos\ \varphi \neq \frac{P}{S} \tag{2-41}$$

Nonlinear load systems have two power factors: true power factor and Displacement power factor. True power factor is measure between power factor of both fundamental and harmonic component in power system whereas displacement power factor is the factor of the fundamental component in the system only. Fig. 2.39 shows the change in the power triangle due to harmonics. Where, P, Q and S are active, reactive and apparent powers respectively. D is distortion power caused by the harmonics.

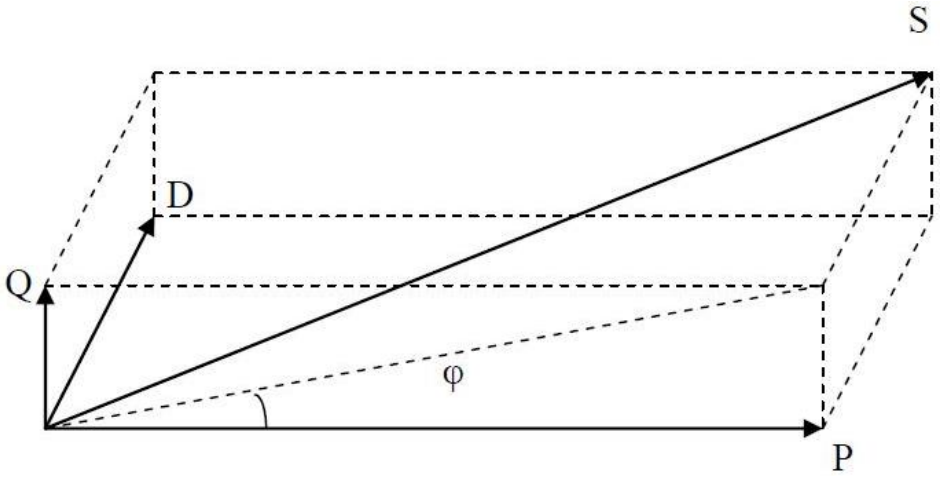

Fig. 2.39: Power factor representation in non-linear load [14]

Total Power factor,

$$pf = cos\ \varphi_1 \frac{1}{\sqrt{1+THD_v^2}} \frac{1}{\sqrt{1+THD_i^2}}$$

$$= cos\ \varphi_{disp}\ cos\ \varphi_{dist} \quad (2\text{-}42)$$

Where, $cos\ \varphi$ = P/S_1

Distortion Power factor,

$$= \frac{1}{\sqrt{1+ THD_v^2}} \frac{1}{\sqrt{1+ THD_i^2}}$$

$$= V_{1rms}\ I_{1rms} / V_{rms}\ I_{rms} = S_1/S \quad (2\text{-}43)$$

Distortion Power D,

$$D = \sqrt{S^2 - P^2 - Q^2} \quad (2\text{-}44)$$

The term cos φ_1 is displacement power factor as it relies on the phase angle between the fundamental components of the voltage and the current similar to the power factor with linear loads. The term $(\frac{1}{\sqrt{1+ THD_v^2}} \frac{1}{\sqrt{1+ THD_i^2}})$ is distortion power factor as it relies on the harmonic distortion of current and voltage. The calculated power factor is called true power factor, which is multiplication of distortion pf, and displacement power factor.

2.3.3 Harmonics Mitigation

It is clear from the previous section that the true power factor will improve if the distortion power factor reduces. In the case of a 3-phase 6-pulse rectifier, as mentioned in previous sections, the power factor will change with the varying conduction angle of the rectifier and with changes in the fundamental frequency of the input voltage i.e. change in motor speed. A specific type of L-C (passive) filter tuned at specific harmonic frequencies, like 5^{th}, 7^{th}, 11^{th}, etc., is used to mitigate the harmonics. This filter not only improves the harmonic distortion but also improves power factor as it contains capacitors.

Resonant frequency,

$$f_o = f_{ripple}\sqrt{\gamma_{filter}} \tag{2-45}$$

Where, f_{ripple} = ripple frequency of the harmonics, γ_{filter} = attenuation

Cut-off frequency,

$$f_{cut-off} = \frac{1}{2\,\pi\,\sqrt{L_f C_f}} \tag{2-46}$$

Where, $f_{cut-off}$ = typical cut-off frequency of filter

L_f = selected inductor value, C_f = selected capacitor value

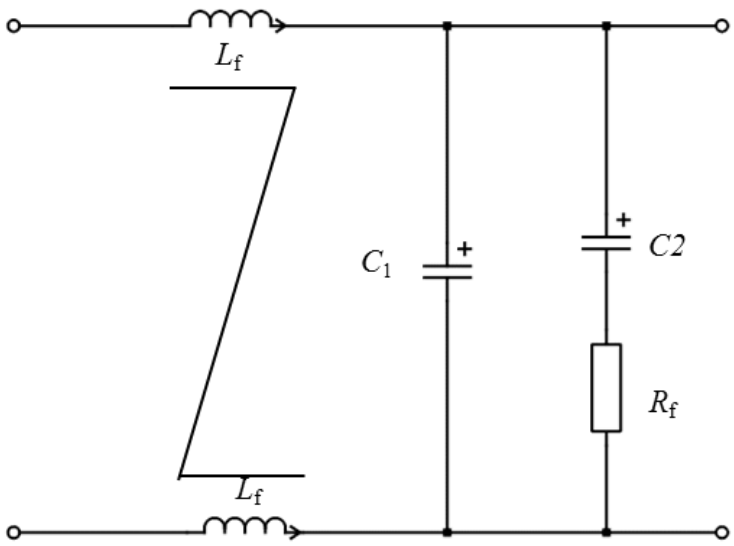

Fig. 2.40: Structure of passive filter

Fig. 2.41 shows typical LC passive filter. To limit the overvoltage at cut-off frequency a damping resistor is used. There are several other ways of mitigating harmonics found in the literature [13] [14].

2.4 Conclusion and remarks

In this chapter, basic rectifier classification based on control, a popular rectifier for PFC (Power factor correction) Vienna rectifier, and brief information on power factor and harmonic distortion were discussed. The simulation of these rectifiers was done in the PLECS Block set. Although there are several controlled rectifiers proposed by researchers the three-phase fully controlled rectifier is widely used, as it is relatively easy to construct and modules are available in the market at reasonable rates. Vienna rectifier is nowadays a popular choice in the PFC applications, as it offers very high frequency and unity power factor. The comparison of three-phase active rectifier and Vienna rectifier can be done keeping many factors in consideration. However, depending upon the application of the system the three-phase active is selected. In this thesis, a SiC-based Active front-end rectifier was used. In Chapter 3, a basic switching technique for the controlled rectifier and basic control scheme is illustrated.

Chapter 3 - Switching and Control

In modern power electronics applications, it is very important to have low harmonic distortion with minimum electromagnetic interference. This chapter will provide discussion on two most common switching techniques: The Sine PWM (SPWM), Third Harmonic injection Sine PWM (THIPWM). This chapter also provides discussion on control technique for the $3-\phi$ AC/DC converter/rectifier. The switching scheme and control technique are modified for attaining unity power factor for experimental setup of the rectifier.

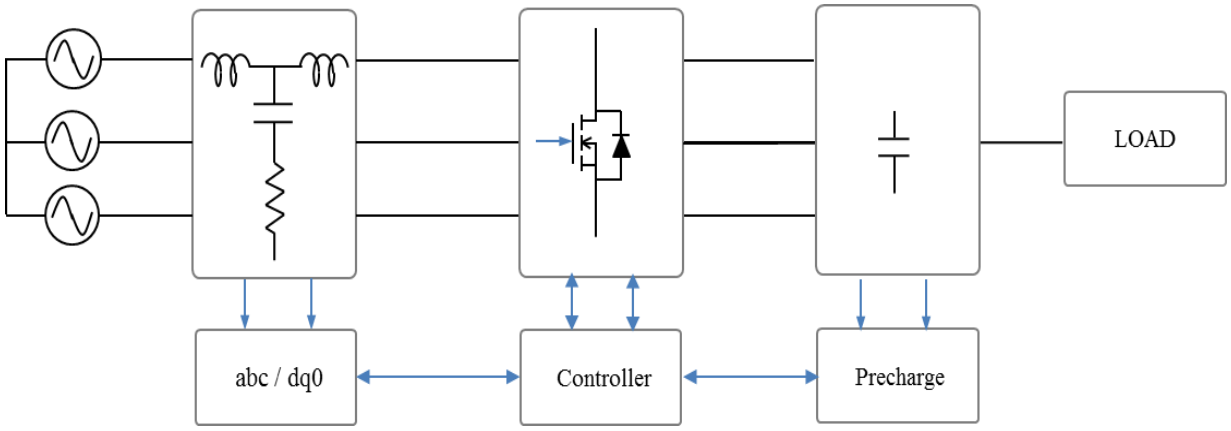

Fig. 3.1: Proposed active rectifier

The proposed active rectifier shown in Fig. 3.1 uses the SPWM with third harmonic injection with constantly modified switching pulses generated using the controller. The following section will give a discussion on SPWM and THIPWM. Explanatory information on the controller and the Pre-charge procedure of the proposed active rectifier is presented in the final section of this chapter. Although the six switch MOSFET gate driver used here operates as a rectifier operation, the switching pattern for Voltage Source Inverter (VSI) is relatively similar.

3.1 Switching Scheme

Switching methods are the most important way of achieving the appropriate goal through the switches. Whether it is the AC-DC converter, DC-AC or DC-DC Buck, Boost or Buck-Boost converter, the switching method determines the size of magnetic components required and Total Harmonic Distortion (THD) and Efficiency, which are important aspects for a converter or rectifier design and operation. Over the course of time, researchers have explored several switching methods. Using Pulse Width Modulation (PWM) technique, Space Vector PWM, Sinusoidal PWM, Selective Harmonic Elimination PWM and Hysteresis PWM are the most common methods of switching of power electronics devices.

3.1.1 Sinusoidal Pulse Width Modulation (SPWM)

The basic SPWM technique compares a triangle carrier with a reference waveform. A low frequency modulating signal is compared with a very high frequency carrier signal. The desired output voltage is achieved by changing the amplitude and frequency of the reference or the modulating voltage. These variations change the patterns of the output voltage. The sinusoidal waveforms are generated by filtering an output pulse waveform with varying width. The switching state is modified when the modulating waveform intersects with the carrier waveform, typically triangular waveform.

Fig. 3.2 shows simulated PWM pattern by comparing three sinusoidal waveforms and triangular carrier waveform. Carrier wave amplitude is A_C and the modulating waveform amplitude is A_m. The pulses generated are two-level; i.e. pulse values are either $+ve\frac{V_d}{2}$ or $-ve\frac{V_d}{2}$. Multi-level inverters have different values of these pulses. +ve $\frac{Vd}{2}$ is achieved when the amplitudes of modulating waveform is greater than carrier waveform i.e. $A_m > A_C$. -ve $\frac{Vd}{2}$ is

achieved when $A_C > A_m$. The resulting square waveform comprises of the desired waveform in its low frequency components and high frequency components are near the carrier wave frequency [17].

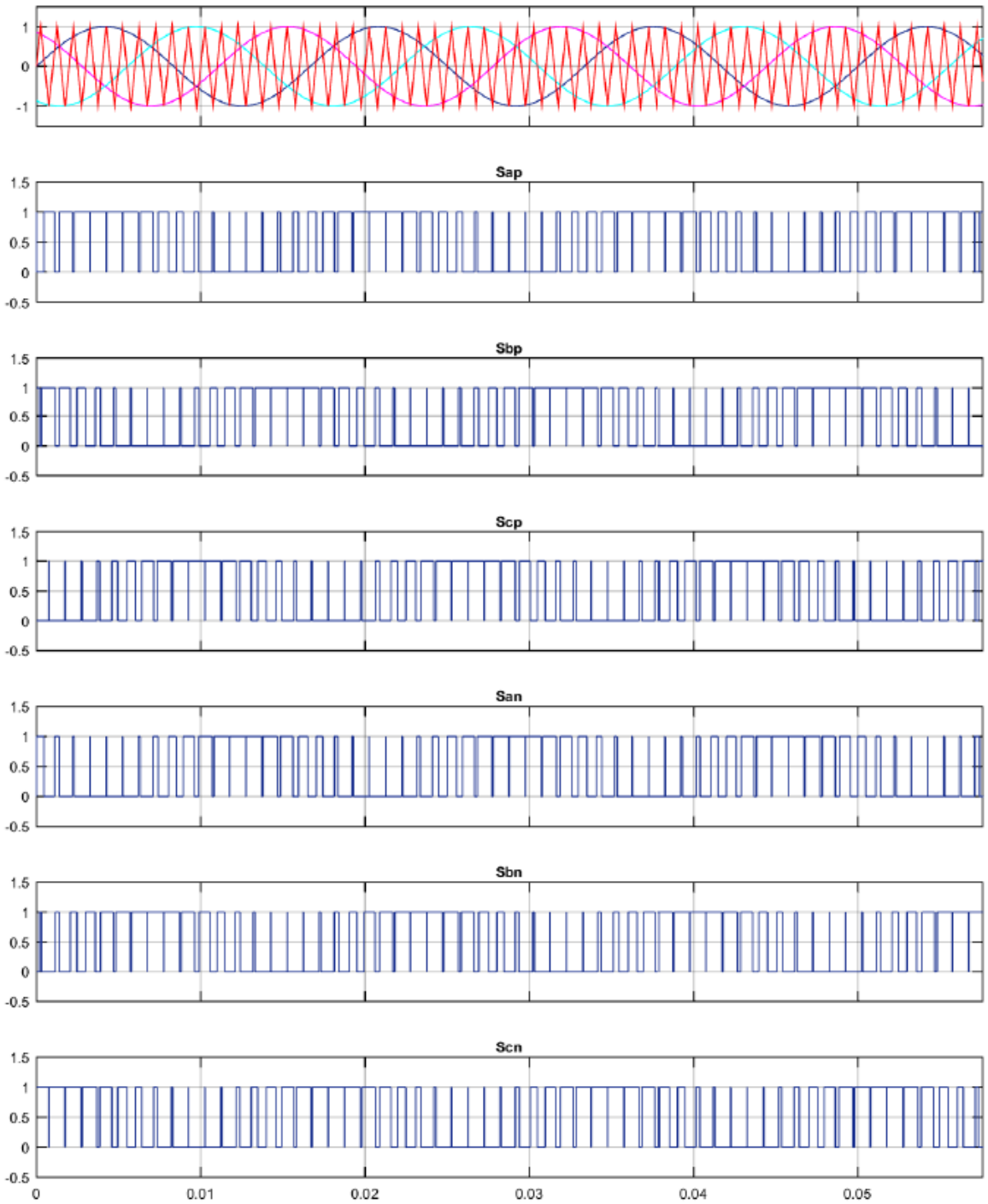

Fig. 3.2: Standard Pulse-Width modulation waveform

When the sinusoidal waveform is greater than the triangular waveform, the switch in the upper leg is turned on and lower switch is turned off. Similarly, when the sinusoidal waveform is less than the triangular carrier waveform the lower switch is on.

In three-phase SPWM, a triangular waveform V_{tri} is compared with three sinusoidal references by 120^{o} out of phase with each other. A two level six-pulse rectifier composed of six switches S1 through S6 was discussed in the previous chapter. Two switches in each phase make one leg, opening, and closing in the corresponding manner. When one switch is open, the other is closed and vice-versa. For the simplicity of explanation, the technique explained here is for a VSI as shown in Fig. 3.3.

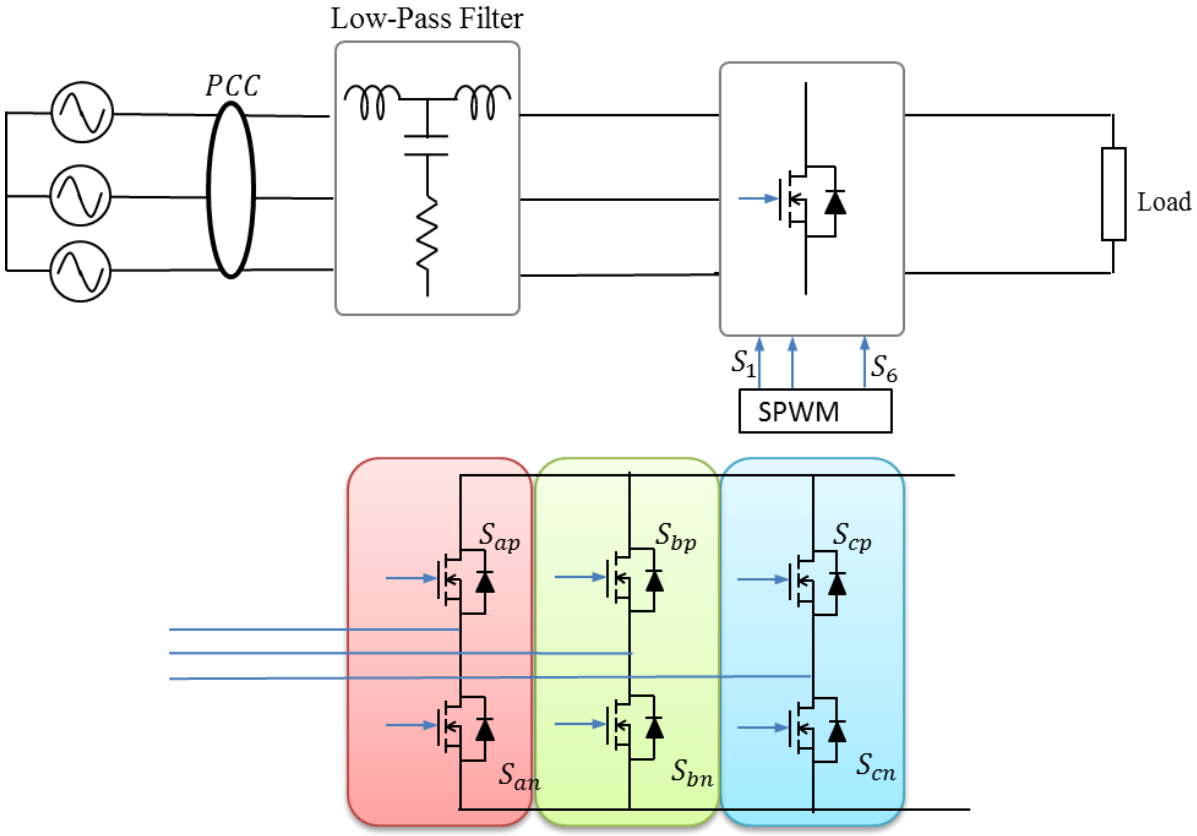

Fig. 3.3: Typical grid connected VSI

Depending upon the state of switching either $+ve\ or\ -ve$ voltage is applied in each phase. Switches are operated in pairs. Upper leg operates in complimentary manner to the lower leg. Fig. 3.4 shows the simulated SPWM waveform for all the switches.

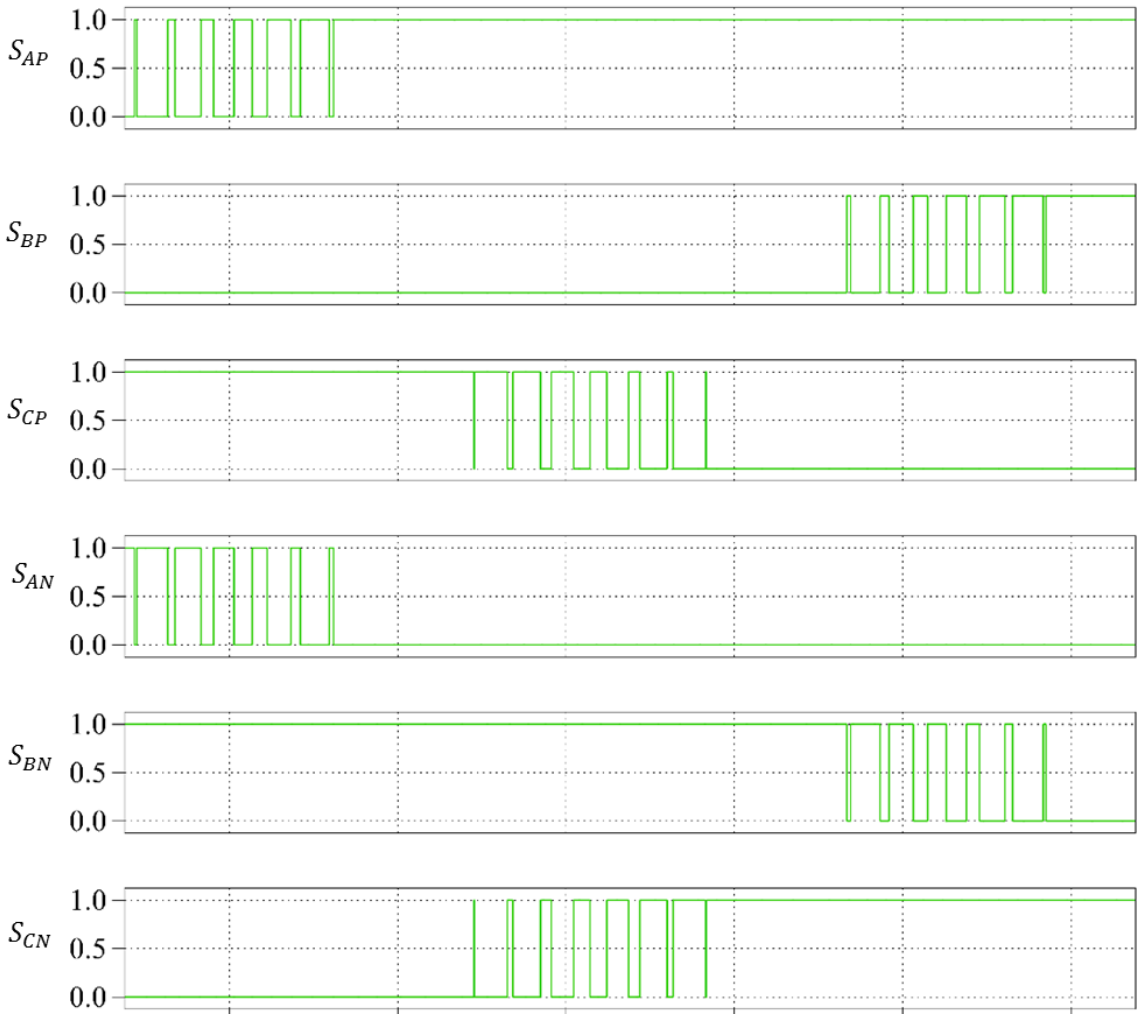

Fig. 3.4: Three-phase sinusoidal PWM switching pattern

Three-reference voltages are given as [17]:

$$V_{an} = V_o cos\ \omega_o t = M\ V_{dc}\ cos\ \omega_o t \quad (3 - 1)$$

$$V_{bn} = V_o \cos\left(\omega_o t - \frac{2\pi}{3}\right)$$

$$= M\ V_{dc}\ cos\ (\omega_o t - \frac{2\pi}{3}) \quad (3 - 2)$$

$$V_{cn} = V_o \cos\left(\omega_o t + \frac{2\pi}{3}\right)$$

$$= M V_{dc} \cos\left(\omega_o t + \tfrac{2\pi}{3}\right) \qquad (3 - 3)$$

Where, V_o = output voltage peak magnitude, M = modulation index and V_{an}, V_{bn} and V_{cn} are reference voltages with respect to a neutral point.

3.1.1.1 Modulation Index (m):

The modulation index is defined as the ratio of the magnitude of reference to carrier signal magnitude. It is used to regulate the magnitude of the output voltage. The value of modulation index lies generally between 0 and 1. In the case of SPWM technique the modulation index $\approx$ 78.55% [17]. Thus, the general SPWM technique does not utilize the full DC bus voltage. To utilize the maximum DC bus voltage the third harmonic is injected with the fundamental following section will provide more information on third harmonic injection.

The line to line volatages are given by the differences between the phase leg voltages as follows,

$$V_{ab} = V_{an} - V_{bn}$$

$$= M \sqrt{3} V_{dc} \cos(\omega_0 t + \pi/6) \qquad (3 - 4)$$

$$V_{bc} = V_{bn} - V_{cn}$$

$$= M \sqrt{3} V_{dc} \cos(\omega_0 t - \pi/2) \qquad (3 - 5)$$

$$V_{ca} = V_{cn} - V_{an}$$

$$= M \sqrt{3} V_{dc} \cos(\omega_0 t + 5\pi/6) \qquad (3 - 6)$$

Detailed methamatical analysis of these voltages can be found in the liturature[17][18].

3.1.2 Third Harmonic SPWM (THIPWM)

The SPWM technique is simplest switching technique but it is unable to fully utilize the available DC bus supply voltage. Due to this limitation THIPWM technique was developed. It is recognized that maximum modulation index of a $3-\phi$ PWM inverter system increases by including a third harmonic term into the target reference waveform of each phase [17]. There is no effect of the third harmonic component on the line-to-line fundamental output voltage as the common mode voltage is canceled between the phase legs but it does reduce the size of peak envelope of each phase leg voltage.

Following reference [17] equations (3-4), (3-5) and (3-6) are shown below to define appropriate sinusoidal target reference waveforms,

$$V_{ab} = V_{dc}\,[M\,cos\,(\omega_0 t) + M_3\,cos\,3(\omega_0 t)] \qquad (3\text{ - }7)$$

$$V_{bc} = V_{dc}\,[M\,cos\,(\omega_0 t - 2\pi/3) + M_3\,cos\,3(\omega_0 t)] \qquad (3\text{ - }8)$$

$$V_{ca} = V_{dc}\,[M\,cos\,(\omega_0 t + 2\pi/3) + M_3\,cos\,3(\omega_0 t)] \qquad (3\text{ - }9)$$

& dividing through $M * Vdc$, these equations can be written in per unit form [17] as

$$v = cos\,\theta + A\,cos\,3\theta \qquad (3\text{ - }10)$$

Where $A = M_3/M$ represents a parameter to be optimized while keeping the maximum amplitude $v(t)$ under unity. The maximum value of Eq. (3-10) is found by setting its derivative with respect to θ equal to zero.

$$\frac{dv}{d\theta} = sin\,\theta + 3A\,sin\,3\theta = 0 \qquad (3\text{ - }11)$$

This function has maximum/minimum at $\theta = 90^{o}$, while depending upon the polarity of A. If it is maximum, the value would be greater than unity and if it is minimum, it is not a matter of concern.

As we know that,

$$\sin 3\theta = \sin 2\theta \cos\theta + \cos 2\theta \sin\theta$$

$$= 2\cos^2\theta \sin\theta + (2\cos^2\theta - 1)\sin\theta$$

$$= (4\cos^2\theta - 1)\sin\theta \qquad (3 - 12)$$

Substituting this expression in (3-11) gives

$$0 = 1 + 3A\,(4\cos^2\theta - 1)$$

Which rearranges as

$$1 - \frac{1}{3A} = 4\cos^2\theta$$

And finally

$$\cos 2\theta = \sqrt{\frac{3A-1}{12A}} \qquad (3 - 13)$$

Similarly

$$\cos 3\theta = \cos 2\theta \cos\theta - \sin 2\theta \sin\theta$$

$$= (2\cos^2\theta - 1)\cos\theta - 2\sin^2\theta \cos\theta$$

$$= (4\cos^2\theta - 3)\cos\theta \qquad (3 - 14)$$

Equation (3-13) can becomes

$$\cos 3\theta = -\frac{6A+1}{6A}\sqrt{\frac{3A-1}{3A}} \qquad (3 - 15)$$

Equations (3-13), (3-14) and (3-15) yields v_{max} as,

$$= -\frac{1}{3}(3A - 1)\sqrt{\frac{3A-1}{3A}}$$

$$= -\frac{1}{3}(3A - 1)\sqrt{1 - \frac{1}{3}A} \qquad (3 - 16)$$

The equation (3-16) v_{max} the maximum value of a function of parameter A.

The maximum possible value of v_{max} is calculated by making the derivative with respect to A equal to zero.

$$d\frac{v_{max}}{dA} = -\sqrt{1-1-\frac{1}{3}A} - \frac{1}{6}\left(\frac{3A-1}{\sqrt{1-1/3A}}\right)\frac{1}{3A^2} = 0 \qquad (3-17)$$

$$0 = -\left(\sqrt{1-\frac{1}{3}A}\right)\left(1+\frac{1}{6A}\right) \qquad (3-18)$$

For this expression to equal to zero, its numerator must be zero, which gives

$$A = \frac{1}{3} \text{ and } -\frac{1}{6} \qquad (3-19)$$

From (3-17), the value A = $\frac{1}{3}$ produces $v_{max} = 0$, which is minimum as the square root term cannot be smaller than zero without becoming imaginary. The value $A = -\frac{1}{6}$ produces a maximum of $v_{max} = \frac{\sqrt{3}}{2} = 0.866$.

From the expression $v_{an} = Mv_{dc}$,

$$v_{an\,max} = \frac{\sqrt{3}}{2} \text{M } v_{dc} \qquad (3-20)$$

Hence, the modulation index can now increase to 2/√3 = 1.15.

Since, $A = \frac{M}{M_3}$, M_3 increases in proportional to M and reaches to value of $M_3 = \frac{\sqrt{3}}{9} = 0.192$, where, $M = \frac{2}{\sqrt{3}} = 1.15$. Fig. 3.5(a) shows the fundamental waveform. Fig. 3.5(b) shows the 1/6 of third harmonic and peak value. Fig. 3.5(c) shows the addition of this third harmonic produces 15.5% increase in the amplitude of the fundamental of the phase voltages.

Injecting the third harmonic component to fundamental component gives the following modulating waveforms,

$$V_{an} = \frac{2}{\sqrt{3}}\left(cos\,\omega_0 t + \frac{1}{6}\,cos\,\omega_0 t\right) \qquad (3-21)$$

$$V_{bn} = \frac{2}{\sqrt{3}}\left(cos\left(\omega_0 t - 2\frac{\pi}{3}\right) + 1/6\ cos\,(3\omega_0 t)\right) \qquad (3-22)$$

$$V_{cn} = \frac{2}{\sqrt{3}}\left(cos\left(\omega_0 t + 2\frac{\pi}{3}\right) + 1/6\ cos\,(\omega_0 t)\right) \qquad (3-23)$$

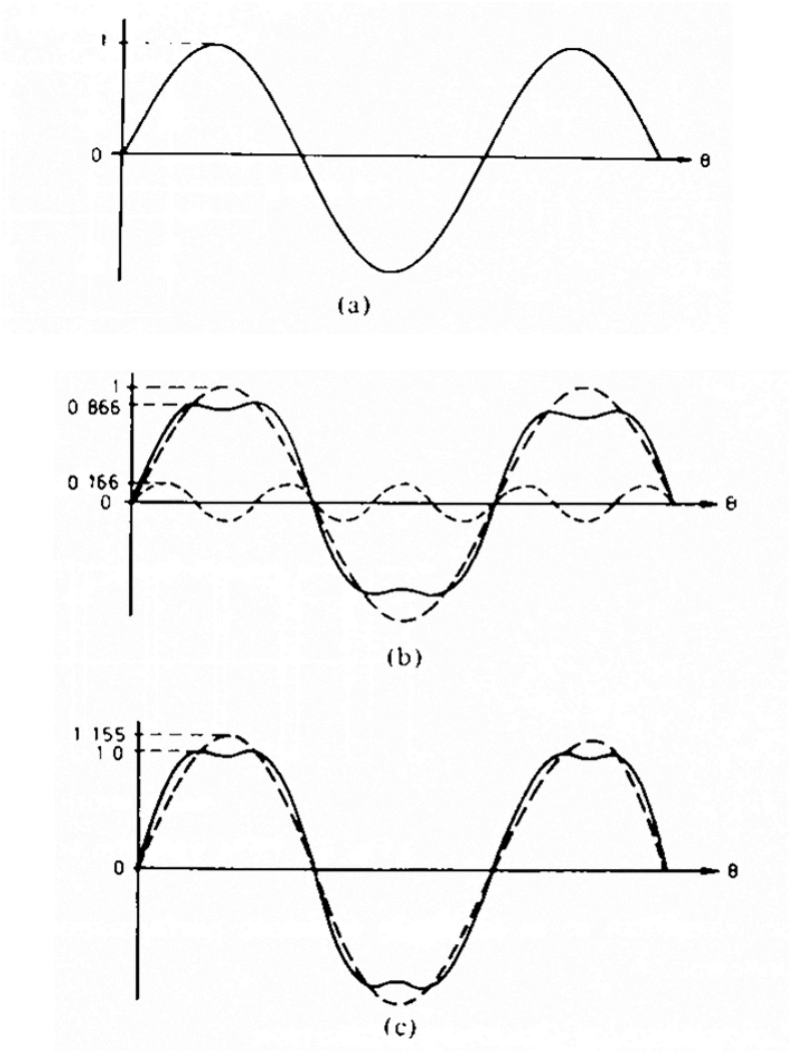

Fig. 3.5: Three-phase sinusoidal PWM with injected third harmonic [18]

3.1.3 Overmodulation:

SPWM works well, for $m \leq 1$. For $m > 1$, some portion of the triangular carrier miss the modulating waveform i.e. there is no intersection between the carrier wave and the modulating wave. Fig. 3.6 shows the overmodulation. Often overmodulation is allowed to some degree to achieve larger AC voltage but rendered voltages are of poor quality.

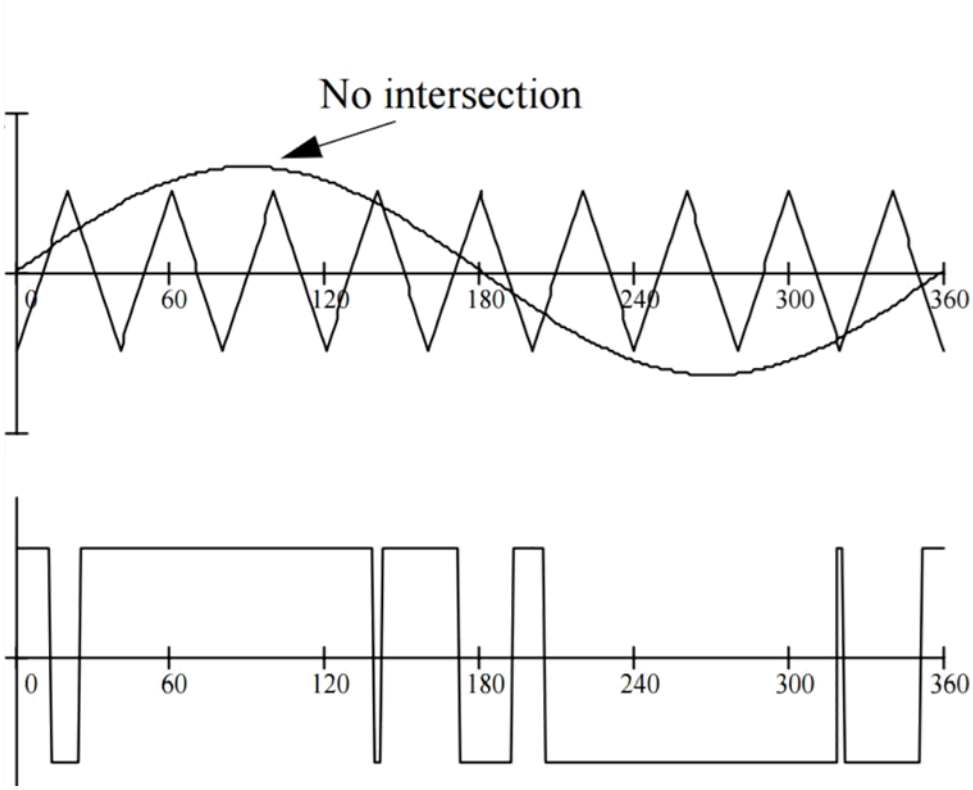

Fig. 3.6: Overmodulation in fundamental and carrier [18]

3.3 Control technique

Control of the system is important to achieve desired response from the system. Feedback control maintains a relationship between the desired or reference input to the output by comparing and using the difference to achieve the desired goal.

In open loop control systems, the output does not have any effect on the control action. In other words, the output is not fed back to the controller for the calculation of difference in error measurement. In the case of closed control systems, a stimulating error signal, which is the difference between the input signal and the feedback signal, is fed to the controller. The feedback single can or cannot be dependent on the input of the system. In the systems when the inputs are known prior and with no disturbances, generally open loop systems are used. Whereas when unprecedented disturbances are expected from the system and constant correction of the error is needed, the closed loop systems are used.

Many of the industrial systems, which are used today, have one or other form of PID (Proportional Integral and Derivative) control. This section will provide brief info on these controllers.

3.3.1 PID Controller

The typical control system can be representated as shown below. The controller compares the real value of plant output or system output with reference input as mentioned earlier. Ultimately, determining the deviation and producing control for system which will decrease the deviation to desired value or zero in many cases.

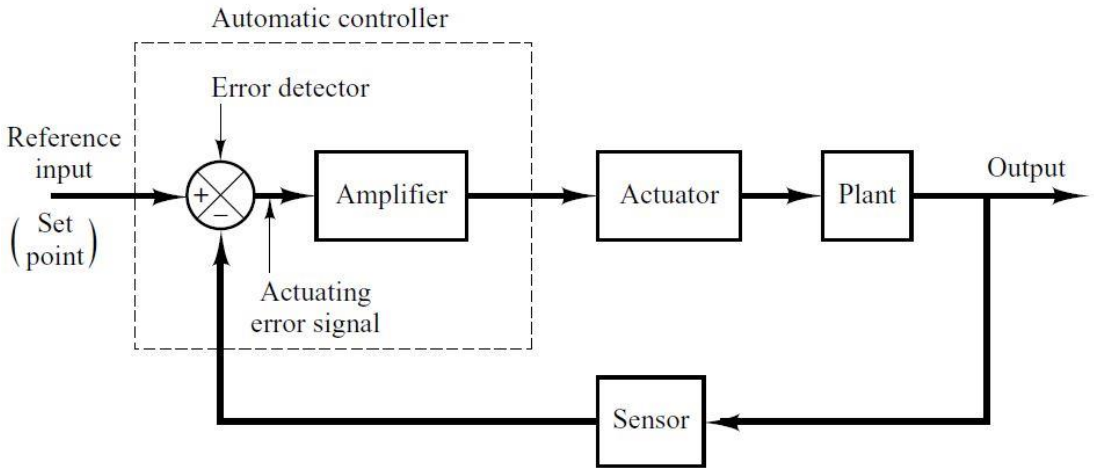

Fig. 3.7: Control system representation with automatic controller [18]

The amplifier in the system increases the error signal level to the higher value. This sufficient higher-level error signal is fed to the actuator, which produces the input signal for plant or system so that output signal will approach to reference input. The sensor converts the output variable to other suitable variable appropriate for the controller. The sensor also provides the feedback path of the closed loop system. Fig. 3.8 shows desired voltage correction in a typical controller.

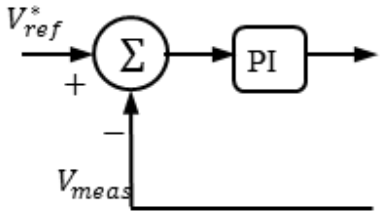

Fig. 3.8: P/I control for desired voltage correction

3.3.1.1 Proportional control action:

In the case for the controller with proportional control action or proportional gain, the error signal $e(t)$ and the output of the controller relationship $u(t)$ is

$$u(t) = K_p\, e(t) \tag{3 - 24}$$

Laplace transform gives

$$K_p = \frac{U(s)}{E(s)} \tag{3 - 25}$$

Where, K_p = proportional gain

The proportional gain gives the amplified error making it an amplifier with variable gain.

3.3.1.2 Integral Control Action:

In the case for the controller with integral control action or integral gain, the error signal $e(t)$ and the output of the controller relationship u (t) is

$$\frac{du(t)}{dt} = K_i\, e(t) \tag{3 - 26}$$

Taking integration with respect to time,

$$u(t) = K_i \int_0^t e(t)\, dt \tag{3 - 27}$$

Transfer function is

$$\frac{U(s)}{E(s)} = \frac{K_i}{s} \tag{3 - 28}$$

Where, K_i = variable integral gain

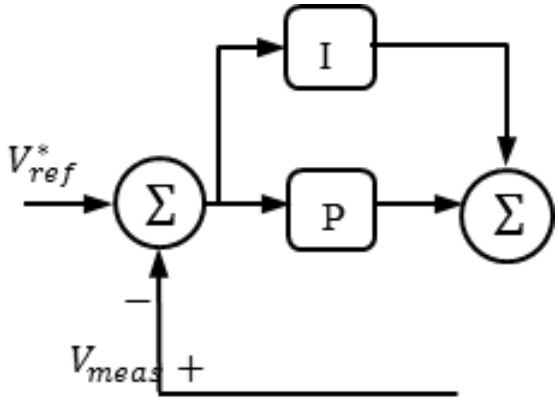

Fig. 3.9: PI control for desired voltage correction

3.3.1.3 Proportional-Integral Control Action:

Similarly, the system with both the actions represented in Fig. 3.9, the output of the controller $u(t)$

$$u(t) = K_p\, e(t) + \frac{K_p}{T_i} \int_0^t e(t)\, dt \qquad (3-29)\ [20]$$

Transfer function gives

$$\frac{U(s)}{E(s)} = K_p\, (1 + \frac{1}{s\, T_i}) \qquad (3-30)$$

Where, T_i = integral time.

There are several other PI and PID (proportional integration and derivation) control designs in the literature [20]. The specifications of the PID controllers are different for different system environments to achieve appropriate transient response and the specifications for transient response in steady state requirements.

3.3.2 Controller of the system

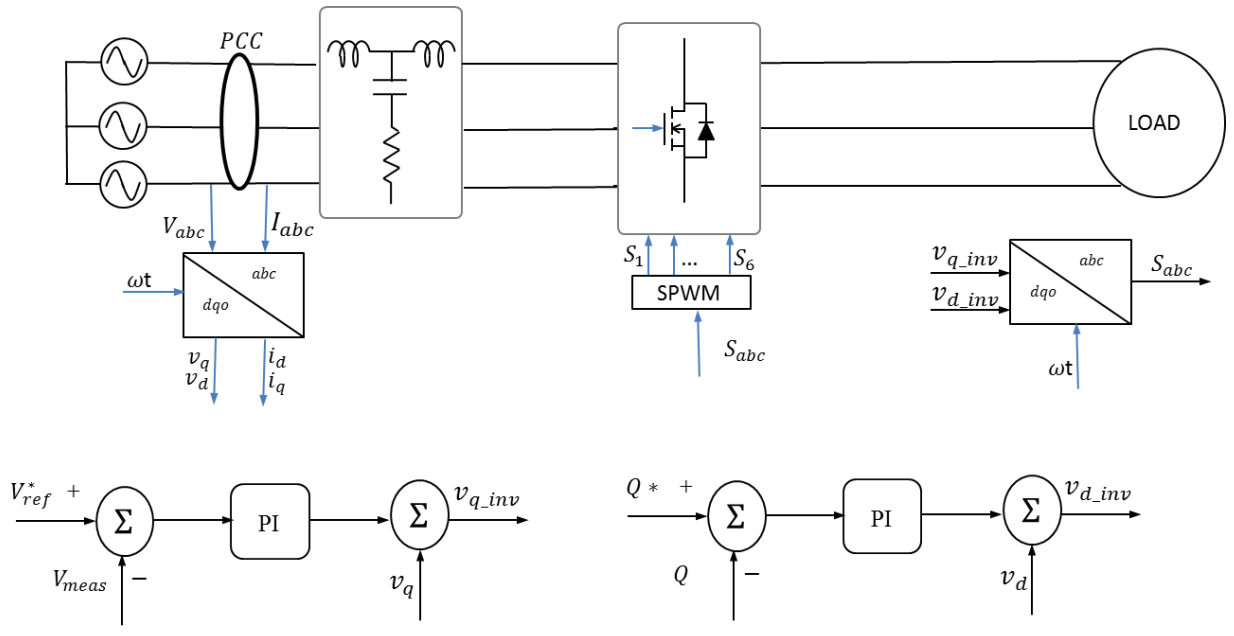

Fig. 3.10: Controller for the system

A controller was designed to regulate the output DC voltage and reactive power from the system. Fig. 3.10 shows the block diagram of the controller. The line to line voltage from the three-phase supply at the point of common coupling (PCC) and line currents from the supply to the system was measured and converted to $dq0$-reference frame to obtain v_q^* and v_d^*. The controller then generates the three reference sinusoidal waveforms to generate switching pattern. P and Q were calculated from the obtained v_q^*, v_d^*, i_q^* and i_d^* using,

$$P = \frac{1}{2}\left((v_q * i_{q)} + (v_d * i_d)\right) \quad (3\text{-}31)$$

$$Q = \frac{1}{2}\left((v_q * i_{d)} - (v_d * i_q)\right) \quad (3\text{-}32)$$

3.3.3 Precharge mechanism

Precharge mechanisms are important for the protection of the entire system. The mechanism or circuitry provide protection against inrush currents. *Inrush currents* or surge currents are maximum instantaneous input current drawn from the supply by the system when initially turned ON. Rectifiers often have these currents due to initial charging of the DC bus capacitor.

System protection elements such as circuit breakers or fuses must be incorporated into the system such that system does not go in faulty condition when there are inrush currents present. Usually, these currents appear for a very short amount of time. Protection against these currents becomes vital as sometimes these currents are higher than the surge current limit of semiconductor devices and other components. Transformers and motors also exhibit these currents when the system starts initially.

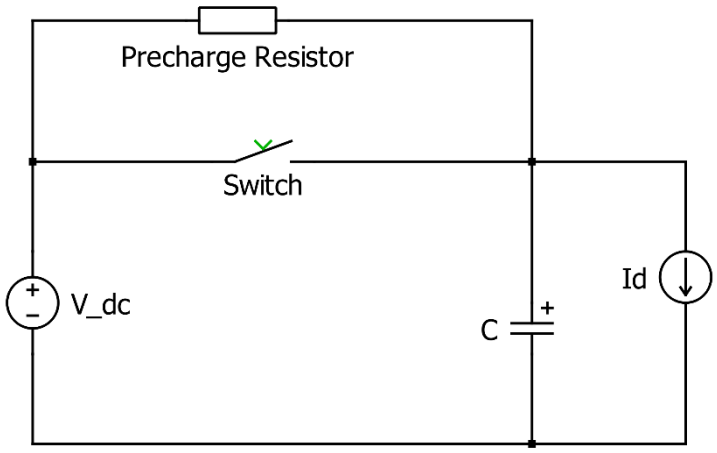

Fig. 3.11: Basic precharge circuit

A precharge mechanism is nothing but a resistor connected in series with the DC side capacitor. Fig. 3.11 shows a basic precharge circuit. The switch is tripped when there is desired charge on the capacitor, in other words, when the capacitor is sufficiently charged. The purpose of the precharge resistor is to reduce the peak of the surge currents. There are several other surge current protection devices, Negative temperature thermistor and circuits available in market, but a series high wattage resistor with a switch (A switch can be a transistor, relay etc.) is most commonly used. The flowchart shown in Fig. 3.12 explains the precharge pulse generation using Hysteresis type method for the IGBT used in the proposed system.

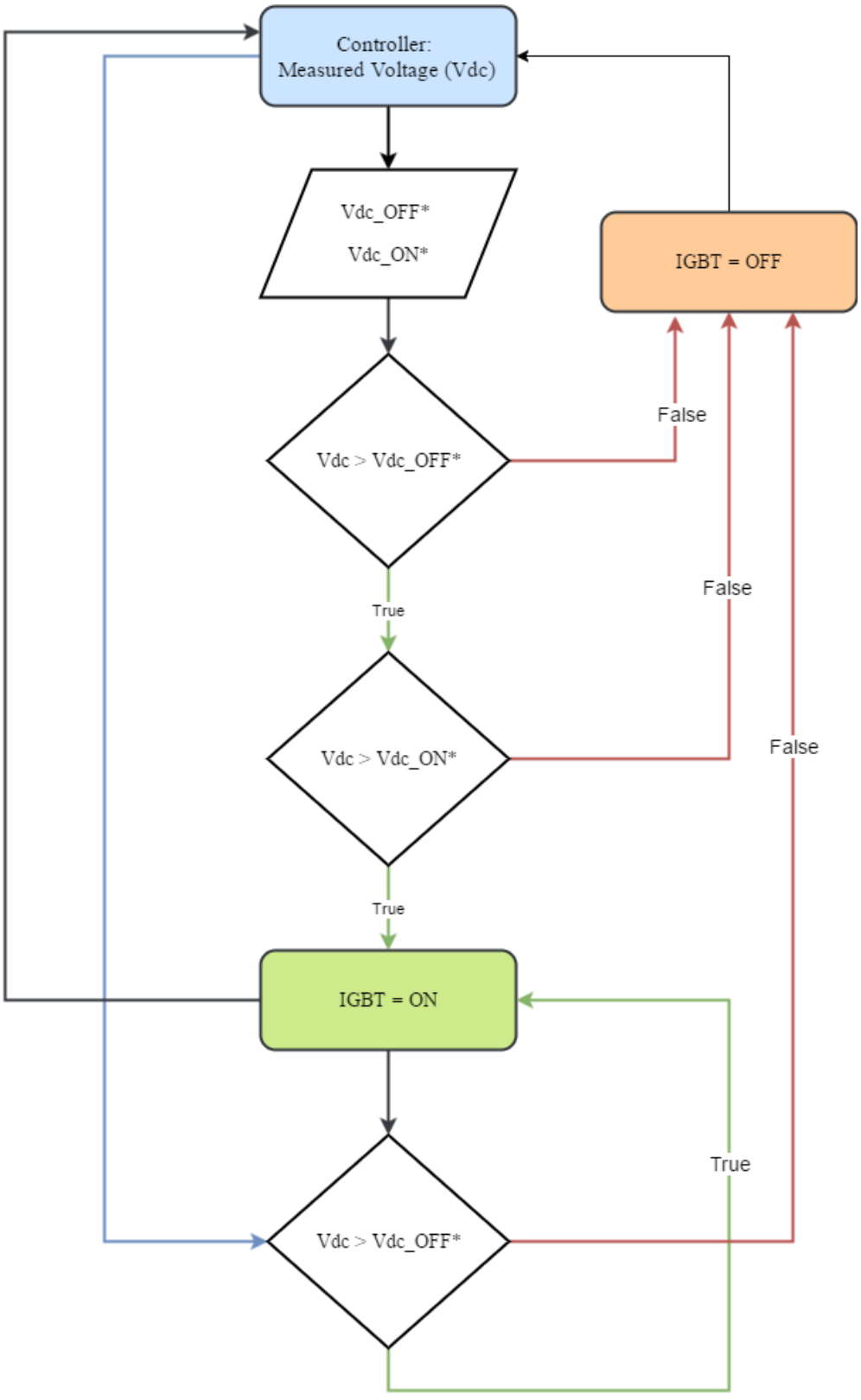

Fig. 3.12: Precharge flowchart

3. 4 Conclusion and remarks

Sine PWM technique with injected third harmonic is used to generate switching for the system. It is certainly possible to use other the switching methods, however, the SPWM technique is relatively easy to design in the hardware. Third harmonic injected PWM utilizes the same level of modulation index as the SVPWM technique. Basic information on the PID controller was presented to provide a general idea of designing a PID controller for beginners. Some extent of the actual controller used in the system and its operation was described. Finally, a basic precharge circuit and the steps to develop the gate pulse the switch used in the precharge mechanism have presented.

Chapter 4 - Laboratory Setup

This Chapter will provide details of Laboratory setup consisting FPGA, dSpace, Measurement Board, Filter.

4.1 Simulation results of system

The simulation uses switching generator inbuilt block from the MATLAB/SIMULINK. The controller and PLCES model were designed by Dr. Behrooz Mirafzal for an aircraft system for variable frequency 300-800 Hz with a constant line to line input voltage of 200 V and desired output voltage of 270 V_{dc}. The controller consists of PI controller with feedback information from the circuit setup. Line currents and line voltages are measured prior to the point of common coupling and fed to the controller.

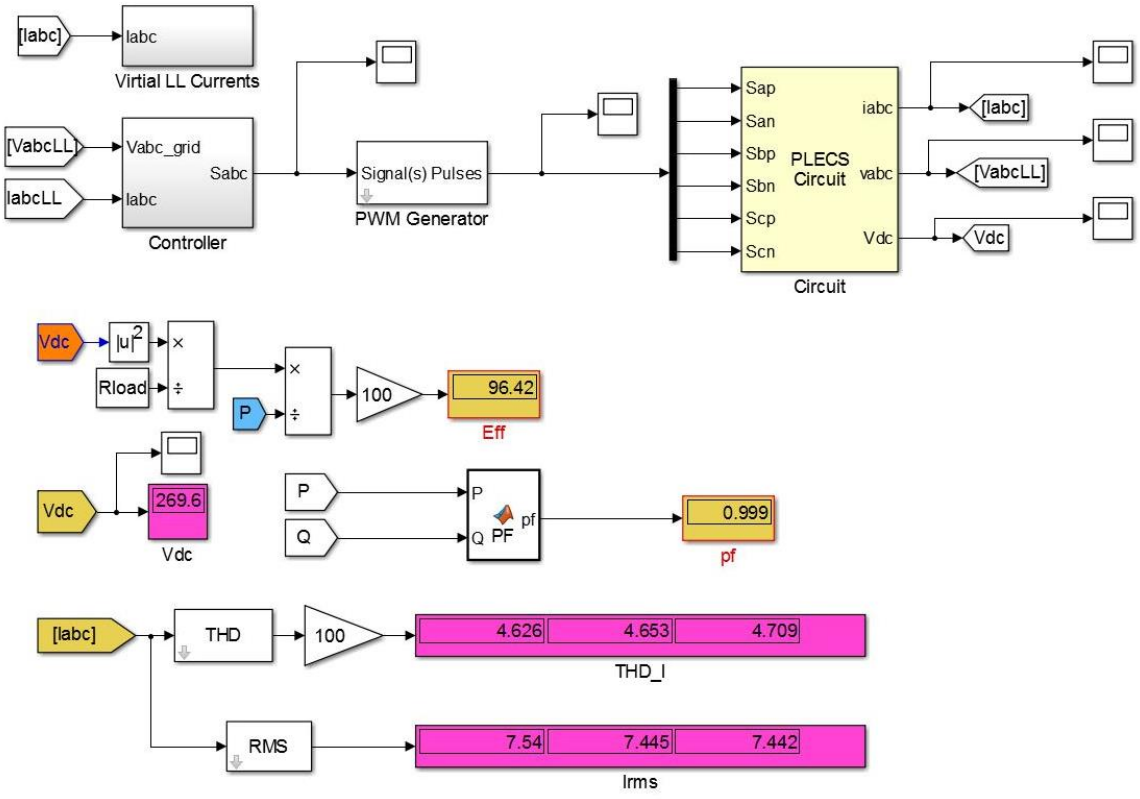

Fig. 4.1: System Simulation

Table 4-1 Simulation parameters

Parameter	Value
V_{llrms}	$200\ V\ @\ 800\ Hz$
L1	$150\ \mu H$
L2	$330\ \mu H$
C (delta connected)	$3\ *\ 27\mu F$
C_{DC}	$2 * 200\mu F$
R_{load}	$30\ \Omega$
$f_{switching}$	$47 * 800\ Hz$

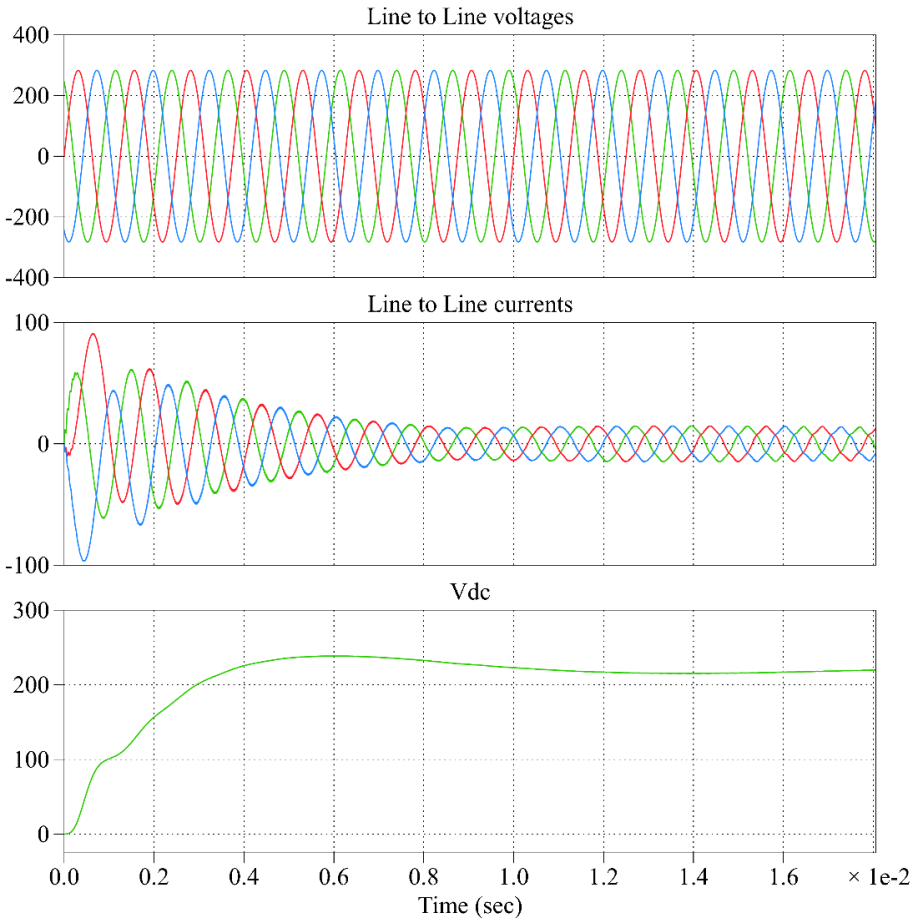

Fig. 4.2: System simulation: Line to Line Voltages, Line currents and Vdc

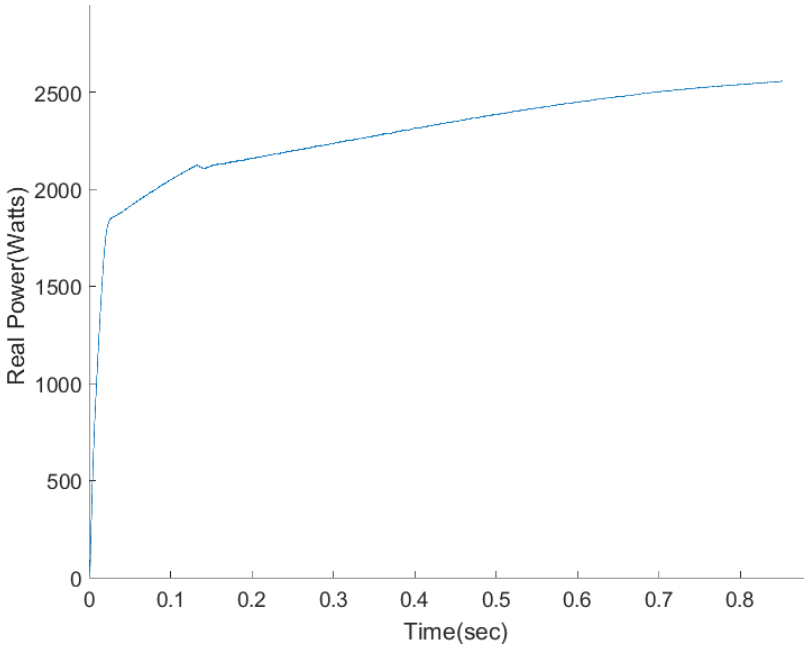

Fig. 4.3: Measured real power from the simulation

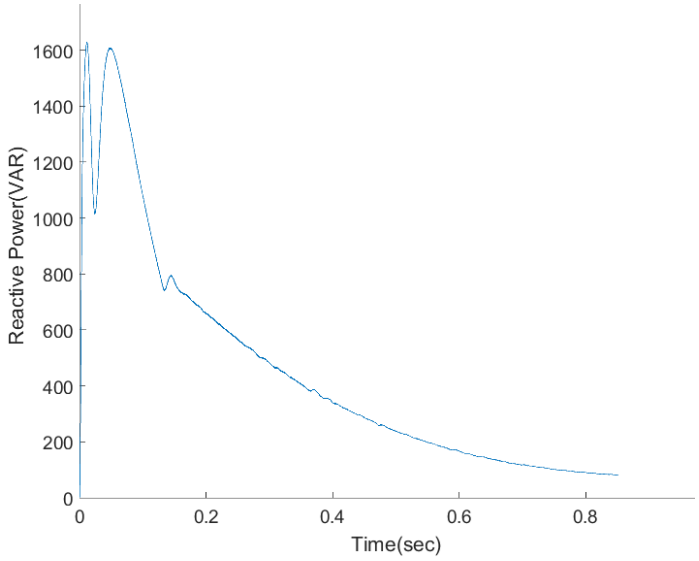

Fig. 4.4: Measured reactive power from simulation

As can be seen from the Fig. 4.5 power factor of the simulated system is almost unity.

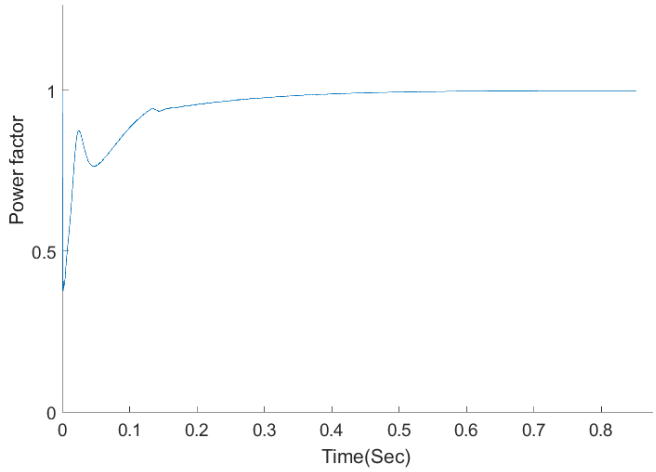

Fig. 4.5: Power factor for the system from simulation

4.2 System arrangement

The experimental setup in Fig. 4.6 shows three boards. The proposed rectifier is a sandwiched rectifier to shrink the overall system size. Here Board-1(measurement board) and Board -2 (CREE SiC MOSFET Gate driver board) are sand-witched with an unoptimized size of heatsink. Board – 3 is filter and pre-charge Board. The built experimental environment is shown in Fig. 4.3. Setup uses the motor drive from Rockwell automation donated to Dr. Mirafzal. Motor drive was run at different input frequencies for the experimental setup. Experimental analysis of the output is discussed in Chapter-5.

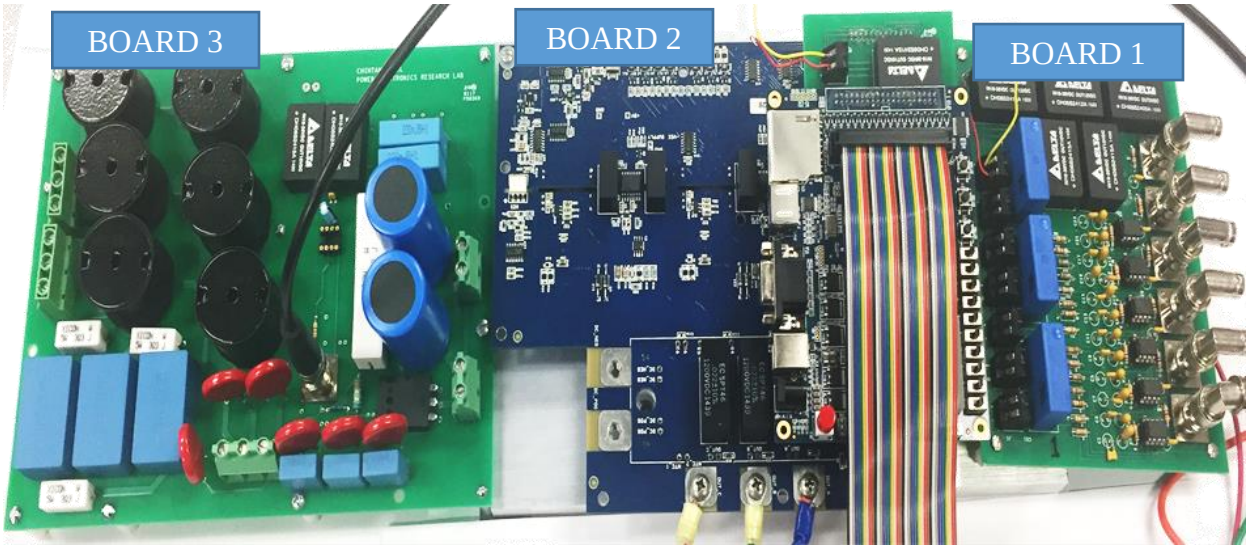

Fig. 4.6: Experimental setup

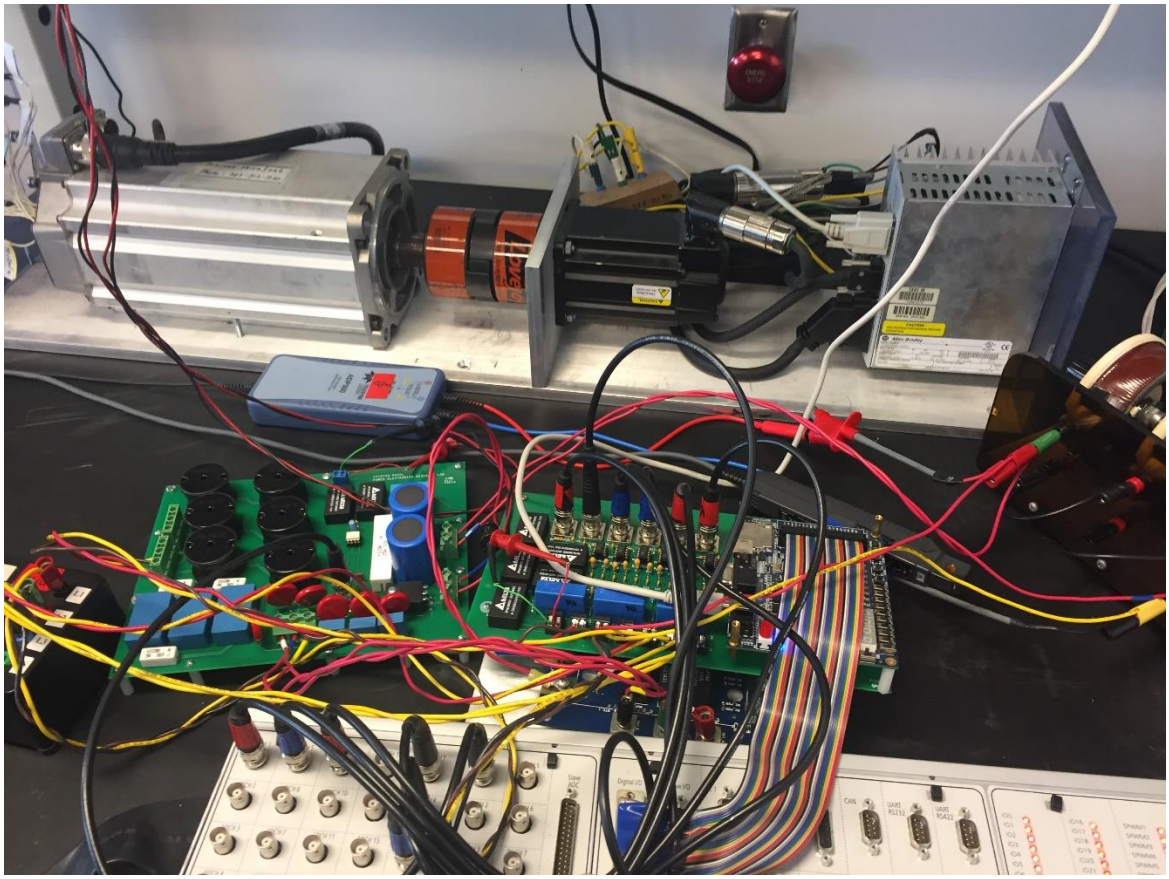

Fig. 4.7: Experimental Environment

Fig. 4.8 shows the final stage of designed active rectifier yet to be tested.

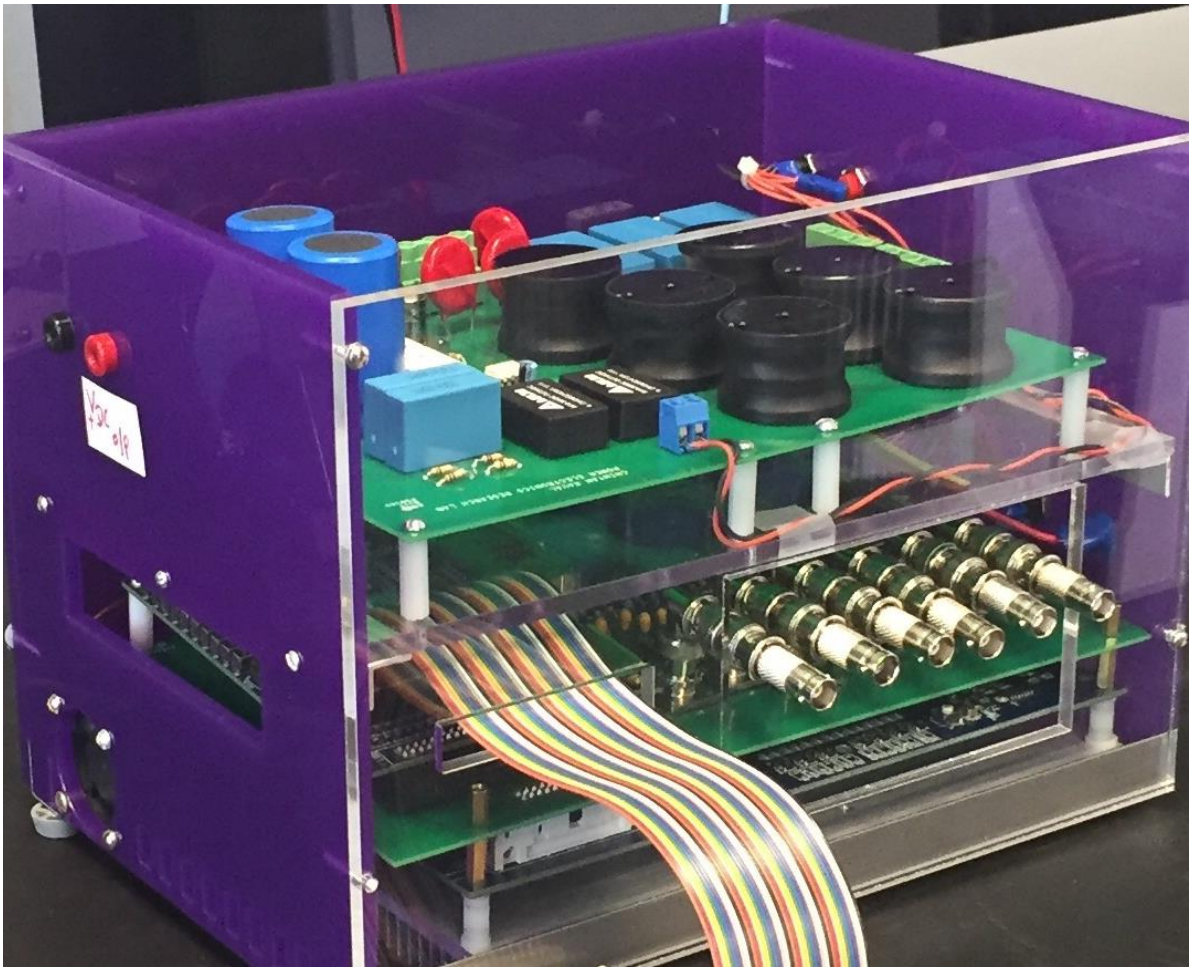

Fig. 4.8: Designed Active rectifier

4.2.1 SiC MOSFET gate driver

Since the required switching frequency in the simulation is very high, conventional power switches cannot be used. Fig. 4.8 shows the SiC MOSFET module used in the experiments and Table 4.2 summarizes the parameters for the module.

Table 4-2: Hardware parameters [23]

Parameter	Value
VS	16 V
V_IH	5 V
V_IL	0 V
Max. switching freq.	150 kHz
V_DS	1200 V
Max. Turn on delay	280 nS
Max. Turn off delay	290 nS

Fig. 4.9: CREE 1200 V SiC 6 pack MOSFET Module

The SiC module has inbuilt over current and desaturation fault protection. By default, the voltage level at the X1 connector shown in Fig. 4.9 for fault signal needs to be kept at LOW. Keeping them floating has a negative effect on the module operation. Similarly, RST and RDY pins must be kept HIGH to have proper operation for the module. Table 4.3 shows the Pinout of the X1 connector.

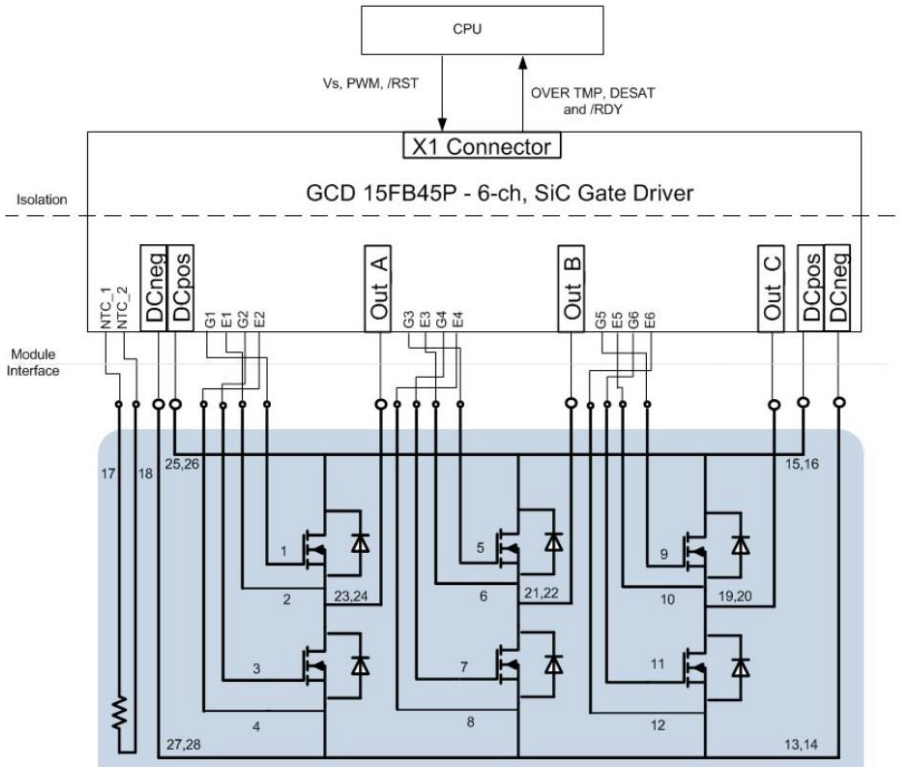

Fig. 4.10: CREE 1200 V SiC 6 pack MOSFET Module [23]

Table 4-3: Pinout table for X1 connector

1	PWM_Upper_A (5V Logic)
3	PWM_Lower_A (5V Logic)
5	PWM_Upper_B (5V Logic)
7	PWM_Lower_B (5V Logic)
9	PWM_Upper_C (5V Logic)
11	PWM_Lower_C (5V Logic)
13	/RST (normally hi)
15	RDY (normally hi)
17	DESAT FAULT (normally low)
19	OVER_TEMP_FLT (normally low)
21,23,25	Vs

4.2.2 Filter Board

Fig. 4.10 show the fabricated PCB board consisting of AC side filter and DC side filter. AC side filter has MOV (Metal – Oxide Varistor) for circuit protection in the case of the overvoltage condition. DC side filter consists of precharge circuitry. The precharge IGBT is triggered after the DC bus voltage reaches a certain level otherwise bypassing through the precharge resistor. Circuit board receives same DC voltage as the measurement board as shown in Fig. 4.11. Table 4.4 summarizes the components used in the filter board and their values.

Table 4-4 Filter board parameters

Parameter	**Value**
$L1$	$150\ \mu H$
$L2$	$330\ \mu H$
C (delta connected)	$3^*\ 27 \mu F$
5-watt damping resistor (R_{damp})	$3.3\ \Omega$
MOV (Varistor)	910V, 10kA
C_{DC}	$200\ \mu F$
PreCharge Resistor (25 watts)	$10\ \Omega$
$C_{coupling}$	$220\ nF$

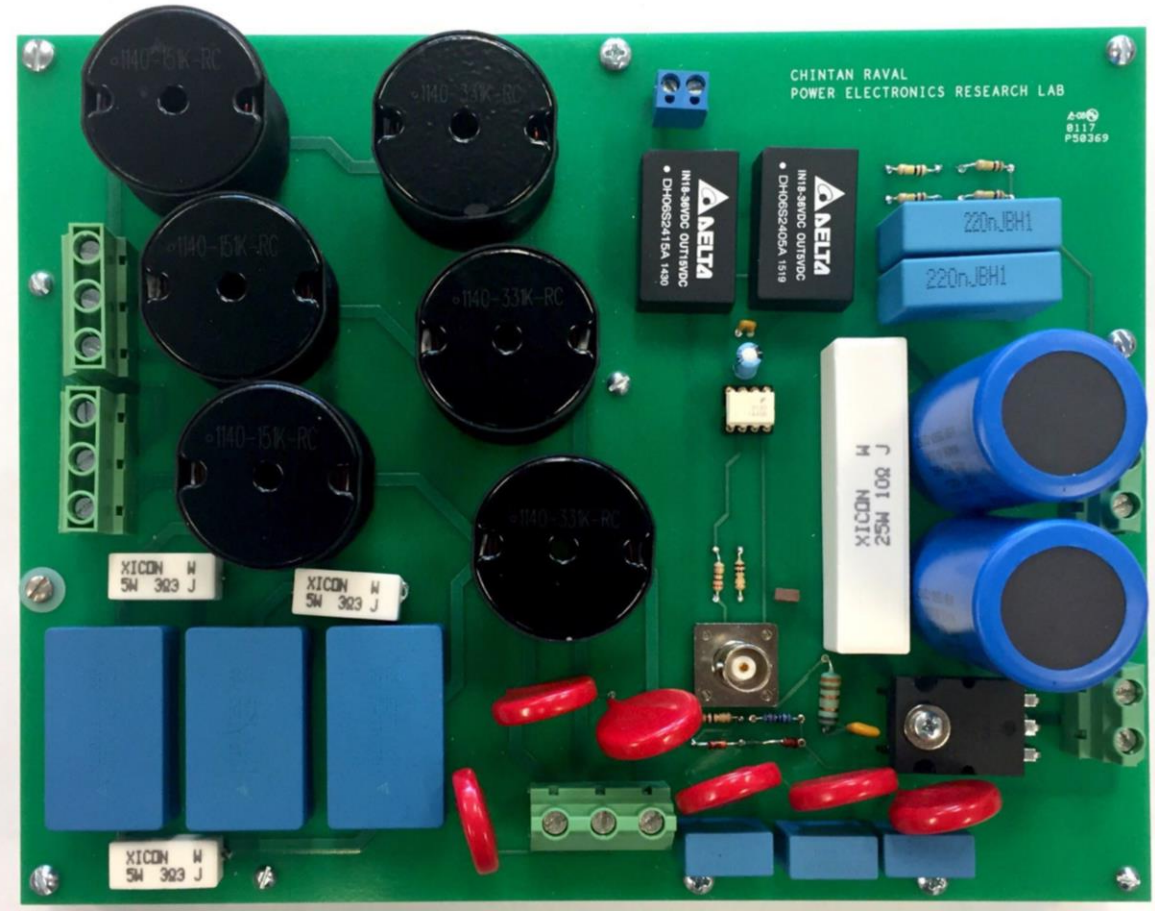

Fig. 4.11: AC side and DC side filter

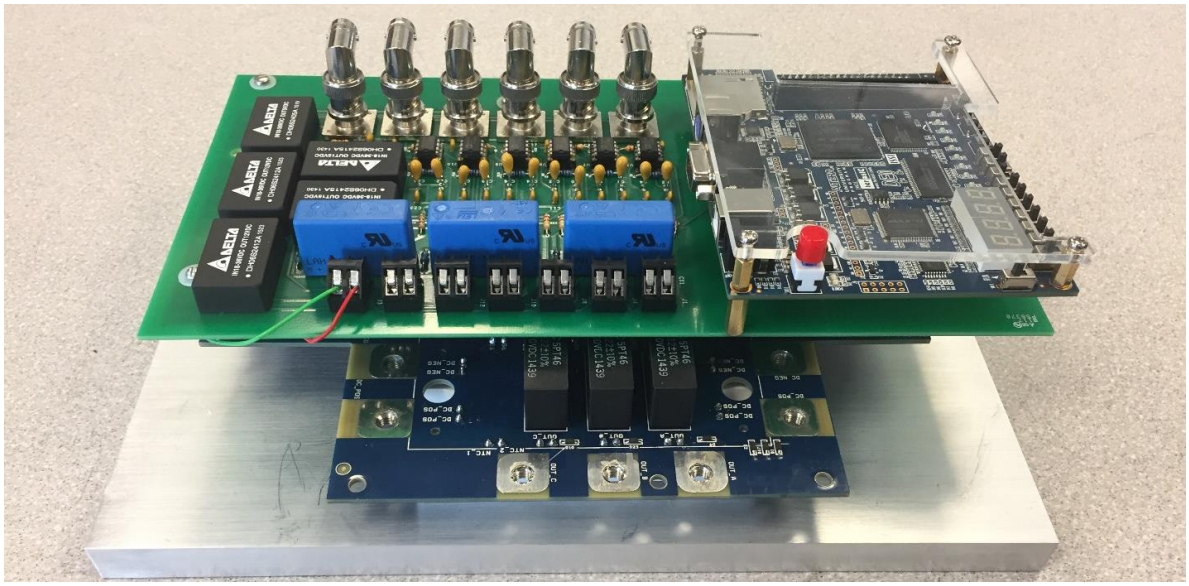

Fig. 4.12: Designed sandwiched layer of FPGA, measurement board and gate driver

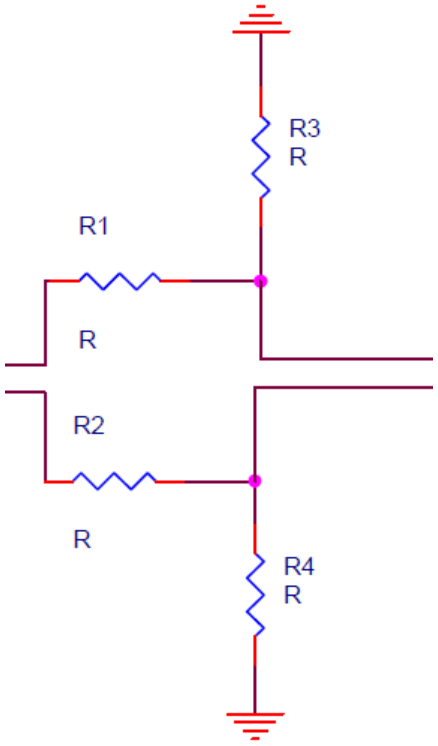

Fig. 4.13: Voltage divider circuit used in the measurement board.

Switching signals are generated using Altera FPGA EP3c16484F. It is required to minimize the distance between gate driver's switching port and FPGA, so the distance for high frequency switching signals to cover is a bare minimum. Thus, reducing the signal noise to as minimum as possible. As shown in Fig. 4.4 Board 1 is a fabricated measurement board designed in the lab. The board consists of current sensors, differential amplifiers, and voltage divider circuit. The measurement is done simply using voltage divider rule. Fig. 4.9 shows a simple schematic for the voltage divider used in the measurement board. The measured quantity is than fed to the instrumentation amplifier. From the specific output values from the instrumentation amplifier, the line voltages, DC voltage and line currents are measured and sent to the dSpace. DSpace converts these quantities to digital form using ADC (Analog to Digital converters).

4.3 Conclusion and remarks

A detailed simulation result was presented in this chapter. From the results, we can see that active rectifier attains near unity power factor eventually. It should be noted that the reactive power is not completely zero even though the power factor is near unity. The reactive power is negligible compared to the active power, which leads to near unity *pf*. Entire experimental-setup was described briefly in this chapter. Designed circuit layouts are attached in Appendix B. Chapter 5 will provide the summary on experimental results.

Chapter 5 - Findings and Analysis

This chapter will display the experimental results from the setup. Experiments were done for different input frequency AC voltages. The results show the controller with proper control on the reactive power of the system. The AC voltages were given using programmable motor drive with a permanent magnet generator. In this chapter, analysis of three different magnitude input supply voltages at different frequencies 30 Hz, 40 Hz, and 50 Hz is presented.

5.1 30 Hz input supply voltage operation

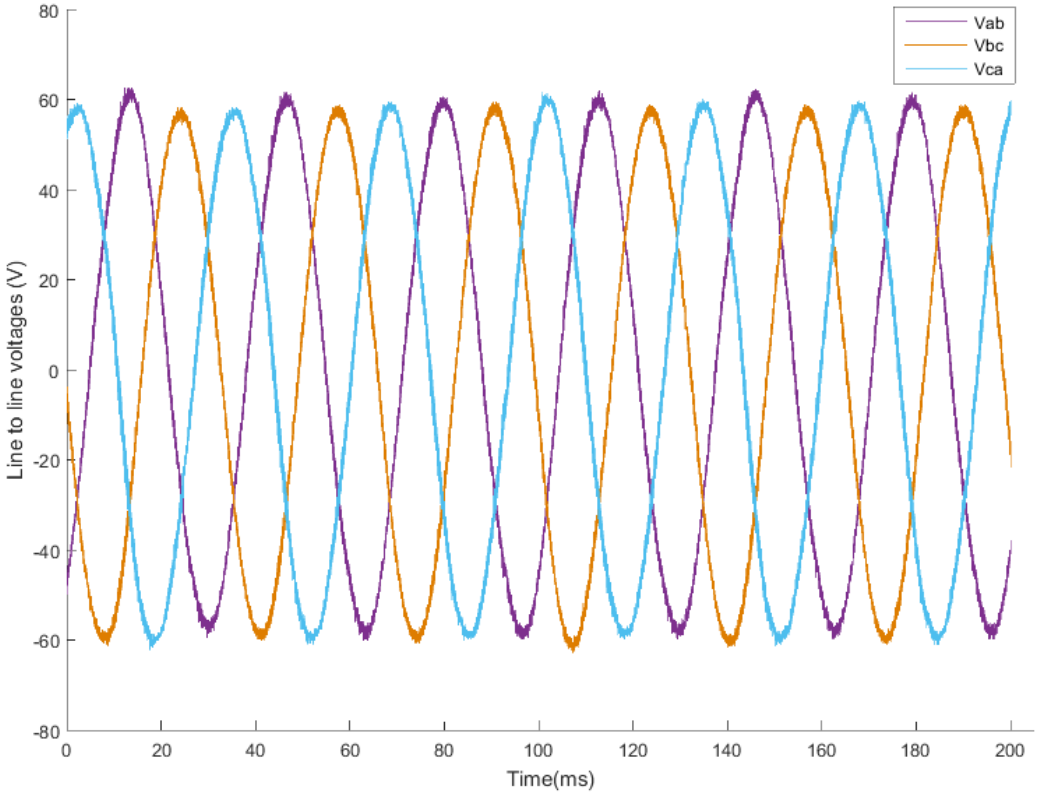

Fig. 5.1: Input: $\boldsymbol{Vin} \approx 45\ V_{LL}$, f = 30 Hz

Fig. 5.1 shows the 30 Hz input voltage at magnitude of nearly equal to 45 V line-to-line r.m.s. The permanent magnet generator was run at 450 rpm to generate this supply.

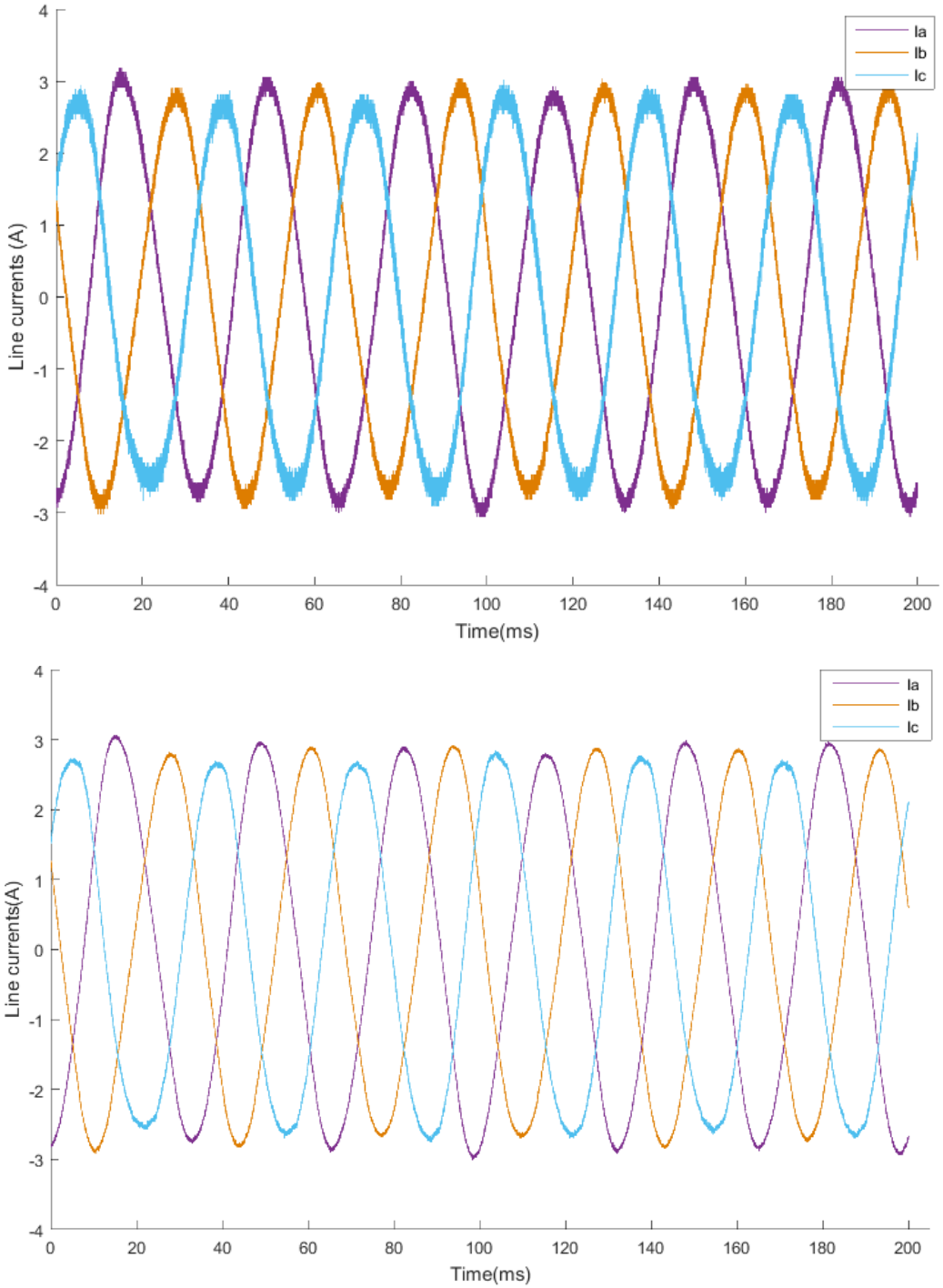

Fig. 5.2: Line currents (Nonfiltered and Filtered)

Fig. 5.2 shows measured line currents in line a, line b and line c respectively. Both the line-to-line voltages and line currents have some low-frequency noise. This low- frequency

noise is then filtered using a simple Butterworth filter and presented as shown in Fig. 5.1 and Fig. 5.2. The single cycle of line currents are shown in Fig. 5.3.

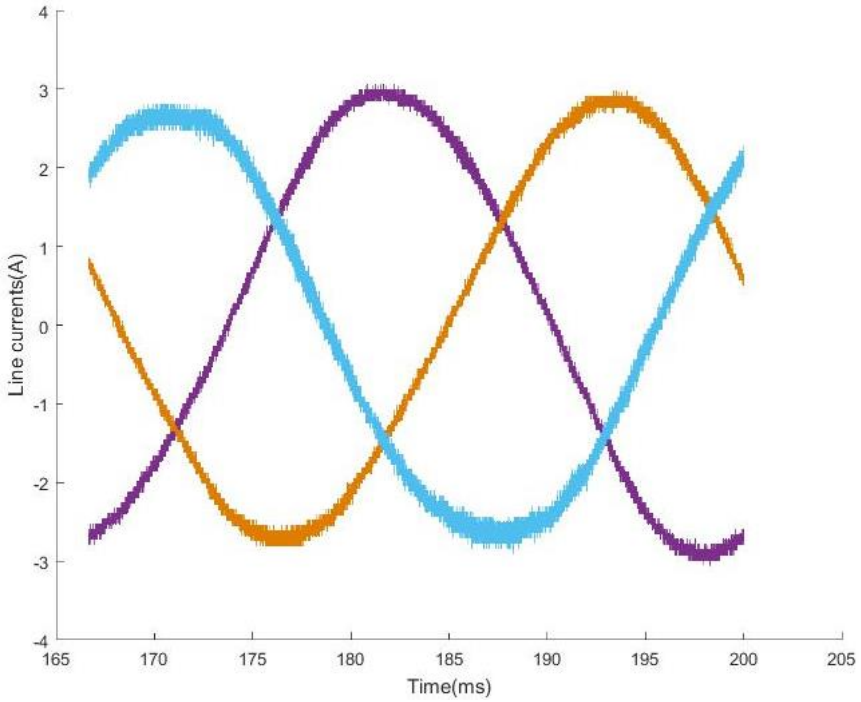

Fig. 5.3: Line currents in a single cycle

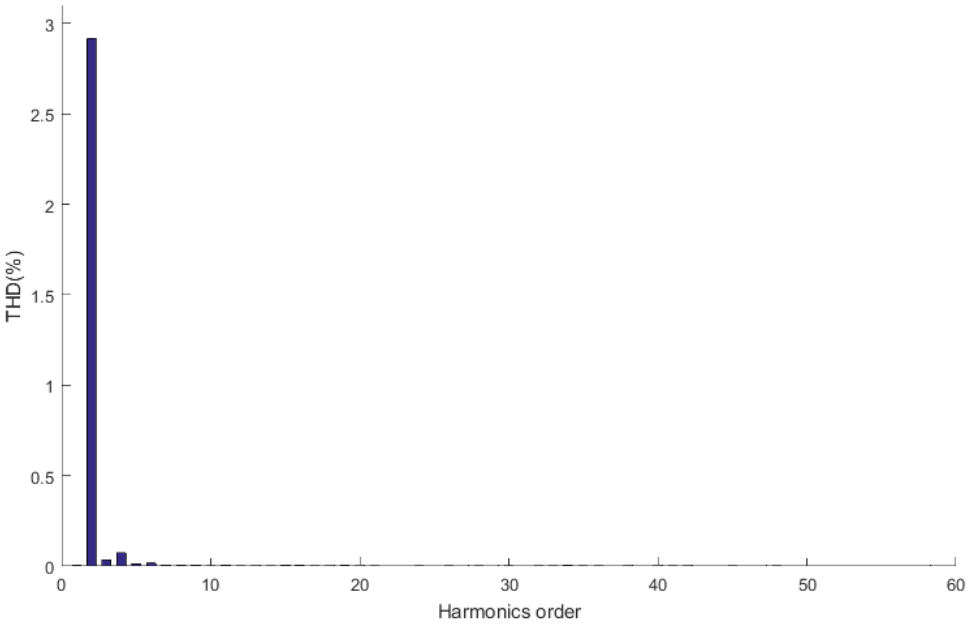

Fig. 5.4: THD in line current I_a

In most rectifiers, the effect of the system is examined based on several factors but the most important one is the distortion present in the mains currents. Fig. 5.3 shows a single cycle of line currents $I_a,\ I_b, and\ I_c$. From this single cycle, the calculated THD in line current I_a has been plotted. Apart from the very low magnitude low frequency noise, the THD in current is about 2.9%. THD in other line currents is under 3%.

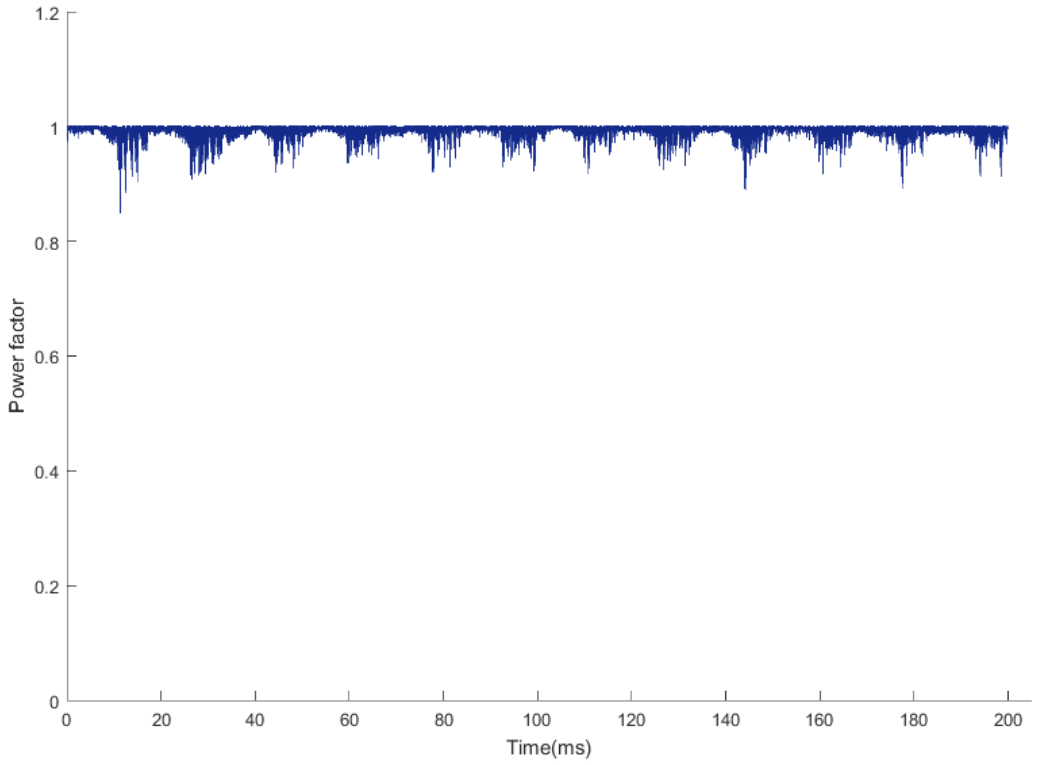

Fig. 5.5: power factor for 30 Hz supply voltage

The purpose of the rectifier was to achieve UPF operation. As can be seen from Fig. 5.5, the *pf* is near unity with the mean of the pf is about 0.99. To calculate the *pf*, the measured line-to-line voltage and line-to-line currents are converted in the *dq0* frame of reference with *q* axis being the reference. It should be noted that the inrush current and initial system transients are not present in the presented data analysis as the experimental data was recorded in steady state condition.

5.2 40 Hz input supply voltage operation

As described from in the previous result, the generator was run at 600 rpm to generate nearly 60 V line-to-line r.m.s voltage. The system setup is built to run for fixed magnitude and variable frequency input supply voltage. However, due to the limitation of the generator, it is not possible to go to a higher magnitude supply voltage than 85 V (i.e. 850 rpm). Fig. 5.6 shows the 40 Hz input voltage. As can be seen clearly, the symmetry in line-to-line voltages is decent. The low-frequency noise was filtered digitally using a simple Butterworth filter. Fig. 5.7 shows two waveforms of line currents: nonfiltered and filtered.

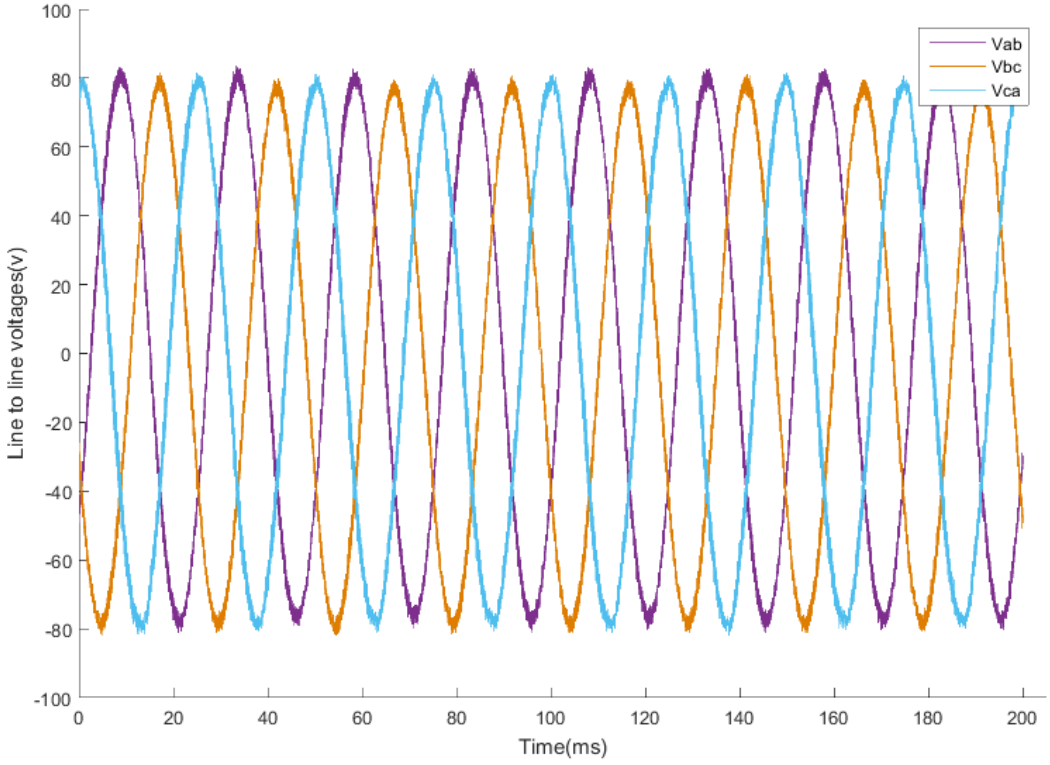

Fig. 5.6: Input: $\boldsymbol{Vin} \approx 60\ V_{LL}$, f = 40 Hz

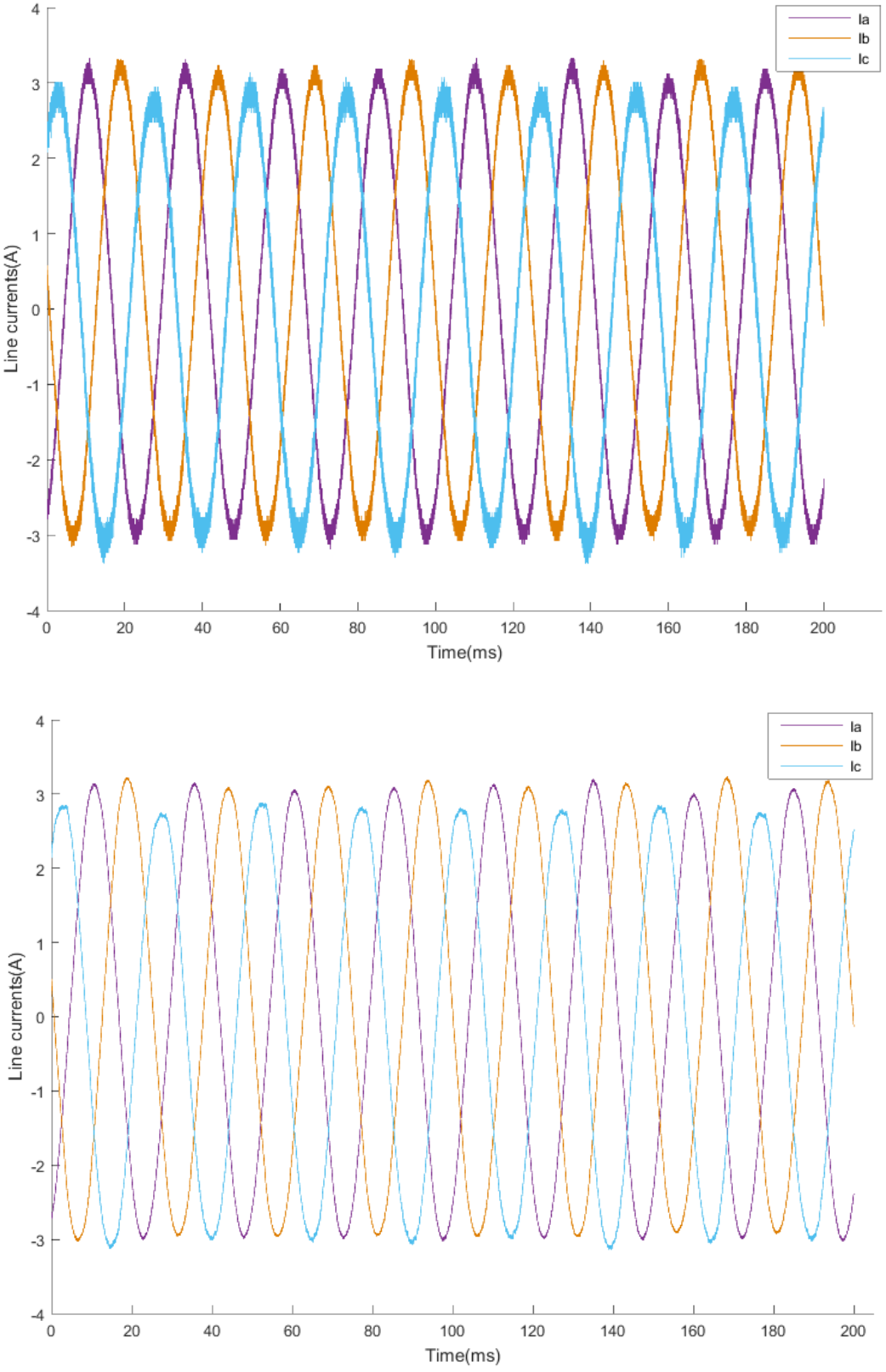

Fig. 5.7: Line currents (Nonfiltered and filtered)

As mentioned in the last analysis, the total harmonic distortion in currents is calculated for a single cycle. In this result, for the final cycle. It is presented in Fig. 5.8.

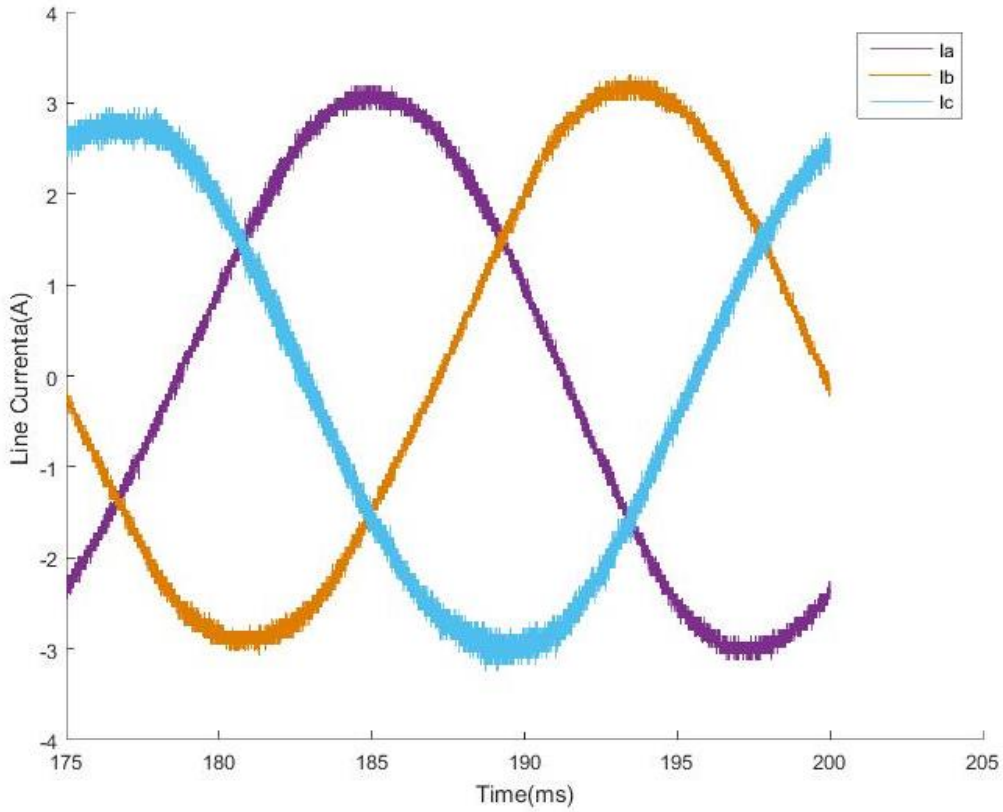

Fig. 5.8: Line currents in single cycle

The calculated THD for the line current I_a shown in Fig. 5.8 is presented in Fig. 5.9. The THD is about 3.04% for the line current I_a. The THD plot shows the distortion until the 60th Harmonic for a single cycle. It is clearly visible that the effect of the low order harmonics is negligible. Fig. 5.10 shows the calculated *pf* for the supply voltage at input frequency 40 Hz. The mean of the calculated *pf* is about 0.99 for recorded data of 200mS. The near unity power factor shows that the controller is able to maximize the difference between real power and reactive power for the system.. The controller is indeed compensating the required reactive power.

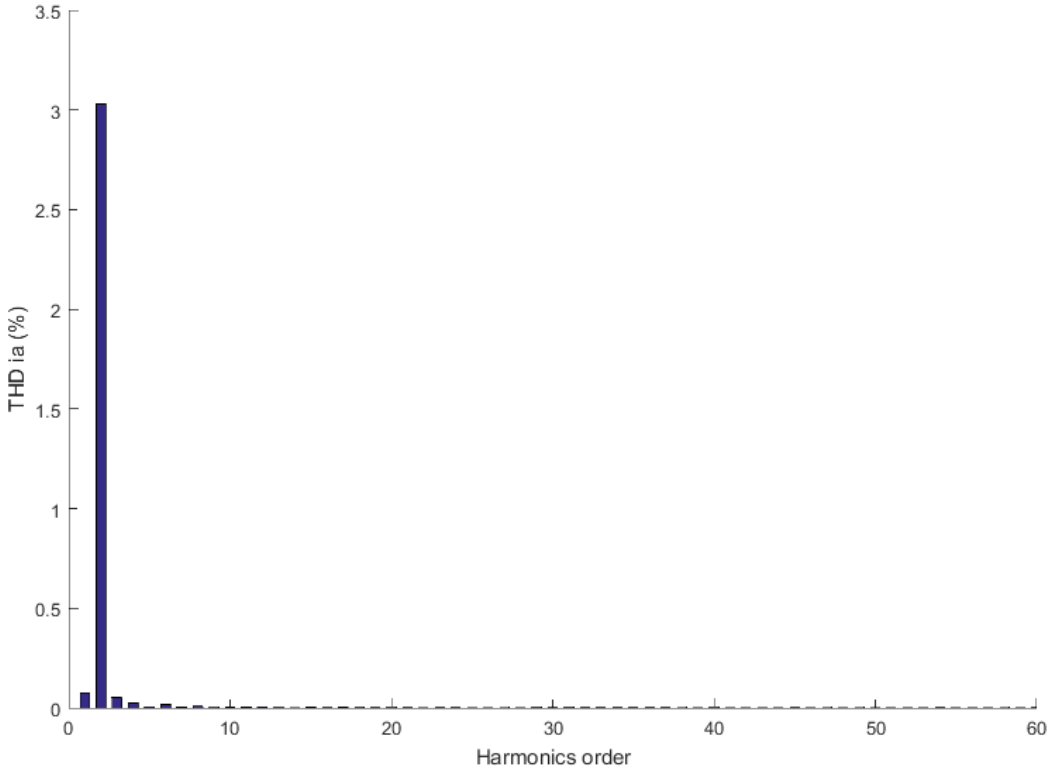

Fig. 5.9: THD in $\boldsymbol{I_a}$ for 40 Hz supply voltage

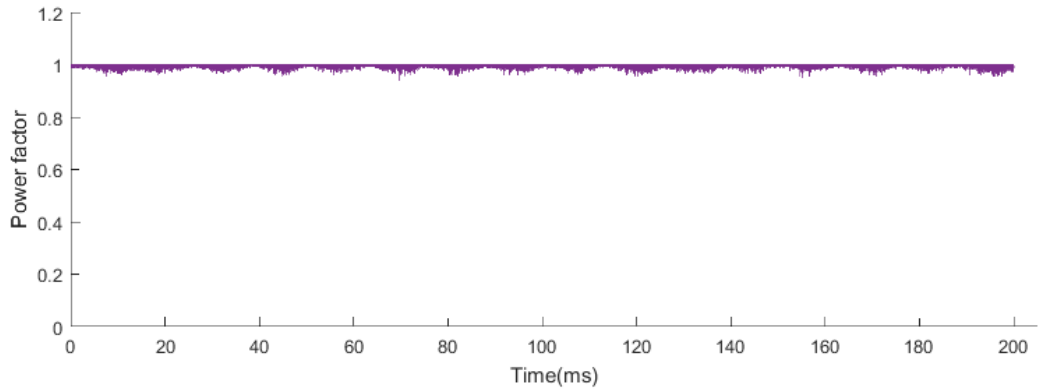

Fig. 5.10: Power factor for 40 Hz supply.

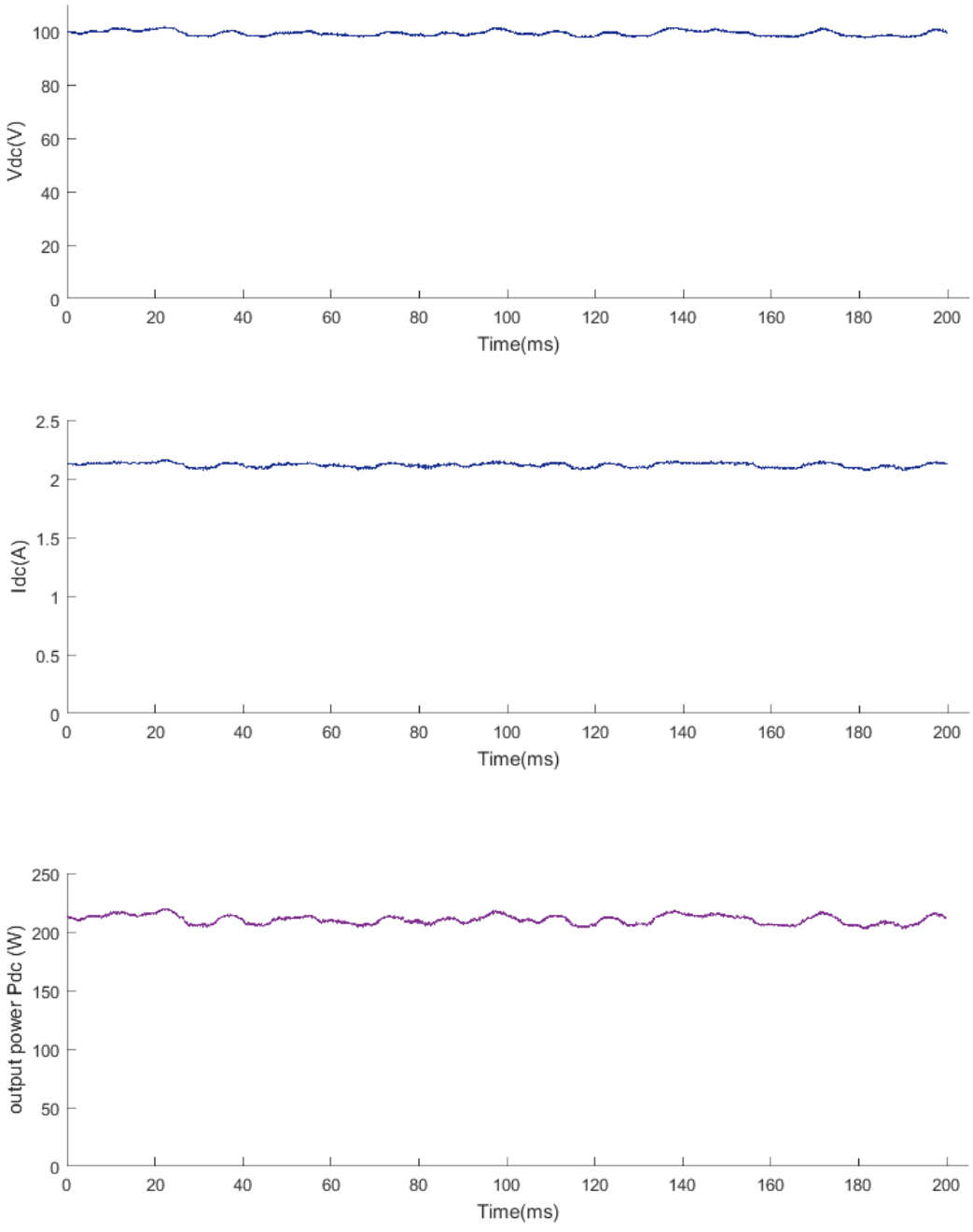

Fig. 5.11: Output DC voltage, DC current and calculated output power

Output summary: Vdc $\approx 100V$, $P_{out} \approx 220\ watts$

Fig. 5.11 shows the rectified DC output by the system. The rectified DC voltage $\approx 1.65 \times V_{LL.rms} \approx 99V$ as discussed in the previous chapter - 2.

A limitation for the experimental setup is that the variable frequency AC voltage generated from the generator also changes the magnitude of the input AC voltage making the stable DC voltage operation difficult. As a contrast to the proposed simulation, the input frequency is varying but the input voltage from the generator is fixed at $200\ V_{LL}rms$.

5.3 50 Hz input supply voltage opearation

To generate input supply voltage at 50 Hz input supply, the generator was run at 750 rpm. It can be seen from Fig. 5.12 the generated voltage from the generator is about 75 V line-to-line r.m.s. A slight unbalance in the magnitude of the voltages is visible. This causes an unbalance in line currents. The unbalance can be due to many factors, one known reason for the unbalance is the PLL (Phase Locked Loop). Which causes unbalance in the line currents. The effect can also be present due to difference line impedance and several other factors.

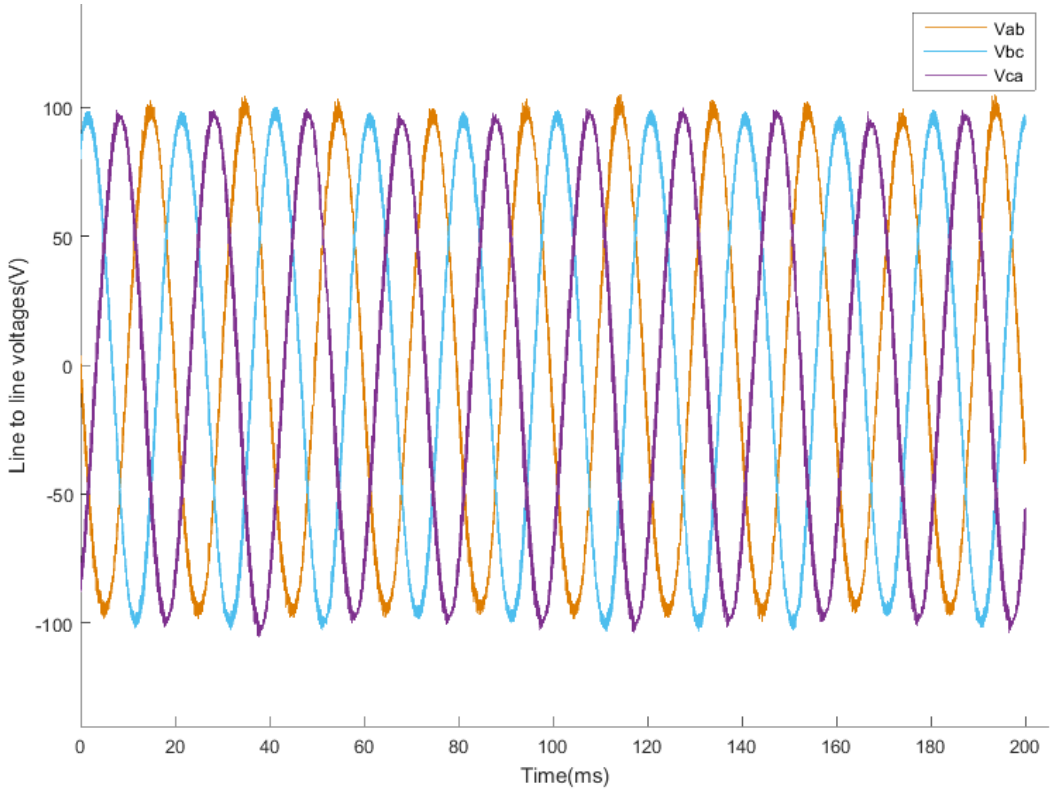

Fig. 5.12: Input: $\boldsymbol{V_{in}} \approx 75\ V_{LL}$, f = 50 Hz

Fig. 5.13 shows the AC main currents from the generator. Similar to prior results, the recorded supply current is filtered using a simple Butterworth filter to get rid of the low-frequency noise.

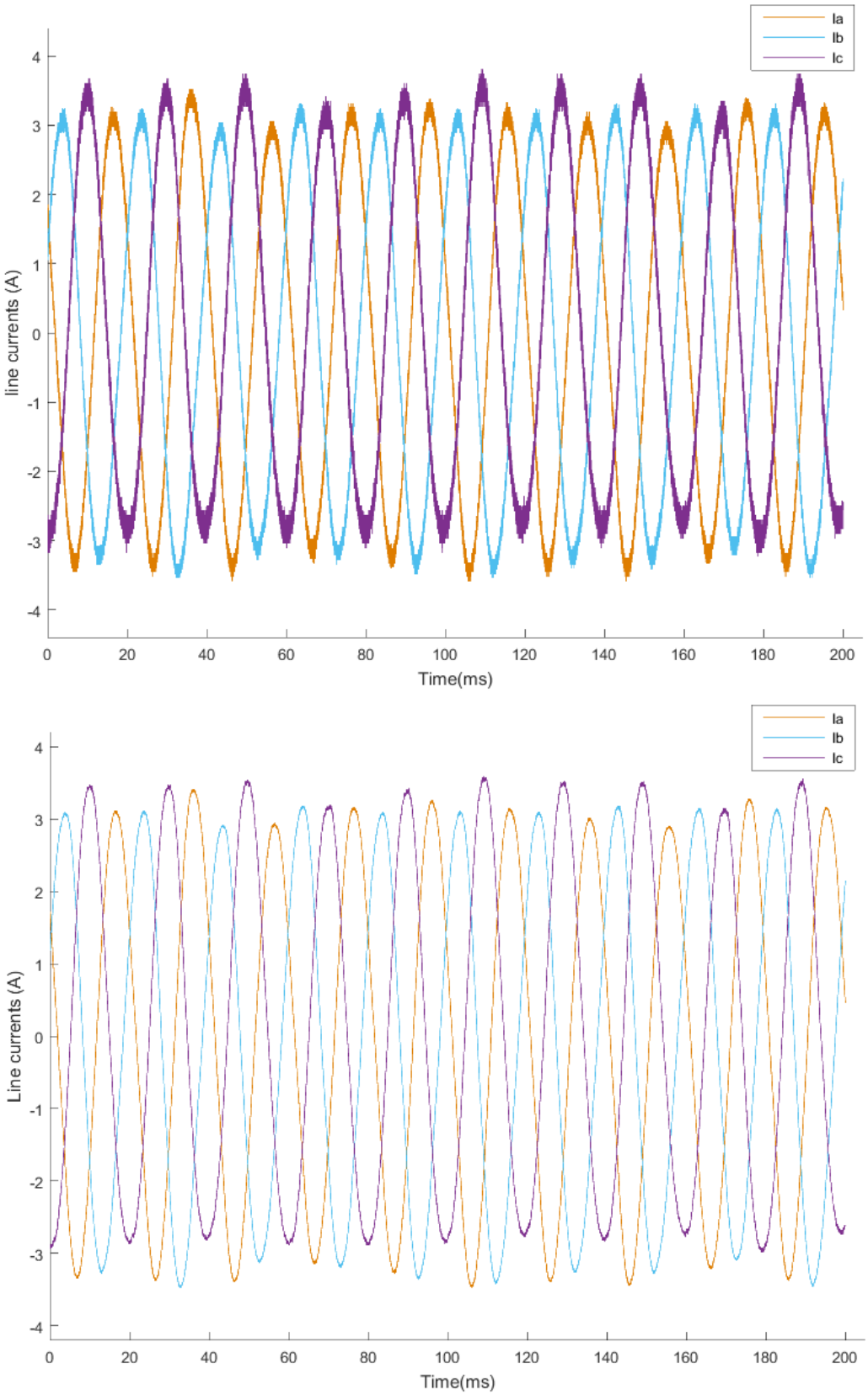

Fig. 5.13: line currents (Non-filtered and filtered) at 50 Hz supply

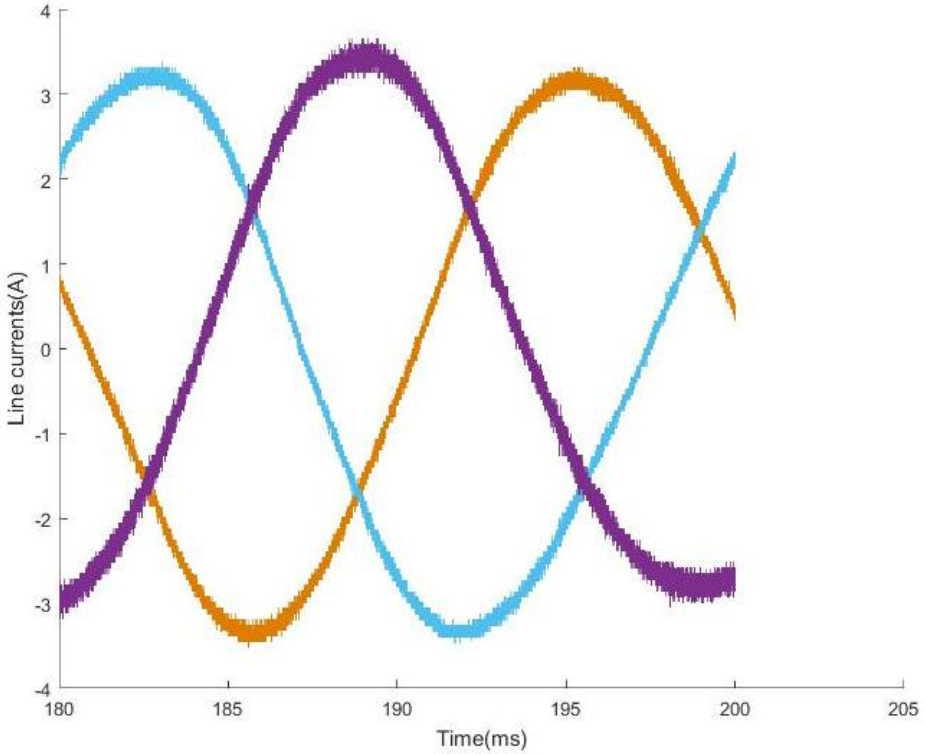

Fig. 5.14: Line currents in a single cycle

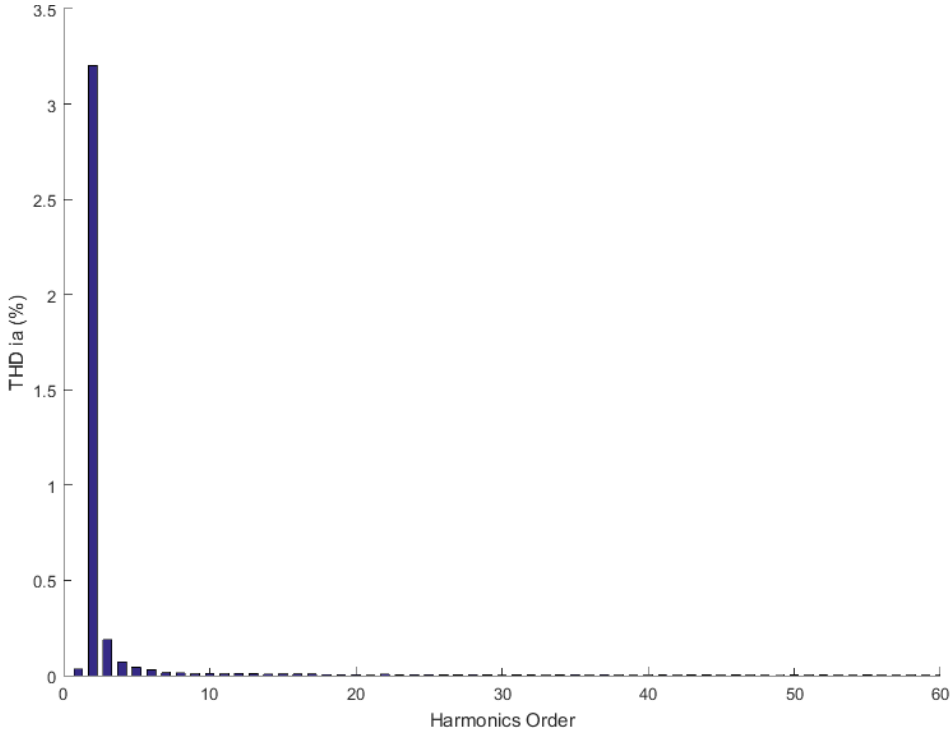

Fig. 5.15: THD in line current Ia

Fig. 5.14 shows a single cycle of line currents. The calculated THD for line current Ia is shown in Fig. 5.15. There is a slight increase in the THD for line current Ia. There is a similar effect on the other line currents. Although the THD for all the line currents is well under 3.5%. For line current Ia THD is about 3.2%.

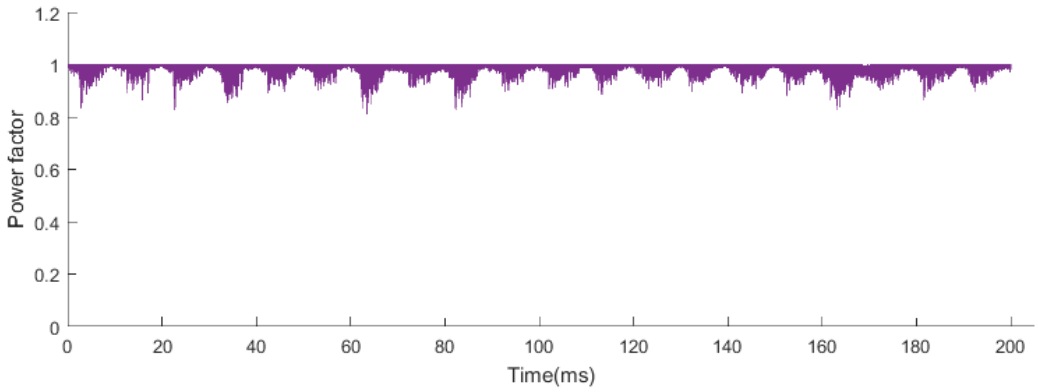

Fig. 5.16: Power factor for 50 Hz supply

Fig. 5.16 shows the calculated power factor for the entire recorded data. The mean *pf* is about 0.992. Comparing the *pf* plots of other results, it is visible that *pf* for the 50 Hz has more periodic deeps although the mean is almost unity.

Fig. 5.17 shows the rectified voltage and current from the system. The mean of the rectified DC voltage is ≈ 115 V. The instantaneous output power is also presented in Fig. 5.17. The mean of calculated output power is about 235 watts.

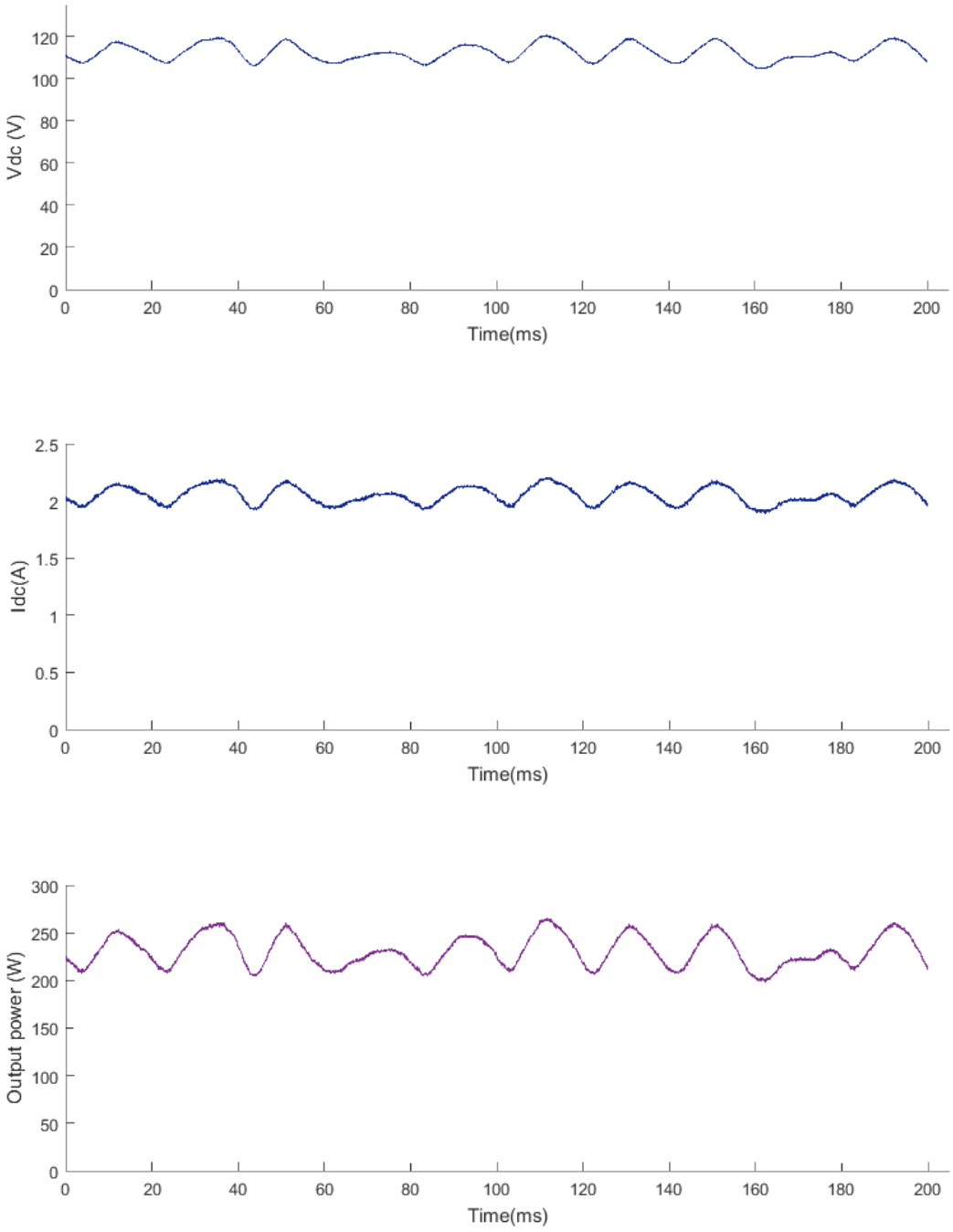

Fig. 5.17: Rectified DC voltage, DC current and calculated output power

Output summary: pf = 0.99, Vdc $\approx 120V$, $P_{out} \approx 240\ watts$

5.4 Conclusion and remarks

Until now, all the measurements were done with the generator. Due to the limitation of the DC current for the generator, it was not possible to go on the higher power than 250 watts. The slight unbalance in term of magnitude of currents is inherent due to generator's operation. The recorded analysis shows that the controller is constantly minimizing the error between desired reactive power and measured reactive power. Hence, the operation of near unity power factor is achieved.

Chapter 6 - Conclusion and Future Work

This chapter presents a summary of work done in this thesis. This chapter also includes suggestions for the future utilization of the experimental setup. Section 6.1 presents a summary of the thesis and 6.2 presents future work suggestions.

6.1 Summary

The major contribution made by this thesis is the development of an active rectifier using a SiC power module with reduced magnetics. The input to the active rectifier is a three-phase variable voltage/frequency supply, while the output is a regulated fixed DC voltage. Both the simulation and experimental results demonstrate the following:

- Simulations shows the proper control of the reactive power in the system leading to a UPF operation.
- The converter performed as expected as shown in Chapter 5, where it is seen that active rectifier operates at different input supply frequency voltages. The obtained power factor from the system is near unity showing the proper control on the reactive power.
- The THD of the line currents for all the experimental tested scenarios is under 3.3%.
- Due to the SiC module, it was possible to go beyond switching a frequency of 40 kHz.

6.2 Future Work

Although the experimental results obtained in this thesis represent a fully functional active rectifier, the following improvements and possible uses of the rectifier are suggested:

- The designed setup can be implemented for the design of a voltage source inverter for optimum performance due to the presence of Wide Bang Gap MOSFETs.

- With the optimized size of the heatsink, the power conversion per weight (power density per weight and volume) can be investigated.
- With the optimized size of heatsink, proper calculation of the efficiency of this rectifier can also be achieved.
- Furthermore, the reduction in the filter size is possible by going to even higher switching frequencies.
- Investigation of a wild frequency power supply is possible.

In addition to investigating the possibilities of solving the existing problems, the designed setup can be improved as follows:

- Making a better performance three-layer PCB board for the filter board.
- Optimize the size of the heatsink can reduce the weight of the system.

References

[1] J. Ito, T. Araki, "Volume evaluation of a PWM inverter with wide band-gap devices for motor drive system", *Proc. ECCE Asia Downunder*, pp. 372-378, 2013.

[2] N. Kaminski, "State of the art and the future of wide band-gap devices", *Power Electronics and Applications,* pp. 1-9, 2009.

[3] https:// energy.gov/eere/amo/downloads/wide-bandgap-semiconductors-pursuing-promise

[4] L. D. Stevanovic K. S. Matocha P. A. Losee J. S. Glaser J. J. Nasadoski S. D. Arthur "Recent advances in silicon carbide MOSFET power devices" *Proc. IEEE Appl. Power Electron. Conf. Expo*. pp. 401-407, Feb. 2010.

[5] J. He T. Zhao X. Jing N.A.O. Demerdash "Application of Wide Bandgap Devices in Renewable Energy Systems. Benefits and Challenges" *Proc. Of IEEE, International Conference on Renewable Energy Research, and Applications (ICRERA),* Oct. 2014.

[6] Muhammad H. Rashid, "Power Electronics Handbook: Devices, Circuits and Applications", 3rd ed. United States: Butterworth-Heinemann publications, 2011

[7] N. Mohan, T. Underland and P. Robbins, "Power Electronics: Converters, Applications and Design", 3rd ed. Wiley Publications, 2002

[8] "Rectifier Application Handbook", 3rd e., Phoenix, Arizona, Motorola, Inc., 1993

[9] M. Weiner, "Analysis of Cockcroft–Walton voltage multipliers with an arbitrary number of stages," *Rev. Sci. Instrum.,* vol. 40, no. 2, pp. 330–333, Feb. 1969.

[10] B. Singh, B. N. Singh, A. Chandra, K. Al-Hadad, A. Pandey, and D. Kothari, "A review of single-phase improved power quality AC-DC converters," *IEEE Trans. Ind. Electron.,* vol. 50, no. 5, pp. 962–981, Oct. 2003.

[11] J. Rodriguez, J. Dixon, J. Espinoza, J. Pontt, P. Lezana, "PWM regenerative rectifiers: State of the art", *IEEE Trans. Ind. Electron.,* vol. 52, no. 1, pp. 5-22, Feb. 2005.

[12] M. M. Reis, B. L. Soares, L. H. S. C. Barreto, C. E. A. Silva, R. P. T. Bascope, and D. S. Oliveira, Jr., "A variable speed wind energy conversion system connected to the grid for small wind generator", *Proc. 23rd Annul. IEEE Appl. Power Electron. Conf. Expo. (APEC 2008),* pp. 751–755. Feb. 2008,

[13] P.C. Sen, Power Electronics, Tata McGraw-Hill - 1988.

[14] G.J. Wakileh, Power Systems Harmonics, Springer, 2001.

[15] K. Yao, X. Ruan, C. Zou, and Z. Ye, "Three-phase single-switch boost PFC converter with high input power factor," *IEEE ECCE Conf.*, pp. 2921-2928, 12-16 Sept. 2010.

[16] J. C. Salmon, "Operating a Three-Phase Diode Rectifier with a Low-Input Current Distortion Using a Series-Connected Dual Boost Converter" *IEEE Trans. on Power Electronics*, vol. 11, no. 4, pp. 592-603, July. 1996.

[17] D.G. Holmes and T.A. Lipo., "Pulse Width Modulation for Power Converters", John Wiley & Sons, Inc. 2003.

[18] C.U. Ogbuka and M.U. Agu, "A Generalized Rectified Sinusoidal PWM Technique for Harmonic Elimination," *The Pacific Journal of Science and Technology*, Vol. 10, No. 2, pp. 21-26, November. 2009.

[19] J.A. Houldsworth, and D.A. Grant, "The Use of Harmonic Distortion to Increase the Output Voltage of a Three-Phase PWM Inverter," *IEEE Trans. Ind. Electron.* Vol. IA-20, No. 5, pp. 1124-1228, September-October 1984.

[20] K. Ogata, "Modern Control Engineering", Pearson Education 2003

[21] J. Kolar, F. Zach, "A Novel Three-Phase Utility Interface Minimizing Line Current Harmonics of High-Power Telecommunications Rectifier Modules". *Conf. Rec. 16th IEEE Int. Telecommunications Energy Conf.*, pp. 367-374, Oct. 1994

[22] Kolar J.W., Drofenik. U., Zach F.C., "Space Vector Based Analysis of the Variation and Control of the Neutral Point Potential of Hysteresis Current Controlled Three-Phase/Switch/Level PWM Rectifier Systems". *Proc. of the Int. Conf. on Power Electronics and Drive Systems*, Vol.1, pp. 22-33 Feb. 1995

[23] CREE Inc., "Six channel SiC MOSFET Driver CGD15FB45P", datasheet, 2014

Bibliography

The books reported as reference in the thesis cover almost all the topics well beyond specific citation. I prefer to cite these books again with additional URLs as sources.

Muhammad H. Rashid, "Power Electronics Handbook: Devices, Circuits and Applications", 3rd ed. United States: Butterworth-Heinemann publications, 2011.

N. Mohan, T. Underland and P. Robbins, "Power Electronics: Converters, Applications and Design", third ed. Wiley Publications.

"Rectifier Application Handbook", 3rd e., Phoenix, Arizona, Motorola, Inc., 1993.

P.C. Sen, “Power Electronics”, Tata McGraw-Hill - 1988.

G.J. Wakileh, “Power Systems Harmonics”, Springer, 2001.

D.G. Holmes and T.A. Lipo., “Pulse Width Modulation for Power Converters.” John Wiley & Sons, Inc. 2003.

K. Ogata, “Modern Control Engineering”, 5th edition. Pearson Education

URLs

https://energy.gov/eere/amo/downloads/wide-bandgap-semiconductors-pursuing-promise

Appendix A - Mathematical Analysis

Mathematical analysis of three-phase controlled bridge rectifier circuit in CCM and DCM

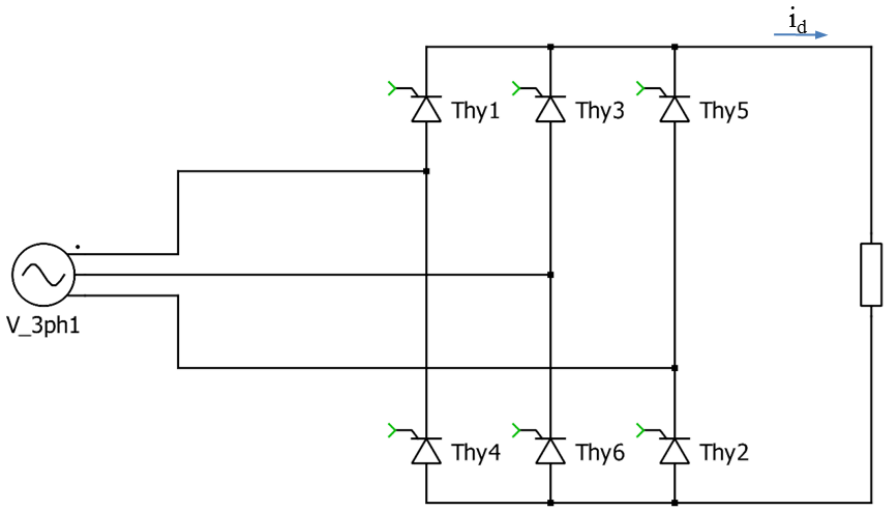

Fig. A.1: Three-phase fully controlled bridge rectifier

Similar to prior assumptions in chapter 2, assuming the switches are ideal and connected with a purely resistive load. The calculated parameters are extracted from [13]

The rectifier is in CCM (Continuous conduction mode) when

$$\mathbf{0} \leq \boldsymbol{\alpha} \leq \frac{\boldsymbol{\pi}}{\mathbf{3}} \tag{A-1}$$

$$V_{DC}(\alpha) = \frac{6}{2\pi}\int_{\alpha}^{\frac{\pi}{3}+\alpha} \sqrt{3}\cdot V_S \cdot \sin\left(\omega t + \frac{\pi}{3}\right) dt$$

$$= \frac{3}{\pi}\cdot\sqrt{3}\cdot V_S \cdot \cos(\alpha) = V_{DC}\cdot\cos(\alpha) \tag{A-2}$$

$$V_L(\alpha) = \sqrt{\frac{6}{2\pi}\int_{\alpha}^{\frac{\pi}{3}+\alpha} 3\cdot V_S^2 \cdot \sin^2\left(\omega t + \frac{\pi}{3}\right) dt}$$

$$= \sqrt{3}\cdot V_S.\sqrt{1+\frac{3\sqrt{3}}{2\cdot\pi}\cos(2\alpha)} \tag{A-3}$$

$$FF(\alpha) = \frac{V_L(\alpha)}{V_{DC}(\alpha)} = \frac{\pi}{3\cos\alpha}\cdot\sqrt{1+\frac{3\sqrt{3}}{2\cdot\pi}\cos(2\alpha)} \tag{A-4}$$

$$I_{DC}(\alpha) = \frac{V_{DC}(\alpha)}{R_L} = \frac{3}{\pi} \cdot \sqrt{3} \cdot \frac{V_S}{R_L} \cdot \cos(\alpha)$$

$$= I_{DC0} \cdot \cos(\alpha) \quad \text{(A-5)}$$

$$I_L(\alpha) = \frac{V_L(\alpha)}{R_L} = \sqrt{3} \cdot \frac{V_S}{R_L} \cdot \sqrt{1 + \frac{3\sqrt{3}}{2 \cdot \pi} \cos(2\alpha)} \quad \text{(A-6)}$$

$$RF(\alpha) = \sqrt{FF^2(\alpha) - 1}$$

$$= \sqrt{\frac{\pi^2}{9\cos^2(\alpha)} \left[1 + \frac{3\sqrt{3}}{2 \cdot \pi} \cos(\alpha)\right] - 1} \quad \text{(A-8)}$$

The rectifier is in DCM (Discontinuous conduction mode) when

$$\boldsymbol{\frac{\pi}{3} < \alpha \leq \frac{2 \cdot \pi}{3}} \quad \text{(A-9)}$$

$$V_{DC}(\alpha) = \frac{6}{2\pi} \int_{\alpha}^{\frac{2\pi}{3}} \sqrt{3} \cdot V_S \cdot \sin\left(\bar{\omega}t + \frac{\pi}{3}\right) dt$$

$$= \frac{3}{\pi} \cdot \sqrt{3} \cdot V_S \cdot \left[1 + \cos\left(\alpha + \frac{\pi}{3}\right)\right] \quad \text{(A-10)}$$

$$V_L(\alpha) = \sqrt{\frac{6}{2\pi} \int_{\alpha}^{\frac{2\pi}{3}} \sqrt{3} \cdot V_S \cdot \sin\left(\bar{\omega}t + \frac{\pi}{3}\right) dt}$$

$$= \frac{\sqrt{3} \cdot V_S}{\sqrt{2}} \cdot \sqrt{\frac{6}{\pi} \cdot \left[\frac{\pi}{3} - \frac{\alpha}{2} + \frac{1}{4} \cdot \sin 2\left(\frac{\pi}{3} + \alpha\right)\right]} \quad \text{(A-11)}$$

$$FF(\alpha) = \frac{V_L(\alpha)}{V_{DC}(\alpha)} = \frac{\pi \cdot \sqrt{\frac{6}{\pi} \cdot \left[\frac{\pi}{3} - \frac{\alpha}{2} + \frac{1}{4} \cdot \sin 2\left(\frac{\pi}{3} + \alpha\right)\right]}}{3 \cdot \sqrt{2} \cdot \left[1 + \cos\left(\alpha + \frac{\pi}{3}\right)\right]} \quad \text{(A-12)}$$

$$I_{DC}(\alpha) = \frac{V_{DC}(\alpha)}{R_L}$$

$$= \frac{3}{\pi} \cdot \sqrt{3} \cdot \frac{V_S}{R_L} \cdot \left[1 + \cos\left(\alpha + \frac{\pi}{3}\right)\right] \quad \text{(A-13)}$$

$$I_L(\alpha) = \frac{V_L(\alpha)}{R_L}$$

$$= \frac{\sqrt{3} \cdot V_S}{\sqrt{2} \cdot R_L} \cdot \sqrt{\frac{6}{\pi} \cdot \left[\frac{\pi}{3} - \frac{\alpha}{2} + \frac{1}{4} \cdot \sin 2\left(\frac{\pi}{3} + \alpha\right)\right]} \qquad \text{(A-14)}$$

$$\eta(\alpha) = \left(\frac{1}{FF(\alpha)}\right)^2 \qquad \text{(A-15)}$$

$$RF(\alpha) = \sqrt{FF^2(\alpha) - 1} \qquad \text{(A-16)}$$

Appendix B - Desired hardware schematics

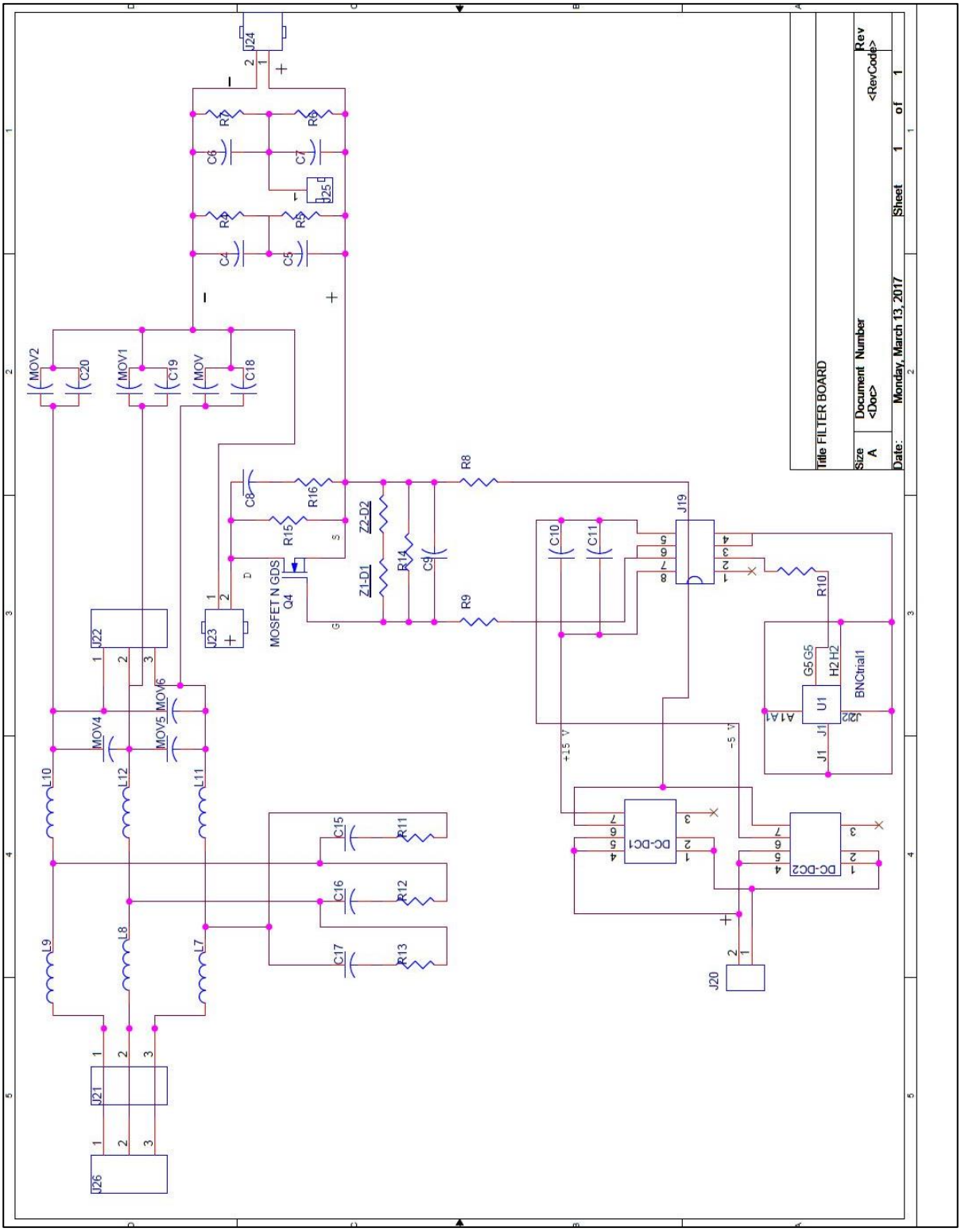

Fig. B-0.1: AC side and DC side filter design schematic in OrCAD

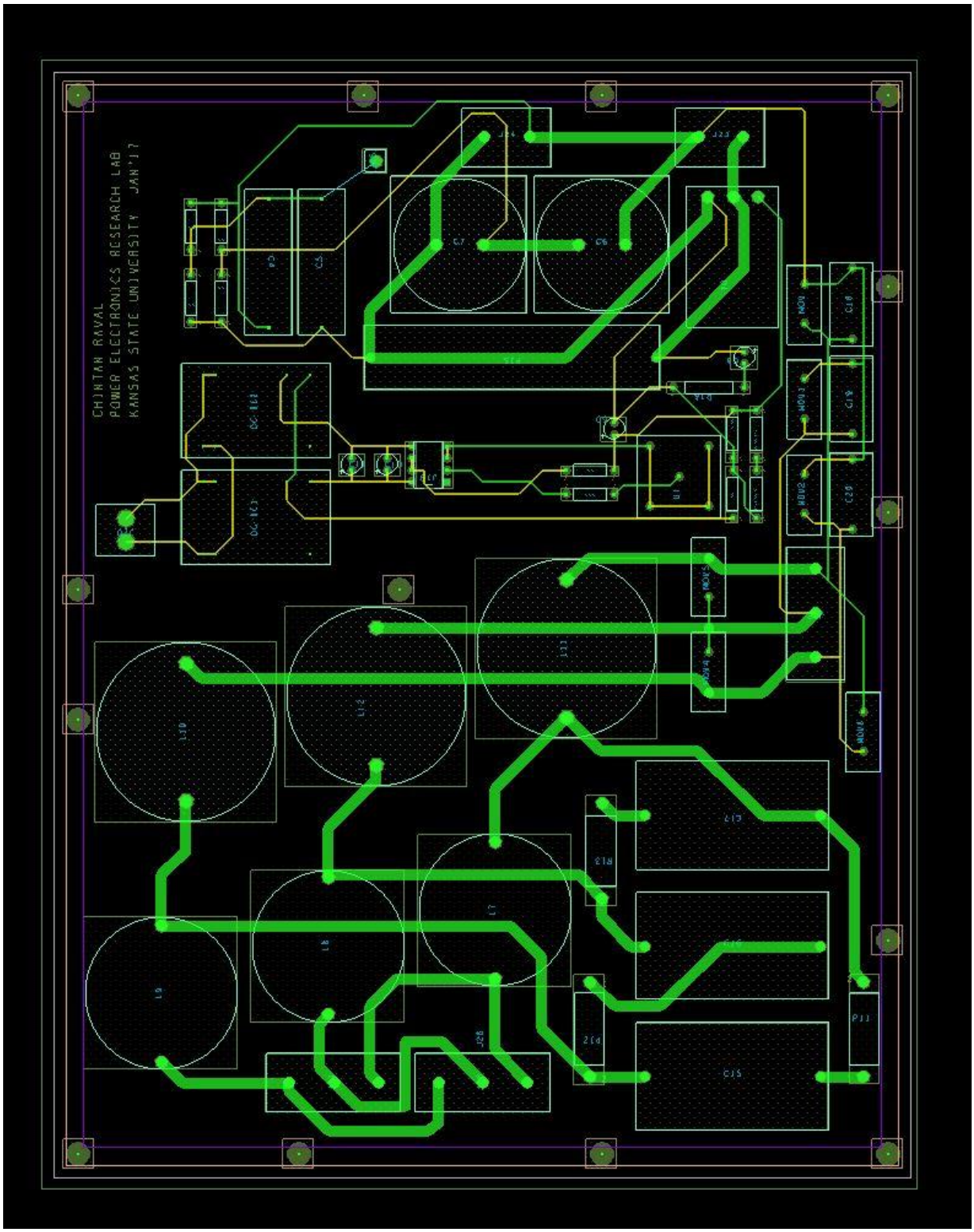

Fig. B-0.2: Circuit layout of the designed the filter board